Energy Reports 15 (2026) 109221

Contents lists available at ScienceDirect

Energy Reports

journal homepage: www.elsevier.com/locate/egyr

Review article

Beyond synchronization: The evolution of grid-following to grid-forming inverters and the quest for power system stability

Ammar Samir Abdelwahab [1,2,*], István Vokony [3]

Department of Electric Power Engineering, Faculty of Electrical Engineering and Informatics, Budapest University of Technology and Economics, Egry József u. 18, Budapest 1111, Hungary

ARTICLE INFO

Keywords:
Grid-Following Inverter (GFL)
Grid-Forming Inverter (GFM)
Power System Stability
Weak Grid, Short-Circuit Ratio (SCR)
Virtual Synchronous Machine (VSM)
Synchronization Instability
Artificial Intelligence (AI)
Adaptive Control, Renewable Energy Integration

ABSTRACT

The global integration of renewable energy is fundamentally reshaping power systems, replacing synchronous generators with inverter-based resources (IBRs). This transition introduces a critical stability challenge: conventional Grid-Following (GFL) inverters, which depend on a stable grid voltage for synchronization, become unstable in weak grids with low Short-Circuit Ratios (SCR). This paper provides a comprehensive review of the paradigm shift from GFL to Grid-Forming (GFM) inverters—the key to stabilizing future power systems. We analyze the core control architectures, operational limitations, and stability mechanisms of both paradigms, with a focused examination of synchronization instability in GFL units, including a precise small-signal impedance model explaining the negative incremental resistance effect and its impact on critical SCR thresholds in multi-inverter systems. We further delve into the voltage-source behavior of GFM strategies like Droop Control and the Virtual Synchronous Machine (VSM), critically comparing their power sharing and frequency regulation capabilities in islanded microgrids and analyzing the stability trade-offs of virtual inertia in ultra-weak grids. The review covers advanced mitigation techniques, including adaptive control and virtual impedance, while also addressing their limitations in P-Q decoupling in resistive grids and exploring novel control paradigms. We provide a bifurcation analysis of large-signal instabilities, clarifying the role of current limiting strategies in catastrophic failures. Furthermore, we highlight the transformative role of Artificial Intelligence (AI) in enabling real-time, self-tuning inverters, and critically examine the optimal role of the AI layer (supervisory vs. direct control) and the attendant risks. Finally, we present a forward-looking research trajectory for developing an AI-augmented GFM inverter capable of stable operation in ultra-weak grids (SCR $<$ 2), including the crucial development of Verification and Validation (V&V) frameworks for AI-based grid controllers to provide formal or probabilistic guarantees against adversarial data and cyber-physical attacks, providing a clear pathway to overcome the most pressing stability barriers in renewable-rich power networks.

1. Introduction

The architecture of the twentieth-century power system was predicated on a centralized, unidirectional paradigm, characterized by large-scale synchronous generation, passive distribution networks, and demand-following operation. This century-old model is now undergoing a foundational transformation, compelled by the imperatives of decarbonization and the proliferation of distributed energy resources. The emergence of inverter-based resources (IBRs), including solar photovoltaics and wind power, is not merely supplementing the existing grid but is fundamentally recalibrating its operational physics and control philosophies (Geekiyanage and Seppänen, 2024; Castilla et al., 2018). This shift from a synchronous machine-dominated system to an inverter-dominated one represents a technological revolution with profound implications for system stability and control (Song et al., 2022). In the nascent stages of this transition, the Grid-Following (GFL) inverter emerged as the predominant interfacing technology. Operating as precision-controlled current sources, GFL converters derive their synchronization from the grid voltage itself via a Phase-Locked Loop (PLL), injecting prescribed active and reactive power commands (Lin

* Corresponding author.
E-mail addresses: aabdelwahab@edu.bme.hu (A.S. Abdelwahab), vokony.istvan@vik.bme.hu (I. Vokony).
[1] https://scholar.google.com/citations?user=KZLsyA8AAAAJ&hl=en
[2] ORCID record is https://orcid.org/0009–0000-7789–3108
[3] https://scholar.google.com/citations?user=0mFLXwEAAAAJ&hl=hu

https://doi.org/10.1016/j.egyr.2026.109221
Received 27 October 2025; Received in revised form 1 February 2026; Accepted 8 March 2026
Available online 27 March 2026

et al., 2025). This grid-feeding strategy proved effective in a robust grid environment, where the voltage and frequency stiffness provided by rotating synchronous masses offered a stable reference for the inverters to follow (Castilla et al., 2018). Consequently, GFL inverters became the de facto standard for integrating renewable generation, functioning as compliant contributors within a system whose stability was guaranteed by other means (Song et al., 2022). Paradoxically, the very success of GFL penetration shows the seeds of its own operational challenges. The large-scale displacement of synchronous generators eviscerates the system's innate inertia and diminishes its short-circuit strength, leading to a decline in the Short-Circuit Ratio (SCR) which is a critical indicator of grid strength (Meraj et al., 2025). In such weakened networks, the foundational assumption of GFL operation, that is, a stable voltage reference that becomes invalid. The PLL, the core of GFL synchronization, enters a destabilizing feedback loop with the grid impedance. This interaction can induce a negative incremental resistance effect, where the inverter effectively injects energy into system oscillations, precipitating synchronization instability, harmonic resonance, and potentially catastrophic voltage collapse (Quan et al., 2020; Kannan et al., 2024). A precise small-signal impedance model is crucial for understanding the genesis of this negative incremental resistance and for dictating the critical SCR threshold for synchronization instability, particularly in multi-inverter systems. Thus, the GFL paradigm, designed to support a strong grid, becomes a liability in the weak-grid conditions it helps create. This instability nexus has catalyzed a paradigm shift in control philosophy, from grid-following to grid-forming (GFM). The GFM inverter represents a conceptual leap, functioning not as a current source but as a controlled voltage source. It autonomously establishes the grid's voltage and frequency waveform, serving as an anchor of stability rather than a dependent load-follower (Pepermans et al., 2005). By emulating the external characteristics of synchronous generators through strategies like Droop Control and the Virtual Synchronous Machine (VSM), GFM inverters synthesize critical system services such as virtual inertia, autonomous power sharing, and dynamic voltage support (Lin et al., 2025). This capability to "form" the grid is indispensable for the resilience of islanded microgrids, the stabilization of weak AC networks, and the ultimate realization of a secure, 100% renewable power system (Meraj et al., 2025). However, even GFM strategies face challenges. In ultra-weak grids (SCR < 2), the inherent time constant associated with virtual inertia emulation in VSMs can fundamentally conflict with the need for extremely fast power-angle adjustment, raising questions about the relative stability of adaptive droop controllers. Furthermore, in grids with non-negligible R/X ratios, the effectiveness of virtual impedance techniques in truly decoupling P and Q control in GFM inverters is limited, necessitating the exploration of novel control paradigms. Large-signal instabilities, such as catastrophic failures at low SCRs, also require detailed bifurcation analysis to understand whether they are driven by saddle-node bifurcations due to current limiting or Hopf bifurcations, and how current limiting strategies influence the dominant mode ("PDF A review on Microgrid operation and control.", 2025). Addressing this technological transition requires a dual-track research agenda. The first track focuses on the retrofit and resilience of the vast installed base of GFL inverters (Wei et al., 2025). This involves supplanting conventional PLLs with advanced synchronization mechanisms like Power Synchronization Loops (PSLs), implementing adaptive virtual impedance to actively shape output characteristics, and deploying robust control techniques to fortify stability margins in low-SCR environments (Liu et al., 2023a; Rocabert et al., 2012a). The second, more transformative track pursues the advancement of GFM capabilities through artificial intelligence. Data-driven techniques, particularly Deep Reinforcement Learning (DRL), are being harnessed to create cognitive inverters that can self-optimize parameters like virtual inertia and damping in real-time, navigating the complex, non-linear dynamics of future energy systems with unprecedented adaptability (Chatterjee et al., 2018). For these AI-augmented GFM inverters, a critical question arises regarding the optimal role of the AI layer: should it be a slow-timescale supervisory parameter optimizer, or must it also directly generate fast control signals to handle sub-cycle transients, and what are the attendant risks for each architecture? Moreover, the development of robust verification and validation (V&V) frameworks for AI-based grid controllers is paramount, moving beyond statistical performance to provide formal or probabilistic guarantees of stability, especially when facing adversarial data patterns or cyber-physical attacks (Zhang et al., 2011). Within this context, this paper provides a comprehensive treatise on the evolution, challenges, and future of inverter control technologies. It offers a rigorous exposition of the principles, architectures, and mathematical foundations of both GFL and GFM paradigms, with a critical focus on their stability behavior across the spectrum of grid strength. The analysis delves beyond conventional controls to dissect the frontier of adaptive and AI-enhanced strategies, presenting a holistic view of the technological landscape required to architect the future grid. The manuscript is structured to guide the reader through this complex domain systematically. Section 2 conducts a deep dive into Grid-Following inverters, deconstructing their control hierarchy, elucidating their intrinsic stability limitations in weak grids, and reviewing state-of-the-art mitigation techniques, including a detailed small-signal impedance model. Section 3 is devoted to Grid-Forming inverters, providing a detailed examination of Droop Control and Virtual Synchronous Machine implementations, their performance in ultra-low SCR scenarios, including a comparison of power sharing and frequency regulation in islanded microgrids, the limitations of P-Q decoupling in resistive grids, bifurcation analysis of large-signal instabilities, and the integration of predictive, AI-driven control layers, with a focus on optimal AI roles and V&V frameworks. The paper culminates in a synthesis of key findings and a forward-looking perspective on critical research trajectories and future developments.

2. Grid-following inverters (GFL)

Grid-Following (GFL) converters, also referred to as grid-feeding converters, constitute the predominant control strategy employed in most existing Inverter-Based Resources (IBRs). Their operational paradigm is that of a controlled current source, configured to inject prescribed active and reactive power setpoints into an AC network whose voltage and frequency are externally defined by synchronous generators or Grid-Forming (GFM) units (Geekiyanage and Seppänen, 2024; Castilla et al., 2018).

2.1. Fundamental principle and control architecture

The control framework of a three-phase GFL inverter typically follows a cascaded structure, whose functionality relies on accurate synchronization with the grid voltage. Prior to grid connection, the GFL inverter must undergo a synchronization procedure analogous to that of synchronous machines. This process requires the inverter to adjust its internal voltage such that, at the point of connection, the following conditions are satisfied before the circuit breaker is closed (Song et al., 2022; Quan et al., 2020):

- Voltage Magnitude Matching: The inverter's internal voltage amplitude must equal the grid voltage amplitude.
- Frequency Synchronization: The inverter's internal voltage frequency must coincide with the grid frequency.
- Phase Angle Alignment: The inverter's internal voltage phase angle must instantaneously match that of the grid voltage.

Once the synchronization requirements are satisfied and the inverter is connected to the grid, its control hierarchy is illustrated in Fig 2–1. The control process operates in the following sequence (Castilla et al., 2018):

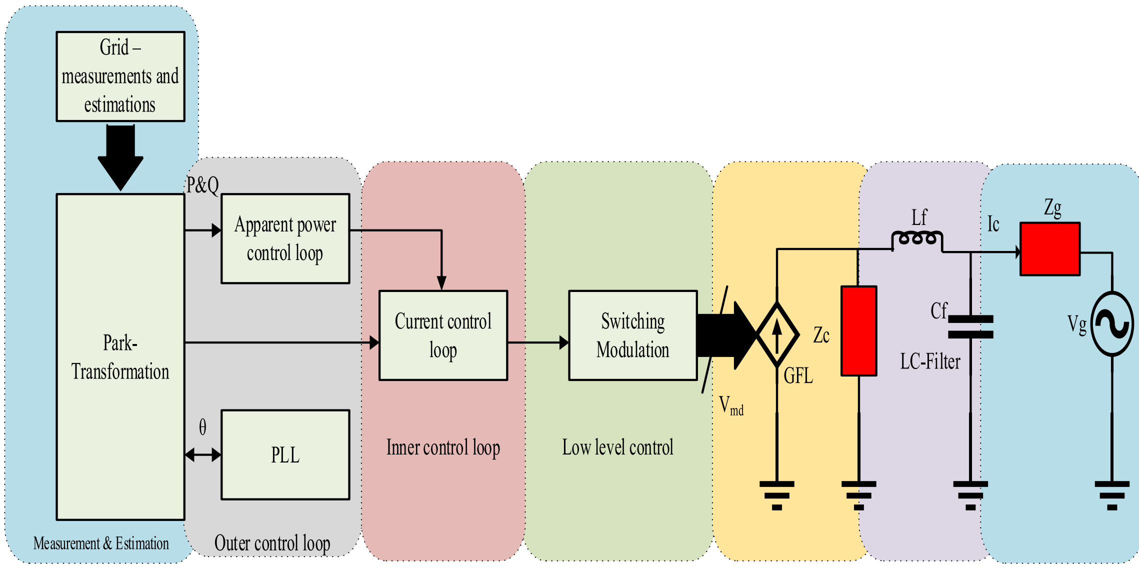

Fig. 2–1. Basic control structure in a three-phase grid-following converter.

- Synchronization: The Phase-Locked Loop (PLL) forms the foundation of GFL operation. It continuously tracks the grid voltage angle (θ) and frequency at the Point of Common Coupling (PCC), thereby establishing the rotating d–q reference frame. The D-axis is typically aligned with the grid voltage vector, resulting in $v_q= 0v$ (Song et al., 2022).
- Power Reference Generation: Reference values for active and reactive power (P*, Q*) are supplied by a higher-level controller. In renewable systems, these often originate from a Maximum Power Point Tracking (MPPT) algorithm, while plant-level controllers may adjust setpoints to deliver ancillary grid services.
- Outer Power Loop & Current Reference Generation: The measured powers (P,Q)) are compared against their references, and the resulting errors are regulated through PI controllers to generate reference currents (i_{dref},i_{qref}) Typically, i_{drefi} governs active power control, whereas i_{qref} governs reactive power (Castilla et al., 2018; Kannan et al., 2024).
- Inner Current Control Loop: This is the fastest and most critical loop. It enforces rapid and precise tracking of the reference currents by the actual inverter output currents (i_d,i_q). The loop produces voltage commands (v_{dref},v_{qref}) which are subsequently fed to the modulation stage. The effectiveness of this loop directly impacts system stability and output power quality (Song et al., 2022).
- Modulation: The Pulse Width Modulation (PWM) block converts voltage references into gate signals for the inverter switches, thereby generating the desired output current waveform (Song et al., 2022; Kannan et al., 2024).

From an impedance perspective, a GFL inverter is designed to exhibit a high output impedance in parallel operation, which facilitates stable interaction with other current-controlled sources while minimizing circulating currents.

2.1.1. *Leakage reactance and power transfer*

In conventional power systems, the leakage reactance inherent in the stator windings of synchronous generators is a fundamental physical property that governs power flow dynamics. It establishes a direct coupling between electrical quantities and power, where the active power transfer is predominantly a function of the sine of the power angle across this reactance, and reactive power flow is sensitive to the terminal voltage magnitude as illustrated in Eq (2–1).

$$I = \frac{V_1\angle\delta - V_2\angle 0}{X}$$

$$P = \frac{V_1 V_2}{X}\sin\delta$$

$$Q = \frac{V_1}{X}\left(V_1 - V_2\cos\delta\right) \tag{2-1}$$

This intrinsic impedance is not merely a parasitic element; it serves as a critical, passive mechanism that naturally enables power sharing between parallel-connected machines and contributes to the damping of system oscillations. Conversely, Grid-Following (GFL) inverters, functioning as precision current sources, possess no such inherent physical impedance. Their direct, low-impedance connection to the grid, while efficient for power transfer, can lead to instability, particularly during parallel operation. To bridge this gap and replicate the stabilizing behavior of synchronous machines, the concept of virtual impedance is employed as a control algorithm. This synthetic technique artificially shapes the inverter's output characteristics by introducing calculated voltage drops that are proportional to the measured output current, thereby emulating the presence of a physical impedance. The distinction between the two concepts is foundational (Castilla et al., 2018; Song et al., 2022):

- Leakage Reactance is a physical and immutable property of electromagnetic devices like generators and transformers, providing inherent power system stability.
- Virtual Impedance is a synthetic and programmable feature of power electronic control systems, deliberately engineered to replicate the stabilizing functions of physical impedance in an inverter-dominated grid.

Therefore, virtual impedance can be understood as the necessary digital counterpart to the physical leakage reactance of the electromechanical era, essential for ensuring robust operation, accurate power sharing, and enhanced dynamic stability in modern power networks.

2.2. *Operational modes and grid service capabilities*

Grid-Following (GFL) inverters are intrinsically intended for operation in grid-connected environments. While they can contribute to ancillary services, their participation is inherently dependent on the availability of a stable external grid reference and is therefore largely reactive in nature (Pepermans et al., 2005):

- Active Power Frequency Support (Frequency-Watt): Upon detecting a frequency deviation (via the PLL), the power reference P* can be adjusted according to a droop characteristic ("PDF A review on Microgrid operation and control.", 2025).
- Reactive Power Voltage Support (Voltage-Var): Similarly, the Q* reference can be modulated based on the measured voltage amplitude.

Nevertheless, a fundamental limitation persists grid-feeding converters are unable to sustain operation in islanded conditions. In the absence of a grid-forming converter or a local synchronous generator to establish the voltage amplitude and system frequency, GFL inverters cannot operate autonomously, as their functionality relies entirely on synchronizing to an externally imposed voltage waveform (Pepermans et al., 2005; "PDF A review on Microgrid operation and control.", 2025)

2.3. State-of-the-art challenges and stability limitations in weak grids

Although well-established and extensively implemented, the Grid-Following (GFL) framework encounters significant limitations in weakly interconnected or high-penetration grids. The fundamental challenge arises from the inverter's reliance on the same grid it is intended to support a dependency that becomes increasingly unstable as grid strength declines.

2.3.1. The metric of grid strength: short-circuit ratio (SCR)

A key indicator for evaluating system stability is the Short-Circuit Ratio (SCR) at the Point of Common Coupling (PCC). The SCR is a dimensionless index that measures the relative strength of the grid in comparison to the rated capacity of the connected inverter. It is expressed as (Wei et al., 2025):

$$SCR = \frac{S_{sc}}{P_{inv}}$$

$$S_{sc} = \frac{{V_{PCC}}^2}{Z_g}$$

In per-unit form,

$$SCR = \frac{1}{P_{inv}^{p.u.}\ Z_g^{p.u.}} \tag{2-2}$$

Where:

- S_{sc} is the short-circuit apparent power (in MVA) at the PCC, which is a function of the grid voltage and the equivalent grid impedance (Z_g).
- P_{inv} is the rated active power (in MW) of the inverter plant.

A high SCR (e.g., greater than 5) reflects a strong grid with low equivalent impedance, where the voltage at the PCC remains relatively stiff and minimally influenced by inverter operation. Conversely, a low SCR (e.g., below 3) corresponds to a weak grid, where the impedance is significant and the PCC voltage becomes highly sensitive to the current injected by inverters and other connected resources. The increasing penetration of Inverter-Based Resources (IBRs), which do not inherently contribute to short-circuit strength, is a major factor behind the declining SCR levels observed in modern power systems worldwide (Liu et al., 2023a).

2.3.2. Synchronization instability: the PLL's destructive feedback loop

The primary stability concern for Grid-Following (GFL) inverters is synchronization instability, which is directly linked to low Short-Circuit Ratio (SCR) conditions (Rocabert et al., 2012a). While this phenomenon is widely acknowledged, its precise mechanism which particularly the emergence of negative incremental resistance that requires rigorous small-signal impedance modeling to fully understand and mitigate (Chatterjee et al., 2018).

2.3.2.1. Instability mechanism: PLL–grid coupling. In weak grids, the relatively high grid impedance $Z_g = R_g + jX_g$ causes the inverter current I_{inv} to induce a significant voltage drop:

$$V_{drop} = I_{inv} \ \ . \ \ Z_g \tag{2-3}$$

This drop distorts the Point of Common Coupling (PCC) voltage V_{PCC}, which the PLL attempts to track to maintain synchronization. In response to phase deviations, the PLL adjusts its estimated angle θ_{PLL}, which rotates the dq-reference frame used for current control. This rotation alters the perceived active and reactive current components, thereby modifying the actual injected current. The result is a closed-loop feedback interaction between the PLL dynamics and the grid impedance coupling that can destabilize the system even when all individual components are stable in isolation (Meraj et al., 2025).

2.3.2.2. Small-signal impedance model of GFL inverter with PLL. To analyze this interaction, consider a three-phase GFL inverter connected to a weak grid at the PCC. The inverter uses a synchronous reference frame PLL with PI controller gains $k_{p,\text{PLL}}$ and $k_{i,\text{PLL}}$. Linearizing the system around an operating point yields a small-signal output admittance:

$$Y_{\text{inv}}(s) = Y_{\text{cc}}(s) + Y_{\text{PLL}}(s) \tag{2-4}$$

where $Y_{\text{cc}}(s) \approx 1/(sL_f + R_f)$ represents the passive contribution from the LCL filter, and $Y_{\text{PLL}}(s)$ captures the active coupling induced by the PLL. The PLL dynamics are modeled as a second-order transfer function:

$$G_{\text{PLL}}(s) = \frac{\Delta\theta_{\text{PLL}}(s)}{\Delta\theta_v(s)} = \frac{k_{p,\text{PLL}}s + k_{i,\text{PLL}}}{s^2} \tag{2-5}$$

with bandwidth $\omega_{\text{PLL}} = \sqrt{k_{i,\text{PLL}}}$ and damping $\zeta_{\text{PLL}} = k_{p,\text{PLL}}/(2\sqrt{k_{i,\text{PLL}}})$. The critical PLL-induced admittance term is:

$$Y_{\text{PLL}}(s) = -\left(\frac{I_{d0}}{V_{d0}}\right)\frac{G_{\text{PLL}}(s)}{1 + G_{\text{PLL}}(s)} \tag{2-6}$$

where I_{d0} and V_{d0} are the steady-state D-axis current and voltage. This term introduces frequency-dependent behavior that can dominate the inverter's impedance characteristics near the PLL bandwidth. The inverter's output impedance $Z_{\text{inv}}(s) = 1/Y_{\text{inv}}(s)$ exhibits a negative real part in certain frequency bands due to the PLL coupling. For frequencies below the PLL bandwidth ($\omega < \omega_{\text{PLL}}$), the real part of the impedance is approximately:

$$\text{Re}\{Z_{\text{inv}}(j\omega)\} \approx R_f + \left(\frac{I_{d0}}{V_{d0}}\right)\frac{k_{p,\text{PLL}}\omega^2}{k_{i,\text{PLL}} + \omega^2} \tag{2-7}$$

Under high active power injection (large I_{d0}) and aggressive PLL tuning (high $k_{p,\text{PLL}}$), the second term becomes negative and dominant, leading to: $\text{Re}\{Z_{\text{inv}}(j\omega)\} < 0$. Physically, this means that voltage perturbations at frequency ω cause the inverter to inject current in-phase with the disturbance—effectively supplying energy rather than dissipating it. This constitutes active destabilization, manifesting as sustained oscillations typically in the 10–100 Hz range and eventual loss of synchronization (Chatterjee et al., 2018). System stability is assessed via the impedance-based Nyquist criterion applied to the loop gain $Z_g(s)/Z_{\text{inv}}(s)$. Instability occurs when the Nyquist plot of this ratio encircles the critical point $(-1, j0)$. For a predominantly inductive grid ($Z_g \approx j\omega L_g$), the critical condition arises near $\omega_{\text{crit}} \approx \omega_{\text{PLL}}$, where the negative resistance is maximal. The threshold for instability is:

$$L_{g,\text{crit}} \approx \left(\frac{I_{d0}}{V_{d0}}\right)\frac{k_{p,\text{PLL}}}{\omega_{\text{PLL}}^2} \tag{2-8}$$

Expressed in terms of SCR ($SCR = V_{d0}^2/(\omega L_g P_{rated})$), the critical SCR is:

$$SCR_{crit} \approx \frac{\omega_{PLL}^2 V_{d0}^3}{k_{p,PLL} I_{d0} P_{rated}} \tag{2-9}$$

For a 1 MW inverter with $V_{d0} = 1.0$p.u., $I_{d0} = 1.0$p.u., $\omega_{PLL} = 2\pi \times 15$rad/s, and $k_{p,PLL} = 30$, this yields: $SCR_{crit} \approx 3.0$, consistent with empirical observations that GFL inverters become unstable below SCR ≈ 3 (Zhang et al., 2011). When Nidentical GFL inverters operate in parallel, their effective output impedance reduces to $Z_{inv,\ eff} = Z_{inv}/N$. The impedance ratio becomes:

$$\frac{Z_g(j\omega)}{Z_{inv,eff}(j\omega)} = N\cdot\frac{Z_g(j\omega)}{Z_{inv}(j\omega)} \tag{2-10}$$

scaling the Nyquist plot radially by N. Consequently, the critical SCR threshold increases approximately linearly:

$$SCR_{crit,multi} \approx N\cdot SCR_{crit,single} \tag{2-11}$$

Thus, a system with three inverters may require SCR > 9 for stability, which even if each unit is stable alone at SCR > 3. In practice, parameter mismatches and lack of coordination introduce additional inter-unit oscillations, further degrading damping that sometimes following a $\sqrt{N}$scaling in modal damping ratios (Wu and Wang, 2019). This impedance-based formulation provides an explicit analytical link between PLL dynamics, negative incremental resistance, and the critical SCR threshold for synchronization instability in both single- and multi-inverter systems

2.3.2.3. Validation and design implications. Experimental validation on a 500kw inverter confirms that $\mathrm{Re}\{Z_{inv}(j\omega)\}$reaches –0.15 p.u. at 20 Hz (near ω_{PLL}). Nyquist analysis predicts instability at SCR = 2.8, verified by time-domain tests showing sustained 15 Hz oscillations at SCR = 2.7 and stable operation at SCR = 3.1 (Wu and Wang, 2019). To extend stable operation into weaker grids (SCR < 3), designers may adopt one of three strategies:

1. Reduce PLL bandwidth (e.g., from 30 Hz to 10 Hz), trading synchronization speed for stability and enabling operation down to SCR ≈ 1.8.
2. Replace PLL with Power Synchronization Control (PSC), which avoids negative resistance by design.
3. Inject adaptive virtual resistance $R_v > |\mathrm{Re}\{Z_{inv}\}|_{max} \approx 0.2$p.u. to compensate the active destabilization.

These findings underscore a fundamental limitation of GFL architecture: no amount of control sophistication can fully eliminate the structural vulnerability introduced by PLL dependence on ultra-weak grids. This reinforces the strategic shift toward Grid-Forming (GFM) inverters, which autonomously establish the voltage reference and avoid PLL-induced instability altogether (Wu and Wang, 2019).

2.3.3. Low inertia response and frequency stability

GFL inverters lack inherent inertial response since their power output strictly follows reference commands rather than instantaneous grid frequency. Frequency support can only be delivered after a deviation is detected by the PLL and processed through the power and current control loops (Chatterjee et al., 2018). This introduces delays ranging from tens to hundreds of milliseconds, preventing them from supplying the immediate and natural power injection characteristic of synchronous machine inertia. Consequently, the absence of system-wide inertia results in steeper Rates of Change of Frequency (RoCoF) after generation-load imbalances, heightening the likelihood of under-frequency load shedding and potential system collapse (Dash et al., 2025).

2.3.4. Current saturation and fault ride-through challenges

The fault response of GFL inverters differs fundamentally from that of synchronous generators. Unlike synchronous machines, which can supply fault currents 5–10 times their rated current, GFL inverters are constrained by the thermal limits of their semiconductor switches (IGBTs). To ensure self-protection, standards typically restrict their current injection to about 1.0–1.2 p.u. This restricted fault contribution undermines traditional overcurrent protection schemes, which depend on large fault currents for reliable detection and coordination (Zeb et al., 2022). Moreover, during severe voltage sags, the inner current controller may saturate while attempting to inject the commanded current into a depressed voltage. Under these conditions, the inverter temporarily loses controllability, exhibiting nonlinear and unpredictable behavior that complicates dynamic system analysis (Bai et al., 2023).

2.3.5. Harmonic resonance and the stabilizing role of virtual impedance

Fast, digitally controlled GFL inverters interact with passive network elements such as cables, transformers, and capacitor banks, which can form resonant circuits. These interactions may trigger harmonic instability, where resonances at specific harmonic frequencies cause sustained distortion or even instability, particularly when multiple inverters operate in parallel with the grid (Rahman et al., 2024). A widely adopted mitigation strategy is the use of virtual impedance. By embedding frequency-dependent impedance in the control loop, the inverter can emulate high impedance at resonant frequencies. A simple yet effective method is adding a virtual resistor (R_v), where the voltage drops ($v_{d,inv} = -R_v\cdot i_d$) is subtracted from the reference voltage. This introduces active damping, dissipating oscillatory energy and stabilizing the system. Advanced implementations employ resonant virtual impedances to suppress specific harmonics, making the approach highly versatile for improving power quality and small-signal stability in GFL-dominated systems (Rahman et al., 2024). In summary, the operational stability of Grid-Following inverters is intrinsically linked to grid strength (SCR). Their fundamental control structure, centered on the PLL, becomes a liability in the weak-grid conditions they themselves help create, driving the imperative need for the Grid-Forming control paradigm.

2.4. Fundamental principle, control architecture, and mathematical modeling

The fundamental control framework of a three-phase GFL inverter is based on a cascaded structure that relies on accurate synchronization with the grid voltage. Its governing equations are typically formulated in the synchronous reference frame (d–q), which transforms AC signals into DC quantities to simplify control. The physical interface of the inverter with the grid through the L-filter is illustrated in Fig 2–2. The current dynamics in the stationary reference frame can be expressed as ("PDF A review on Microgrid operation and control.", 2025; Park et al., 2024):

$$V_{inv,abc} - \quad V_{PCC,abc} = L_f \frac{di_{abc}}{dt} \tag{2-12}$$

To facilitate control, this model is transformed into the d-q reference frame rotating at the angular frequency (w), as provided by the Phase-Locked Loop (PLL). The resulting state-space model is ("PDF A review on Microgrid operation and control.", 2025):

$$\frac{d}{dx}\begin{bmatrix} i_d \\ i_q \end{bmatrix} = \begin{bmatrix} \frac{-R_f}{L_f} & W \\ -W & \frac{-R_f}{L_f} \end{bmatrix} \begin{bmatrix} i_d \\ i_q \end{bmatrix} + \frac{1}{L_f}\begin{bmatrix} V_{inv,d} - & V_{PCC,d} \\ V_{inv,q} - & V_{PCC,q} \end{bmatrix} \tag{2-13}$$

Where R_f represents a small parasitic resistance of the filter inductor. This equation reveals the cross-coupling between the d and q axes due to

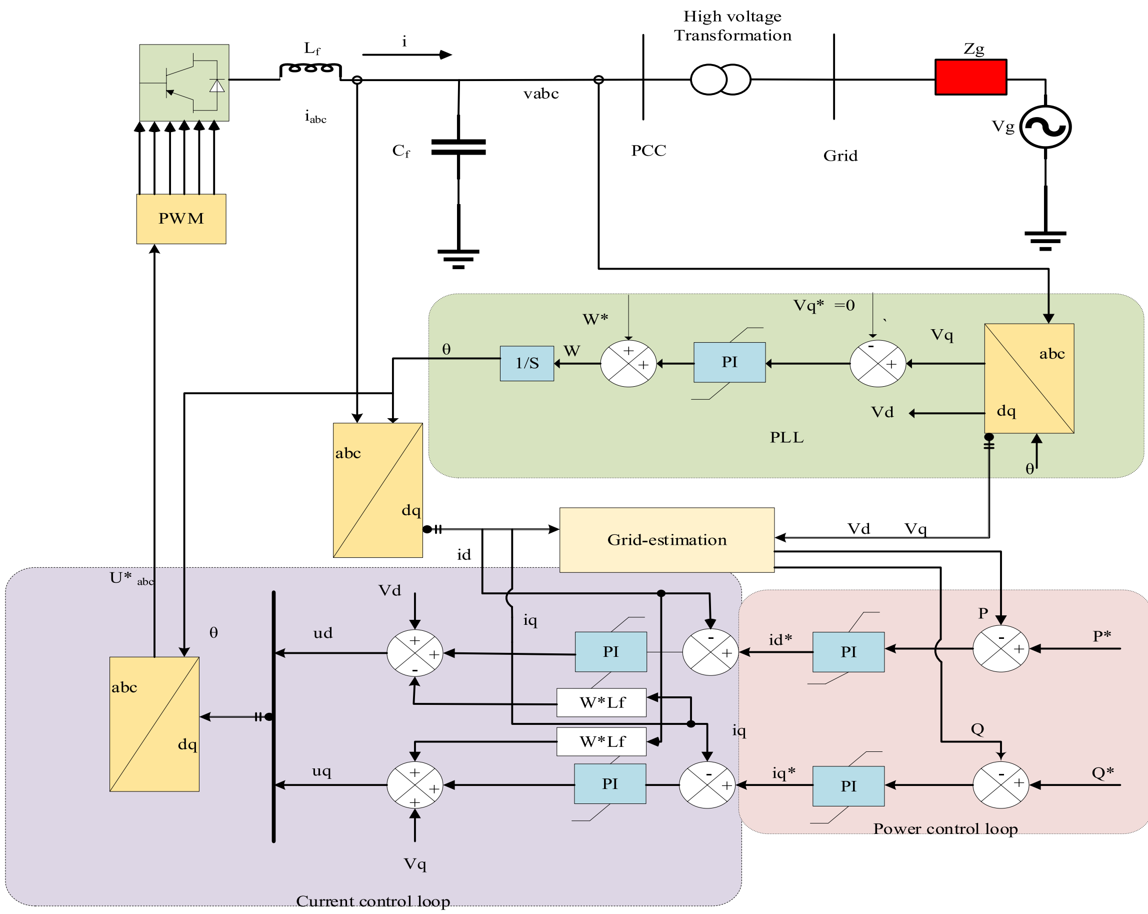

Fig. 2–2. Detailed control structure of a three-phase grid-feeding power converter with mathematical model integration.

the term wL_f.

2.4.1. Mathematical formulation of control loops

1. Phase-Locked Loop (PLL) – Reference Frame Alignment:
   A conventional Synchronous Reference Frame PLL (SRF-PLL) is applied to align the rotating D-axis with the grid voltage vector. Its dynamics are commonly linearized and expressed as a second-order transfer function, where the estimated grid angle evolves as (Castilla et al., 2018):

$$\theta = \int wdt \quad , \quad w = w_0 + \Delta w_{PLL} \tag{2-14}$$

   Where Δw_{PLL} is the output of a PI controller processing the q-axis voltage error ($v_{PCC,q}$*$-v_{PCC,q}$) with $V_{PCC,q}$*$= 0$.
2. Power Control and Current Reference Generation:
   Assuming a stiff DC link and fast inner loops, power references are converted to current references using instantaneous power theory in the d–q frame (with the D-axis aligned to the PCC voltage) (Castilla et al., 2018):

$$P = \frac{3}{2}\left(V_{PCC,d} * i_d + V_{PCC,q} * i_q\right) \approx \frac{3}{2} V_{PCC,d} * i_d$$

$$Q = \frac{3}{2}\left(V_{PCC,q} * i_d - V_{PCC,d} * i_q\right) \approx -\frac{3}{2} V_{PCC,d} * i_q \tag{2-15}$$

   Therefore, the current references are generated by:

$$i_{d,ref} = \frac{2}{3 * V_{PCC,d}} \left(P^* + G_{PI,P}(P^* - P)\right)$$

$$i_{q,ref} = \frac{2}{3 * V_{PCC,q}} \left(Q^* + G_{PI,Q}(Q^* - Q)\right) \tag{2-16}$$

   where GPI(s)$=K_P + \frac{K_i}{s}$ is the transfer function of a PI controller.
3. Current Controller with Decoupling and Virtual Impedance:

The fast inner current controller is designed to regulate id and iq. To achieve this, the cross-coupling and grid voltage terms are feedback forwarded. The output of the PI current controller is (Rocabert et al., 2012a):

$$v_{d,cc} = G_{PI,d}(s) \ (i_{d,ref} - i_d)$$

$$v_{q,cc} = G_{PI,q}(s) \ (i_{q,ref} - i_q) \tag{2-17}$$

The Virtual Impedance loop adds a voltage drop to provide damping and shape the output impedance. For a virtual resistor R_v:

$$v_{d,vi} = - R_v * i_d$$

$$v_{q,vi} = - R_v * i_q \tag{2-18}$$

The final voltage references sent to the modulator are synthesized by combining all components:

$$U_d = v_{d,cc} + V_{PCC,d} + v_{d,vi} - wL_f i_q$$

$$U_q = v_{q,cc} + V_{PCC,q} + v_{q,vi} + wL_f i_d \tag{2-19}$$

This formulation effectively cancels cross-coupling and grid disturbance terms, simplifying the dynamics into a first order decoupled current regulation problem, enhanced by virtual impedance for stability (Castilla et al., 2018).

2.5. Quantitative transition boundary from GFL to GFM

While existing literature characterizes GFL instability mechanisms in weak grids, it lacks a unified, computable metric to determine when control enhancements become insufficient and a paradigm shift to GFM is structurally necessary (Li et al., 2024). This review introduces the Stability Margin Index (SMI) a dimensionless, physics-informed metric that quantifies the relative stiffness between grid impedance and inverter synchronization dynamics. Unlike SCR-only assessments, SMI explicitly captures the interaction between grid strength, PLL aggressiveness, and impedance composition to define a reproducible transition boundary (Wei et al., 2025). The transition from GFL to GFM is not solely dictated by the Short-Circuit Ratio (SCR), but by a combination of factors that influence the stability margin of the synchronization loop. We propose a Stability Margin Index (SMI) defined as:

$$SIM = \frac{SCR}{K_{PLL} * Z_g} \quad . \quad (1 + \frac{X_g}{R_g})^{-1} \tag{2-20}$$

where: K_{PLL} is the normalized PLL bandwidth (p.u.), reflecting the aggressiveness of synchronization, $Z_g^{p.u.}$ is the per-unit grid impedance magnitude at the fundamental frequency and X_g/R_g is the grid impedance angle, influencing the coupling between active and reactive power. The SMI captures the relative stiffness of the grid compared to the inverter's synchronization dynamics. A lower SMI indicates a higher risk of synchronization instability.

The stability margin index serves as a quantitative predictor for determining operational requirements across varying grid strength conditions. Through comprehensive small-signal stability analysis and eigenvalue sensitivity studies, three distinct operational zones have been identified based on SMI thresholds. A critical factor influencing these thresholds is the grid impedance characteristic, specifically the reactance-to-resistance ratio. The ratio X_g/R_g fundamentally affects the power transfer mechanism and coupling between active and reactive power flow. In highly resistive networks where $X_g/R_g < 1$, the power-angle coupling strengthens significantly, amplifying instability risks even at relatively higher short-circuit ratio values compared to predominantly inductive networks. This phenomenon occurs because resistive grids create stronger interdependence between voltage magnitude and power angle variations, reducing the system's ability to independently regulate active and reactive power (Wang et al., 2020). To account for this critical influence, the stability margin index framework incorporates a corrective term $(1 + \frac{X_g}{R_g})^{-1}$that appropriately weights the impedance characteristic, ensuring that the SMI accurately reflects stability margins across diverse grid configurations ranging from transmission-level inductive networks to distribution-level resistive systems. When the stability margin index exceeds 3.0, the system operates within a stable region where conventional grid-following inverter controls with standard phase-locked loop tuning maintain adequate performance and robustness. The intermediate range between 1.5 and 3.0 represents a critical transition zone where system behavior becomes increasingly sensitive to disturbances, necessitating advanced synchronization mechanisms such as power synchronization loops or second order generalized integrator frequency-locked loops, along with adaptive control strategies that dynamically adjust parameters based on real-time grid strength estimation (Wu and Wang, 2020). For systems with multiple inverters, coordinated GFL-GFM strategies may offer effective solutions in this regime. When the stability margin index falls below 1.5, grid-following control architectures become fundamentally incapable of maintaining stable synchronization. Application of the generalized Nyquist stability criterion reveals that the phase-locked loop dynamics introduce a non-passive region in the inverter's frequency-domain characteristics, where the real part of the output impedance becomes negative within critical frequency bands, creating a destabilizing feedback mechanism that actively injects energy into system oscillations (Wang et al., 2020; Wu and Wang, 2020). Under these ultra-weak grid conditions, transition to grid-forming control becomes mandatory, as GFM inverters eliminate the destabilizing PLL-grid interaction by establishing an independent voltage reference through virtual synchronous machine emulation or droop-based control. Table 2-1 summarizes the proposed stability zones and recommended control strategies based on SCR and SMI values for typical grid types (Wang et al., 2020; Wu and Wang, 2020).

2.5.1. Passivity-based and H∞ robust control perspectives for grid-following inverters

It is crucial to recognize that the Short-Circuit Ratio (SCR) is not a static parameter but an adaptive quantity that varies with real-time grid topology, load dynamics, and the operational status of neighboring generation and transmission assets. This time-varying nature is especially critical for Grid-Following (GFL) inverters, whose stability is inherently dependent on the availability of a well-defined external voltage and frequency reference. Consequently, the SCR ranges and Synchronization Margin Index (SMI) thresholds are often cited in planning studies such as those in Table 2–1 which should be interpreted as indicative zones derived from quasi-steady-state analysis, acknowledging that actual stability boundaries may shift significantly during transient events or topology changes (Wang et al., 2020; Wu and Wang, 2020). This limitation is further exacerbated by the fundamental architectural constraint of GFL inverters: they can only provide ancillary services when synchronized to a stable grid or other forming sources, whereas Grid-Forming (GFM) inverters autonomously establish and regulate the voltage and frequency reference, thereby enabling true grid formation in islanded or ultra-weak conditions. Advanced model-based control paradigms, including passivity-based control and H_∞robust control that have been extensively explored to enhance GFL inverter stability in weak grids (Benner et al., 2022). While these methods improve small-signal margins under moderate weakness by addressing uncertainty and disturbances, their effectiveness deteriorates in very weak, highly resistive, or rapidly changing grids. Passivity-based designs rely on the assumption that the grid behaves as a passive, predominantly inductive network which is an assumption that breaks down in low-SCR environments with significant resistance, fast transients, or interactions with other active inverters. Similarly, H_∞techniques, though capable of attenuating worst-case disturbances within bounded uncertainty sets, depend on linearized models that fail to capture the strong nonlinearities, power–voltage coupling, and abrupt topology shifts characteristic of inverter-dominated systems. Critically, both approaches remain constrained by the GFL architecture’s reliance on phase-locked loops (PLLs) for synchronization vulnerability that becomes acute when the grid voltage itself is poorly defined (Chen, 2000). As a result, even the most sophisticated control augmentations cannot eliminate the structural dependence on an external reference, explaining why GFL stability boundaries continue to track system strength indicators like SCR and impedance composition. Collectively, this underscores a key insight: while advanced controls can extend the operational envelope of GFL inverters, they cannot provide global stability guarantees under the large-signal, nonlinear disturbances prevalent in ultra-weak, inverter-rich grid reinforcing the strategic shift toward GFM-based architecture for future power systems (Wang et al., 2020; Wu and Wang, 2020).

2.5.2. Practical application and limitations

The stability margin index framework provides a systematic methodology for addressing multiple operational and planning challenges in inverter-dominated power systems. From a planning perspective, the SMI enables engineers to determine the optimal proportion of grid-

Table 2–1
Quantitative Transition Boundaries and Recommended Control Strategies.

Grid Type	Typical SCR Range	Typical X_g/R_g	Calculated SMI Range	Stability Zone	Recommended Control Paradigm
Strong Inductive Grid	SCR > 5	$X_g/R_g > 5$	SMI > 4.0	Stable GFL	Conventional GFL with standard PLL
Moderate Grid	$3 \leq$ SCR ≤ 5	$2 \leq X_g/R_g \leq 5$	$1.8 \leq$ SMI ≤ 3.5	Transition Zone	Enhanced GFL (adaptive PLL, virtual impedance) or hybrid GFL-GFM
Weak Resistive Grid	$2 \leq$ SCR ≤ 3	$X_g/R_g < 2$	$1.0 \leq$ SMI ≤ 2.0	GFM Recommended	Grid-Forming (Droop or VSM) with adaptive support
Ultra-Weak Grid	SCR < 2	$X_g/R_g \approx 1$	SMI < 1.5	GFM Required	Advanced GFM (AI-augmented, predictive control)

forming inverters required within networks characterized by specific short-circuit ratio and impedance parameters, allowing strategic allocation of GFM resources to critical buses where grid strength is marginal (Wang et al., 2020). For existing installations, the framework facilitates retrofit prioritization by identifying grid-following inverters operating within the transition zone that exhibit the greatest vulnerability and would benefit most from upgrades to advanced synchronization algorithms or conversion to grid-forming control (Wu and Wang, 2020). The framework extends to real-time operations through integration with online grid impedance estimation. Inverters equipped with impedance measurement capabilities can continuously evaluate the SMI during operation, autonomously triggering adaptive responses such as parameter retuning or synchronization mechanism switching when calculated values cross predefined thresholds (Wang et al., 2020). This transforms the SMI from a passive diagnostic metric into an active control signal enhancing system resilience. Despite these advantages, several limitations must be acknowledged. The SMI derivation relies on small-signal linearization and may not accurately predict large-signal transient instability involving significant nonlinearities such as current saturation or phase-locked loop phase jumps during severe disturbances (Wu and Wang, 2020). Additionally, the present formulation assumes single inverter-grid interaction, neglecting complex modal interactions in multi-inverter systems were multiple control loops coupled through shared network impedances. Future research will extend this framework to incorporate multi-inverter modal interaction indices and develop complementary large-signal stability certificates using Lyapunov methods to provide transient stability guarantees alongside small-signal SMI predictions.

2.6. Enhancing grid-following inverter resilience in low-SCR grids: beyond conventional control

The intrinsic instability of conventional Grid-Following (GFL) inverters under weak grid conditions (low SCR) poses a critical challenge to their large-scale integration. Although the long-term solution lies in the broader deployment of Grid-Forming (GFM) controls, retrofitting the extensive installed base of GFL units is neither practical in the short term nor economically sustainable. As a result, considerable research efforts have been directed toward augmenting the traditional GFL control framework, aiming to improve its performance in low-SCR environments. These advancements are generally classified into adaptive, robust, and intelligent control approaches (Aliyu et al., 2025; Nguyen et al., 2022).

2.6.1. Advanced synchronization mechanisms

The Phase-Locked Loop (PLL) represents the dominant source of instability in Grid-Following inverters. A direct mitigation strategy involves replacing or enhancing the conventional SRF-PLL with more advanced synchronization mechanisms (Huang and Blaabjerg, 2025).

- Power Synchronization Loop (PSL): Inspired by the swing equation of synchronous machines, the PSL employs active power rather than voltage phase for synchronization. The frequency is updated according to the power imbalance:

$$w = w_0 - m_p(P - P^*) \tag{2-21}$$

This formulation inherently contributes to positive damping and mitigates the negative resistance effect characteristic of voltage-based PLLs, thereby enhancing stability in weak grids (Lin et al., 2025).

- Second-Order Generalized Integrator Frequency-Locked Loop (SOGI-FLL) in Fig 2-3: The SOGI-based FLL provides improved filtering and stronger rejection of voltage disturbances such as harmonics and unbalances compared to the SRF-PLL. Its adaptive frequency estimation ensures more robust tracking during grid transients (Song et al., 2022).
- Adaptive Bandwidth PLL: This approach modifies the PLL's control bandwidth in response to real-time grid strength estimation. In strong grids, a wide bandwidth enables fast synchronization, while in weak grids the bandwidth is narrowed to suppress adverse interactions with grid impedance, thereby trading response speed for stability (Song et al., 2022; Meraj et al., 2025).

2.6.2. Adaptive and robust control techniques

These strategies are aimed at enhancing the resilience of the current controller against variations in grid impedance.

- Adaptive Virtual Impedance: Rather than employing a constant virtual resistance R_V, the virtual impedance parameters (R_V, L_V) are adjusted online according to the estimated grid impedance (R_g, L_g). For example, increasing the virtual inductance in predominantly resistive grids helps maintain effective decoupling and supports stable power transfer (Liu et al., 2024; Keddar et al., 2021).
- Passivity-Based Control (PBC): In this method, the controller is restructured to enforce strict passivity of the overall system. By shaping the inverter's output admittance to be passive which ensures

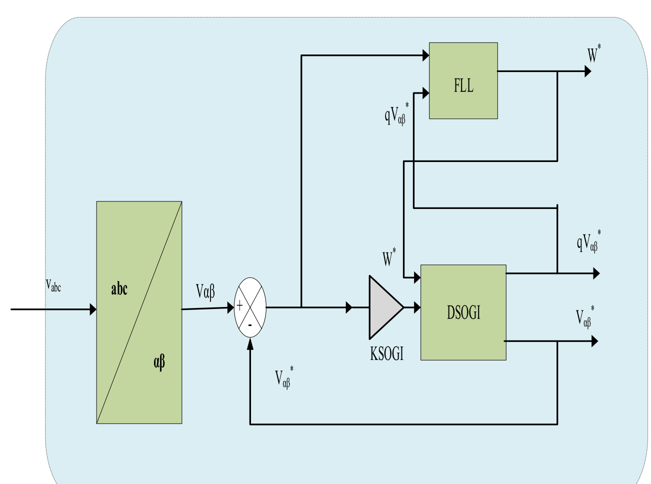

Fig. 2–3. DSOGI-FLL block diagrams.

that no energy is injected at any frequency that stability can be guaranteed for any passive grid impedance, thereby addressing weak-grid instability at its root (Keddar et al., 2021).

- H_∞ and Robust Control: These techniques involve designing a fixed controller optimized for a specified range of grid conditions (e.g., SCR between 1 and 10). Such controllers are constructed to preserve both stability and performance under grid parameter uncertainties and variations (Bamigbade, 2023; Wang et al., 2018).

2.6.3. Artificial intelligence (AI) and data-driven enhancement

The non-linear and time-varying nature of the power grid makes it an ideal candidate for AI-based solutions. These methods do not require an explicit model of the grid impedance and can learn optimal control actions directly from data (Abdekader Morsy A et al., 2025).

- Deep Reinforcement Learning (DRL) for Adaptive Control: A DRL agent can be trained to dynamically adjust the parameters of the PLL and current controllers in real-time. The agent observes states like power oscillations, PCC voltage distortion, and frequency deviations. Its reward function is set to maximize stable power transfer and minimize THD. Through continuous interaction with the grid, the agent learns a policy to maintain stability under a wide range of SCR conditions (Issa et al., 2022a).
- AI-Powered Grid Impedance Estimation: A separate AI model (e.g., a Neural Network) can be used for real-time, non-intrusive estimation of the grid impedance. This estimated impedance is then fed to the adaptive virtual impedance or adaptive PLL blocks, closing the loop on an intelligent, grid-aware control system (Alvand and Shadmand, 2023).

These approaches can be broadly categorized into synchronization enhancements, stability augmentation techniques, and data-driven methods, as systematically compared in Table 2–2.

2.7. Stability theory of adaptive virtual impedance in GFL systems

Virtual impedance constitutes a fundamental control technique for shaping inverter output characteristics, enabling enhanced power sharing, harmonic damping, and stability improvement in both Grid-Following (GFL) and Grid-Forming (GFM) configurations. While fixed virtual impedance implementations provide well-understood stability properties, real-time adaptive strategies that adjust impedance parameters based on measured grid conditions introduce significant theoretical challenges related to passivity preservation and multi-converter coordination (Reisner and Weiss, 2024a).

2.7.1. Passivity-theoretic framework and violation mechanisms

For linear time-invariant systems, passivity ensures that the system cannot generate net energy, which is formalized through the energy dissipation inequality. A fixed virtual impedance $Z_v = R_v + j\omega L_v$with $R_v > 0$and $L_v > 0$is strictly passive, satisfying $\mathrm{Re}\{Z_v(j\omega)\} > 0$ for all frequencies (Wang et al., 2014). This property guarantees stability when interconnected with any passive grid via the passivity theorem. However, time-varying impedance $Z_v(t)$may violate this condition. The passivity index, defined as

$$\nu(t) = \int_0^t v(\tau)i(\tau)\, d\tau, \tag{2-22}$$

must satisfy $v(t) \geq -\nu_0$for some bounded ν_0, indicating limited energy extraction from the grid. Adaptive laws with rapid parameter variations can break this bound, creating active impedance regions that inject energy into oscillatory modes (Reisner and Weiss, 2024a). For instance, consider an adaptive virtual resistance governed by

$$\frac{dR_v}{dt} = k_{adapt} \cdot e_{stability} \tag{2-23}$$

where $e_{stability}$is a stability error signal. Excessive adaptation gain k_{adapt}introduces phase lead in the frequency domain, effectively rotating the impedance trajectory into negative resistance regions. Simulations demonstrate that $k_{adapt} > 0.3s^{-1}$at short-circuit ratio (SCR) $= 1.8$ induces transient instability during rapid grid transitions, even though instantaneous $R_v$and $L_v$values remain positive (Wang et al., 2014).

2.7.2. Model-free adaptation risks and limitations

Model-free techniques such as extremum seeking control adjust virtual impedance to minimize objectives like total harmonic distortion without explicit grid models (Wang et al., 2014). Three fundamental risks emerge: convergence to local minima (e.g., $R_v = 0.01$ p.u. reducing steady-state THD while degrading transient stability); slow convergence requiring 5–10 s, inadequate for transients occurring within 100–200 ms; and absence of formal stability certificates distinguishing them from Lyapunov-certified model-based adaptive control (Bao et al., 2014).

Table 2–2
Comprehensive Comparison of Advanced Control Methods for Enhancing GFL Inverter Stability in Low-SCR Grids.

Control Method	Core Principle	Advantages	Limitations
Power Synchronization Loop (PSL)	Replaces voltage-based PLL with power-based synchronization using swing equation emulation	Inherent damping capabilityEliminates negative impedance behaviorNaturally stable in weak gridsSimple physical interpretation	Slower dynamic responseSensitive to power measurement accuracyLimited performance during fault transients
SOGI-FLL	Uses adaptive filtering and Frequency-Locked Loop for robust grid tracking	Superior harmonic rejectionExcellent unbalance handlingEnhanced filtering capabilityGood transient performance	Complex parameter tuningHigher computational requirementsLimited very weak grid performance
Adaptive PLL Bandwidth	Dynamically adjusts PLL bandwidth based on real-time grid strength estimation	Maintains conventional PLL structureAdaptive stability-performance tradeoffEasy integration with existing systems	Requires accurate grid impedance estimationLimited improvement in very weak gridsDependent on estimation algorithm
Adaptive Virtual Impedance	Dynamically shaped output impedance based on real-time grid conditions	Active power decouplingEnhanced damping injectionImproved power sharingFault current management	Requires grid parameter identification Complex stability analysisParameter tuning challenges
Passivity-Based Control (PBC)	Ensure system passivity by shaping energy dissipation characteristics	Guaranteed stability for any passive gridRobust to grid parameter variationsStrong theoretical foundation	High mathematical complexityRequires accurate system modelDifficult practical implementation
H∞ Robust Control	Optimizes worst-case performance under bounded uncertainty	Robust to large parameter variationsHandles model uncertainties wellSystematic design approach	Conservative performanceComplex controller designHigh-order controllers
AI/Deep Reinforcement Learning	Learning optimal control policy through environment interaction	No explicit system model neededAdapts to complex nonlinearitiesOptimal performance in trained conditions	Extensive training data requiredBlack-box nature raises reliability concernsHigh computational resources needed
AI-Powered Grid Impedance Estimation	Uses machine learning for real-time grid parameter identification	Fast, accurate impedance estimationnon-intrusive measurementAdapts to grid topology changes	Training data dependencyLimited to trained scenariosIntegration complexity with controllers

2.7.3. Multi-converter interaction pathologies

When multiple inverters employ independent adaptive impedances in parallel operation, three interaction pathologies arise. First, positive feedback loops occur when one inverter's adaptation alters the local grid impedance observed by others, triggering cascading adjustments. Three-inverter case studies show virtual resistance oscillating between 0.05–0.4 p.u. at 3 Hz, preventing steady-state convergence (Reisner and Weiss, 2024a). Second, impedance resonance amplification emerges when converters adapt to similar values, yielding an equivalent parallel impedance

$$Z_{eq} = \frac{Z_v}{N} \tag{2-24}$$

which can shift system resonance into the control bandwidth. For example, three inverters with $L_v = 3\text{mH}$produce a resonance at $f_{res} = 1.2\text{kHz}$, coinciding with the current controller bandwidth and triggering harmonic instability (Bao et al., 2014). Third, unequal power sharing degrades when adaptive algorithms optimize local rather than global objectives, causing disproportionate reactive power absorption and premature current saturation (Wang et al., 2014).

2.7.4. Passivity-preserving design principles

Four mitigation strategies ensure safe adaptation. First, rate-limited adaptation constrains $|dZ_v/dt| < \Delta_{max}$(typically 0.1 p.u./s), maintaining quasi-static behavior that preserves passivity (Wang et al., 2014). Second, real-time passivity monitoring computes $\nu(t)$online and reverts to a safe impedance $Z_{v,safe}$when $\nu(t) < -\nu_{threshold}$. Third, consensus-based coordination shares impedance values among inverters via low-bandwidth communication, computing an average $Z_{v,avg}$as the adaptation reference to prevent divergence (Reisner and Weiss, 2024a). Fourth, Lyapunov-certified adaptation employs an energy function

$$V = \frac{1}{2}i^2L + \frac{1}{2\gamma}(Z_v - Z_{opt})^2 \tag{2-25}$$

The adaptation selection gain $\gamma < \omega_c L$ to ensure $\dot{V} < 0$, thereby guaranteeing convergence with bounded trajectories (Bao et al., 2014).

3. Grid-forming inverters: the architects of the modern grid

Grid-Following inverters are fundamentally constrained by their reliance on an external voltage reference, making them inadequate as the core of future power systems where synchronous generation is declining. In contrast, Grid-Forming (GFM) inverters provide a transformative solution by acting as controlled voltage sources that can independently establish and regulate both grid voltage and frequency. Rather than tracking an existing grid signal, they generate the reference waveform that other units, including GFL inverters, must align with. This functionality is crucial for islanded microgrids, weak grid environments, and, ultimately, for a 100% renewable-powered system (Ma, 2025). Table 3–1 provides a comprehensive comparison of these two technologies, highlighting their distinct roles in modern power systems with high penetration of renewable energy resources.

Table 3-1
Comprehensive Comparison Between Grid-Following (GFL) and Grid-Forming (GFM) Inverters.

Feature	Grid-Following (GFL) Inverter	Grid-Forming (GFM) Inverter
Fundamental Control Principle	Controlled current source	Controlled voltage source
Synchronization Mechanism	Phase-Locked Loop (PLL) tracks grid voltage	Internal oscillator sets grid voltage and frequency
Current Control	Essential and fast - Primary control objective. Inner current loop directly regulates output current.	Protective function - Secondary control objective. Current control acts as a protective limiter.
Voltage & Frequency Control	Indirect - Cannot control grid V/f directly. It can only be influenced through current injection.	Direct - Directly sets and regulates grid voltage magnitude and frequency.
Power Flow Control	Direct power control - Regulates active and reactive power injection according to references.	Indirect power control - Power output is determined by load demand and grid conditions.
P-Q Coupling	Decoupled control - Independent control of active and reactive power through dq-axis current regulation.	Coupled behavior - Natural coupling between P-ω and Q-V similar to synchronous generators. Requires virtual impedance for decoupling.
Islanded Operation	Cannot operate - Requires existing voltage source for synchronization. Cannot black start.	Can operate independently - Can establish and maintain microgrids. Capable of black start.
Grid Strength Dependency	High dependency - Performance degrades significantly in weak grids. PLL instability issues.	Low dependency - Naturally robust in weak grids. Can operate in very low SCR conditions.
Inertia Provision	No inherent inertia - Can provide synthetic inertia with additional control loops.	Virtual inertia - Can emulate rotational inertia through control algorithms (e.g., VSM).
Fault Response	Current-limited - Naturally current-limited. May trip during severe faults.	Voltage source behavior - Tries to maintain voltage. Requires sophisticated current limiting.
Stability Issues	Synchronization instability - PLL instability in weak grids. Harmonic instability.	Power-angle stability - Similar to synchronous generator stability. Small-signal stability.
Control Hierarchy	Grid → PLL → Power Control → Current Control → Gate Signals	Power Calculation → V/f Control → Voltage Control → Current Limiter → Gate Signals
Typical Applications	Grid-connected renewables - Solar PV, Wind farms, HVDC	Microgrids, weak grids, black start units - ESS, diesel generators, weak grid connections
Complexity	Moderate - Well-established control structure. Standard industrial practice.	Higher - More complex control algorithms. Requires careful parameter tuning.

3.1. From electromechanical stability to digital control

For more than a century, the stability and reliable operation of AC power systems have relied on the fundamental physics of synchronous machines (SMs). These rotating electromechanical units contribute far beyond power generation; they underpin system integrity through two key properties. First, synchronous inertia: the large rotating masses store kinetic energy that inherently resists frequency deviations. In the event of a power imbalance, this stored energy is instantly exchanged with the grid, as described by the swing equation:

$$J\frac{dw}{dt} = P_m - P_e \tag{3-1}$$

Where J is Moment of inertia of the synchronous machine rotor and it represents the stored kinetic energy capacity, w is the angular velocity of the rotor, P_m is the mechanical input power from the prime mover and P_e is the Electrical output power delivered to the grid.

This mechanism slows the Rate of Change of Frequency (RoCoF) and buys critical time for primary control actions. Second, automatic voltage regulation (AVR): excitation systems adjust the field current to stabilize terminal voltage, offering dynamic reactive power support during load changes and faults. Together, these attributes create a "stiff" grid with robust voltage and frequency characteristics, ensuring stable operation of all connected devices. However, the gradual replacement of synchronous machines with inverter-based resources (IBRs) weakens this foundation, reducing system inertia, lowering short-circuit strength, and introducing potentially unstable dynamics.

The Grid-Forming (GFM) inverter is envisioned as the digital counterpart to the synchronous machine, reproducing its stabilizing role through advanced control algorithms instead of mechanical rotation. Its primary function is to operate as a controlled voltage source behind an impedance, independently defining the grid's voltage and frequency reference. Core GFM control approaches, such as Droop Control and the Virtual Synchronous Machine (VSM), are modeled after synchronous machine behavior:

- Droop Control mimics the primary frequency and voltage response of synchronous generators, allowing autonomous load sharing across multiple units.
- Virtual Synchronous Machine (VSM) directly embeds the swing equation and AVR into its control, digitally reproducing inertia (J) and damping (D) to achieve a similar dynamic reaction to power disturbances.

A standalone GFM inverter directly linked to an intermittent renewable source (such as PV) cannot consistently fulfill its role, since it lacks assured power delivery. The true effectiveness of GFM control emerges when paired with an Energy Storage System (ESS). Acting as a 'digital prime mover,' the ESS supplies the necessary energy buffer that enables the GFM inverter to: (i) ensure firm active power injection as dictated by the control algorithm, independent of renewable variability; (ii) deliver real inertial response by rapidly injecting or absorbing power through its stored energy, something renewables alone cannot provide; and (iii) perform black start by supplying the initial energy required to establish grid voltage and frequency after a blackout.

3.2. Fundamental principle and control architecture

The key distinction between GFL and GFM inverters lies in their intrinsic operating nature: GFL inverters function as current sources with high output impedance, whereas GFM inverters behave as voltage sources with low output impedance. This voltage-source characteristic imparts the stiffness required to sustain a stable voltage waveform at the Point of Common Coupling (PCC), even under varying loads and grid disturbance. The generic structure of the GFM inverter is depicted in Fig 3–1.

Key Operational Principles:

- Voltage and Frequency Formation: A GFM inverter establishes its own internal voltage reference waveform (V*abc) from a specified amplitude V* and frequency W*. The phase angle θ is obtained by integrating the frequency reference, which makes the inverter the master of phase and frequency, unlike a GFL inverter that must follow the grid.
- Power-Coupled Regulation: Unlike fixed values, the specified amplitude V* and frequency W* are adaptively tuned in response to the measured active P and reactive Q power through a defined control strategy (e.g., droop control, virtual synchronous machine, or Matching control diagram). This enables autonomous balancing of generation and demand without external coordination.
- Hierarchical Control Loops: The control architecture typically includes a virtual impedance loop that shapes the output impedance and provides current-limiting capability. This is complemented by a voltage control loop, which regulates the inverter's output capacitor voltage. At the innermost level, a fast current control loop ensures the inductor current closely tracks its reference, thereby protecting the semiconductor devices. This architecture allows the GFM inverter to seamlessly transition between grid-connected and island modes and to provide vital system-wide stability service

3.3. Droop control: mathematical modeling and loop equations

Droop control replicates the primary frequency and voltage regulation of synchronous generators by applying fixed proportional relationships between power output and system frequency or voltage. Fig 3–2 presents the Droop-control loop. When power demand increases, the generator's rotor speed decreases, causing a drop in frequency. The frequency is restored to its nominal value by increasing power generation. When power demand decreases, the generator's rotor speed increases, leading to a rise in frequency. To restore the frequency to its nominal value, power generation must be reduced.

3.3.1. Active and Reactive Power-Frequency Droop

This mechanism regulates the inverter's output angular frequency (ω) based on its measured active power output (P). The frequency of the GFM is allowed to decrease linearly with increasing Active power:

$$w = w^{\circ} - M.(P - P^{*}) \tag{3-2}$$

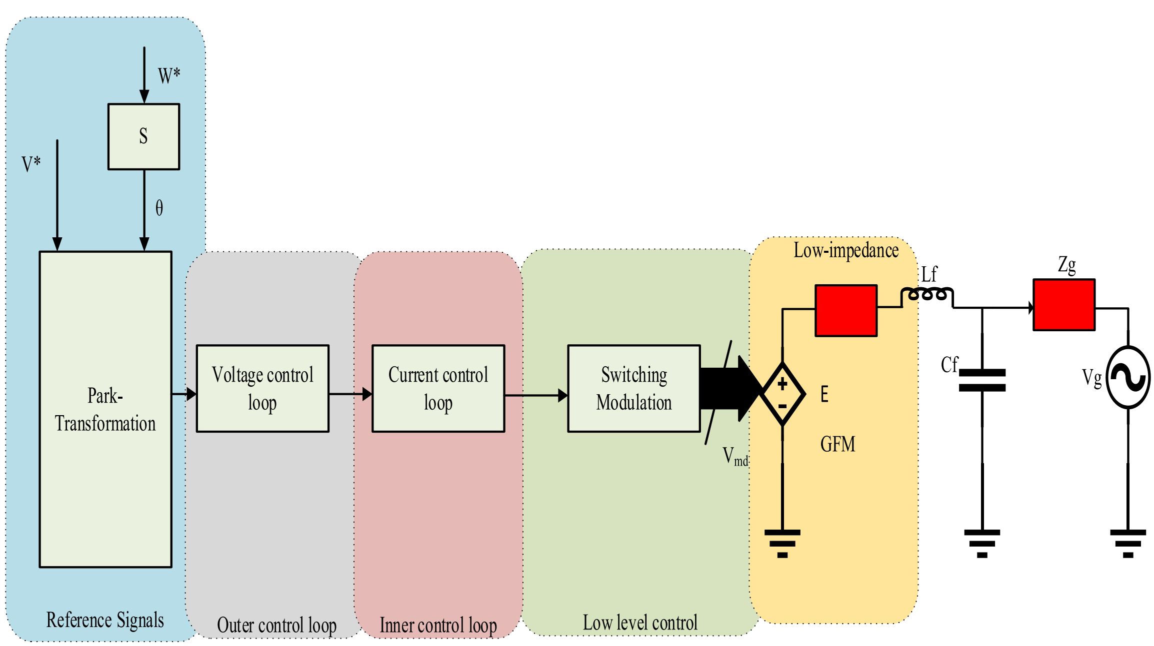

Fig. 3–1. Basic control structure of a grid-forming voltage source inverter.

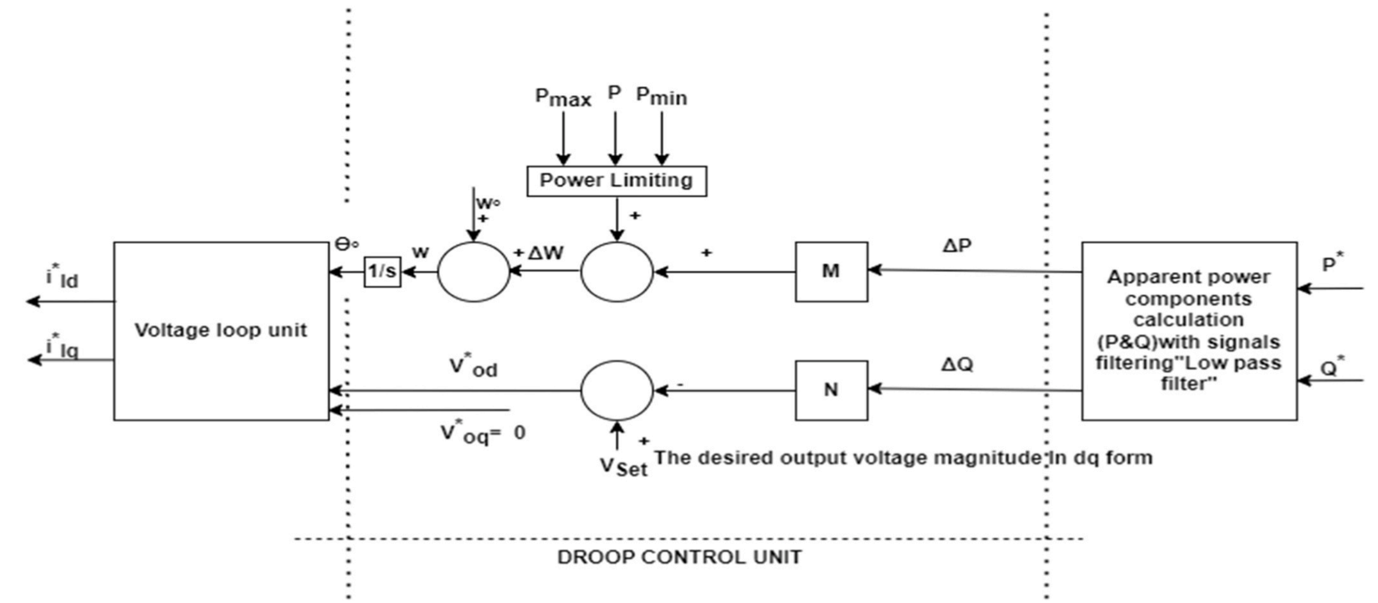

Fig. 3–2. The droop control loop (P-F Droop &Q-V droop).

where:

- w is the angular frequency.
- w° is the reference angular frequency.
- M is the droop coefficient for frequency.
- P is the measured active power output.

M is the droop coefficient determines the sensitivity of the frequency to active power changes. According to Equation (3–3), A negative correlation implies that as GFM supplies more active power, its output frequency slightly decreases, facilitating load sharing. Fig 3–3 illustrates the P-f droop and Q-V Droop characteristic curve (Fazal et al., 2022).

$$w = w^{\circ} - mp.(P - P^{*})$$

$$\delta_p = \delta_E - \delta_V$$

$$P = \frac{E.V}{X_L} \sin \delta_p$$

$$P \sim \frac{E.V}{X_L}\delta_p \tag{3-3}$$

In case of Q-V Droop, this mechanism regulates the amplitude of the GFM's output voltage (V) based on its reactive power output (Q):

$$V = V_{Set} - nq.(Q - Q^{*})$$

$$\delta_p = \delta_E - \delta_V$$

$$Q = \frac{E^2 - E.VCOS\delta_p}{X_L}$$

$$Q \sim \frac{E(E - V)}{X_L} \tag{3-4}$$

Where N is reactive Power Droop Coefficient, defines how much the voltage amplitude changes in response to reactive power variations. This helps with reactive power sharing and voltage regulation within the microgrid (Fazal et al., 2022). To protect the GFM from overloads and maintain system stability, power limiting functions are often integrated with droop control. These functions restrict the GFM's active and reactive power output within predefined safe operational boundaries (Saleh et al., 2022). Fig 3–4 Shows the mechanism of the power limiting control unit. In this graph, there are two power limits: a maximum and a minimum. These limits define the safe operational range of the system's

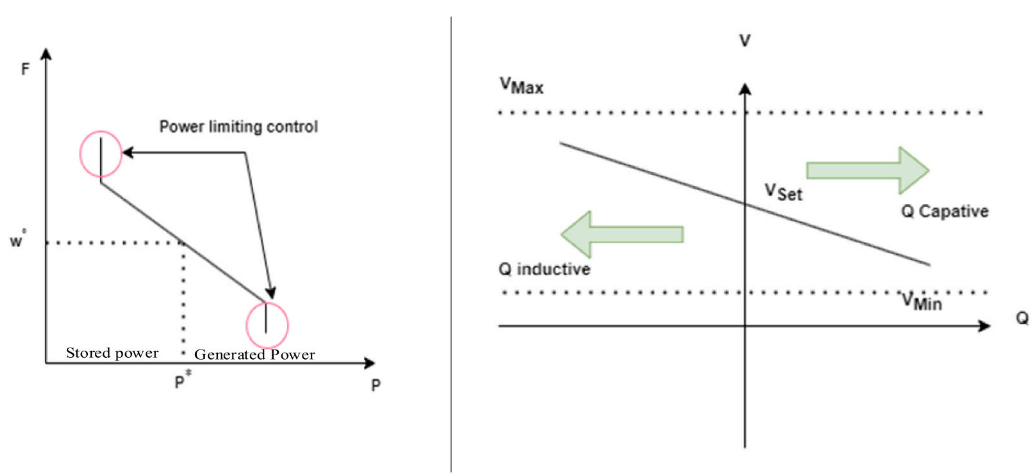

Fig. 3–3. Characteristic curves of the active and reactive power droop control.

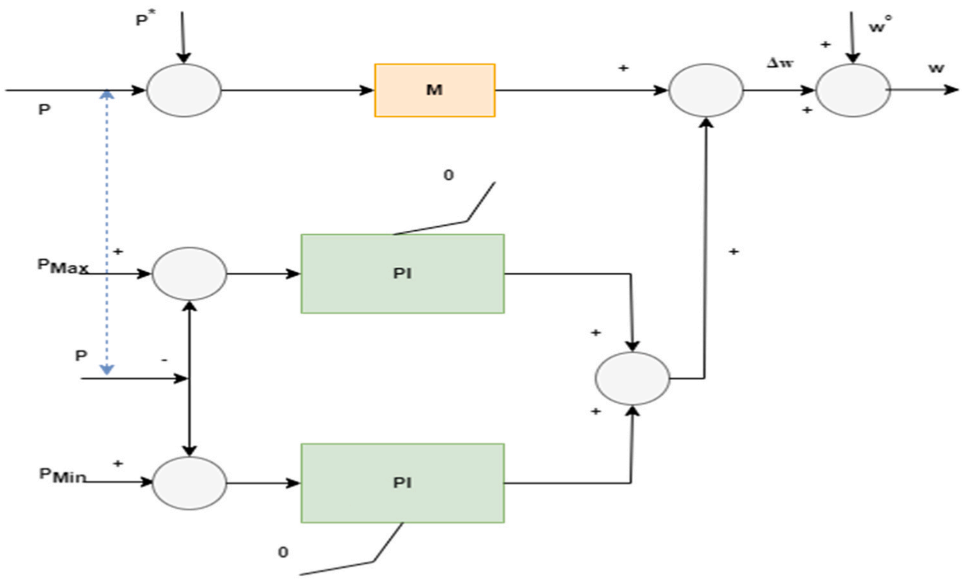

Fig. 3–4. Block diagram of power limiting.

power output, ensuring that the GFM operates within its capabilities

3.3.2. Power calculation and filtering

Consider a GFM inverter with an internal voltage E∠δ connected to the grid voltage Vg∠0∘ through a line or leakage impedance Zg∠ϕg=Rg+jXg, as shown in Fig 3–5. This circuit forms the basis for deriving the fundamental power flow equations that govern active and reactive power transfer between the inverter and the grid (Chatterjee et al., 2018).

The instantaneous powers are calculated from the measured voltages and currents in the DQ-reference frame (with D-axis aligned to the voltage vector, making $V_q \approx 0$) (Rocabert et al., 2012a):

$$P_{inst} = \frac{3}{2}\left(V_{PCC,d} * i_d + V_{PCC,q} * i_q\right) \approx \frac{3}{2} V_{PCC,d} * i_d$$

$$Q_{inst} = \frac{3}{2}\left(V_{PCC,q} * i_d - V_{PCC,d} * i_q\right) \approx -\frac{3}{2} V_{PCC,d} * i_q \quad (3\text{-}5)$$

To eliminate high-frequency noise and oscillations from switching and measurement noise, the instantaneous powers are filtered (Castilla et al., 2018):

$$P = \frac{w_f}{s + w_f} P_{inst}$$

$$Q_{inst} = \frac{w_f}{s + w_f} Q_{inst} \quad (3\text{-}6)$$

Where ω_f is the cutoff frequency [rad/s] of the first-order low-pass filter. The output voltage references are generated using the frequency and voltage magnitude calculated by the droop laws (Castilla et al., 2018):

$$\theta = \int w dt = \int (w^0 - m_p(P - P^*))$$

$$v_a^* = \mathrm{V}\sin\theta = (V_{Set} - nq.(Q - Q^*)\sin\theta$$

$$v_b^* = (V_{Set} - nq.(Q - Q^*)\sin(\theta - \frac{2\Pi}{3})$$

$$v_c^* = (V_{Set} - nq.(Q - Q^*)\sin(\theta + \frac{2\Pi}{3}) \quad (3\text{-}7)$$

To enhance stability, provide damping, and decouple power flow in resistive networks, a virtual impedance is added (Rodriguez-Cabero

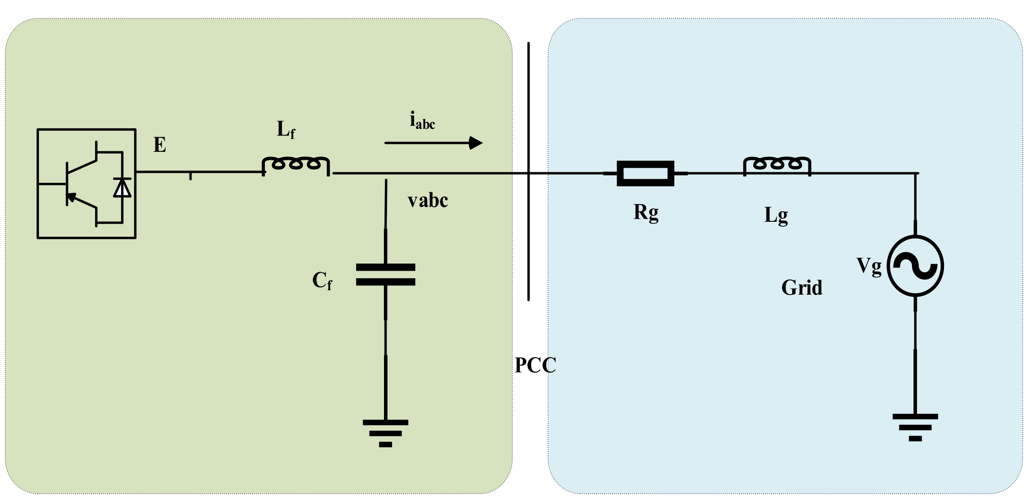

Fig. 3–5. Equivalent circuit diagram of a grid-forming inverter interfaced with the AC grid.

et al., 2020):

$$V_{d,vi} = -R_V * i_d + W * L_V * i_q$$
$$V_{q,vi} = -R_V * i_q - W * L_V * i_d$$
$$V_d^{**} = V_d^* - V_{d,vi}$$
$$V_q^{**} = V_q^* - V_{q,vi} \tag{3-8}$$

Where R_V is virtual resistance and L_V is the virtual inductance. The voltage controller (in dq-frame) loop regulates the capacitor voltage at the inverter output.

$$I_{d,ref} = \left(K_{P,V} + \frac{K_{I,V}}{s}\right)(V_d^{**} - V_d) - w\, C_f\, V_q$$
$$I_{q,ref} = \left(K_{P,V} + \frac{K_{I,V}}{s}\right)\left(V_q^{**} - V_q\right) + w\, C_f\, V_d \tag{3-9}$$

While the current controller is the innermost and fastest loop, responsible for protecting the semiconductors by regulating the inductor current.

$$U_d = \left(K_{P,I} + \frac{K_{I,I}}{s}\right)(I_{d,ref} - i_d) - w\, L_f\, i_q + V_d$$
$$U_q = \left(K_{P,I} + \frac{K_{I,I}}{s}\right)(I_{q,ref} - i_q) + w\, L_f\, i_d + V_q \tag{3-10}$$

These equations (Ud &Uq) are the final voltage references that are sent to the PWM modulator to generate the gate signals for the inverter's power switches.

3.3.3. Fundamental power flow physics for grid-forming inverters

The mechanism of power transfer in Grid-Forming (GFM) inverters is inherently distinct from that of conventional synchronous generators because of their electronic interface with the grid. Whereas synchronous machines primarily exchange power through reactance, the output of a GFM inverter depends on both the resistive and reactive parts of the grid impedance. This interaction is expressed by the general power flow equations for an inverter with an internal voltage $E\angle\delta$ connected to a grid voltage $V_g\angle 0^\circ$ via an impedance $Z_g=R_g + j\, X_g$.

General Power Flow Equations (Castilla et al., 2018):

$$P = \frac{3}{R_g^2 + X_g^2}\left[R_g\left(EV_g\cos\delta - V_g^2\right) + X_g EV_g \sin\delta\right]$$
$$Q = \frac{3}{R_g^2 + X_g^2}\left[X_g\left(EV_g\cos\delta - V_g^2\right) - R_g EV_g \sin\delta\right] \tag{3-11}$$

These equations reveal that active and reactive power flow depends explicitly on both grid resistance (R_g) and reactance (X_g), creating a coupled relationship that must be properly managed for stable inverter operation. The grid impedance acts as a dynamic filter, shaping how voltage deviations are converted into current flow and, consequently, power exchange. Its resistive and reactive parts contribute in different ways: the resistive component dissipates real power, producing in-phase current that dictates active power transfer, while the reactive component alternately stores and releases energy, generating quadrature current that primarily regulates reactive power flow. This perspective highlights the significance of the grid's R/X ratio, as it directly impacts the power-sharing behavior of GFM inverters and plays a key role in defining system stability limits (Gao et al., 2023). The interdependence of the power flow equations creates major challenges for control design. Since active power P is influenced by both R_g and X_g, tuning the inverter frequency to adjust the power angle δ simultaneously alters active and reactive power. Likewise, changes in the voltage magnitude E affect both components of power. This intrinsic P–Q coupling requires advanced control schemes capable of decoupling these interactions to maintain stable inverter performance under varying grid condition. The magnitude of grid impedance is a direct indicator of system strength. In strong grids with low Z_g, the voltage remains largely unaffected by inverter current injections, enabling stable and predictable power transfer. In contrast, weak grids with high Z_g exhibit significant voltage distortion from inverter currents, introducing complex feedback dynamics that may threaten overall system stability (Reisner and Weiss, 2024a).

3.4. Virtual synchronous machine (VSM)

The Virtual Synchronous Machine (VSM), often referred to as a Synchronverter, is among the most advanced grid-forming control strategies, as it explicitly reproduces the full electromechanical behavior of a synchronous generator (Thommessen and Hackl, 2024). Unlike static droop-based methods, VSM control emulates both the inertial dynamics and excitation mechanisms of rotating machines, thereby serving as a vital transitional framework between conventional synchronous systems and inverter-dominated grids (Roldan-Perez et al., 2019; Barsali et al., 2025).

3.4.1. Core principle and mathematical foundation

The VSM architecture is built upon two fundamental pillars: the swing equation emulation for active power control and the excitation system emulation for reactive power regulation. A synchronous generator naturally possesses inertia because of its spinning rotor. When the load changes, the rotor either slows down or speeds up, which helps balance the system frequency (Thommessen and Hackl, 2024). In contrast, an inverter has no moving parts, so it does not provide natural inertia. To overcome this limitation, the Virtual Synchronous Machine (VSM) control strategy enables the inverter to "pretend" to be a generator by embedding the equations of a synchronous machine into its control system (Barac et al., 2021). Through this approach, the inverter creates virtual inertia and damping, allowing it to react to system changes much like a real generator. It also mimics excitation control, regulating voltage and reactive power. As a result, the inverter is capable of setting both voltage and frequency, just like a traditional synchronous generator, which is why it is classified as a grid-forming unit (Mallemaci et al., 2023). When frequency oscillations occur after a disturbance, the system requires a mechanism to slow them down. In real generators, this role is performed by friction and damper windings. In the case of a VSM, a damping factor (D) is added into the swing equation to stabilize frequency. Without damping, frequency behaves like a swinging pendulum that continues oscillating. With damping, however, oscillations settle smoothly back to their nominal value, ensuring system stability (Wald et al., 2024). Excitation control is another fundamental function. In a synchronous generator, excitation refers to the adjustment of field current in the rotor, which directly controls terminal voltage and reactive power output. In a VSM, there is no physical rotor, so this function is implemented digitally. The inverter's control system modifies the voltage magnitude in a way that mirrors the operation of an Automatic Voltage Regulator (AVR). This ensures the inverter contributes to voltage stability and supports reactive power sharing within the grid (Rodriguez-Cabero et al., 2020; Wald et al., 2024). The core dynamic behavior is governed by the electromechanical swing equation (Wald et al., 2024):

$$\frac{dw}{dt} = \frac{1}{J}\left[P_m - P_e - D_P(w - w_0)\right] \tag{3-12}$$

Where:

- J: Virtual inertia constant [kg·m^2] or [Ws^3 /rad^2]
- D_P: Damping coefficient [N·m·s/rad]
- P_m: Mechanical power input (setpoint) [W]
- P_e: Electrical power output (measured) [W]

- w: Angular frequency [rad/s]

The frequency dynamics are determined by integrating the swing equation (Wald et al., 2024):

$$w = w_0 + \frac{1}{J}\int P_m - P_e - D_P(w - w_0)$$

$$\theta = \int w dt \tag{3-13}$$

Excitation System Emulation (Reactive Power Control): AVR, which stands for Automatic Voltage Regulator, is a key component in voltage control. In a synchronous generator, the AVR manages the excitation current of the rotor winding to keep the terminal voltage close to its reference value (Wald et al., 2024). In a Virtual Synchronous Machine (VSM), the same function is performed digitally through control software. Instead of adjusting rotor excitation, the AVR modifies the internal electromotive force or the inverter's voltage reference (E_0), ensuring that the output terminal voltage remains aligned with the desired setpoint. The voltage regulation follows the automatic voltage regulator principle (Das et al., 2024; Reißner and De Carne, 2024):

$$E = E_0 + \left(K_{P,q} + \frac{K_{I,q}}{s}\right) (Q^* - Q) \tag{3-14}$$

3.4.2. Current limiting and protection strategies for VSM

One of the biggest challenges in Virtual Synchronous Machine (VSM) control is current limiting. Unlike synchronous generators, which can safely carry 3–5 times their rated current for a few seconds, VSM inverters rely on semiconductor switches that can only tolerate about 1.2–1.5 times rated current for very short durations (Panya et al., 2024). This makes effective current protection essential to prevent device damage while still maintaining grid stability. The core current limiting algorithm operates in the synchronous reference frame (dq-frame) and implements a magnitude-based limitation (Barac et al., 2021).

Current Magnitude Calculation:

$$I_{\max} = \sqrt{(i_d^2 + i_q^2)} \tag{3-15}$$

Limiting Condition:

$$\text{If} I_{\max} > I_{limit} \quad : \quad i_d^* = i_d^* * \frac{I_{limit}}{I_{\max}} \quad , \quad i_q^* = i_q^* * \frac{I_{limit}}{I_{\max}} \tag{3-16}$$

Where:

- I_{max}: Instantaneous current magnitude [A].
- I_{limit}: Maximum allowable current threshold [A].
- i_d^*, i_q^*,: Current references in dq-frame [A].

This approach maintains the relative proportion between active (D-axis) and reactive (q-axis) current components while ensuring the total current magnitude does not exceed the safe operating area of the semiconductor devices (He et al., 2025).

Priority-Based Current Limiting:

During severe current limitations, priority can be given to specific current components based on system requirements:

$$\text{If} I_{\max} > I_{limit} \quad : \begin{cases} i_d^* = i_d^* * \frac{I_{limit}}{I_{\max}} \quad , \quad i_q^* = i_q^* * \frac{I_{limit}}{I_{\max}} \\ i_d^* = sign(i_d^*) . \sqrt{(I_{limit}^2 - i_q^2)} \quad (Active\ Priority) \\ i_q^* = sign\left(i_q^*\right) . \sqrt{(I_{limit}^2 - i_d^2)} \quad (Reactive\ Priority) \end{cases} \tag{3-17}$$

To prevent abrupt current changes that could destabilize the system:

$$\frac{di^*}{dt} \leq (\frac{di}{dt})\max \tag{3-18}$$

The process of current limiting poses major challenges for VSM performance. Synchronization stability: When current limiting is active, the inverter may not be able to sustain its internal voltage, which can eventually cause it to lose synchronism with the grid. Power imbalance: By capping current, the VSM cannot always supply the power dictated by the swing equation, leading to mismatches that disturb frequency stability. Voltage collapse: Under severe grid faults, strong current limitation may reduce the PCC voltage drastically, risking a local voltage collapse (Fan et al., 2022). Complete control block diagram of a Virtual Synchronous Machine (VSM) grid-forming inverter, showing the implementation of the swing equation, automatic voltage regulation, virtual impedance, and current limiting protection is shown in Fig 3–6 (Mallemaci et al., 2023).

3.4.3. Stability trade-off in ultra-weak grids: VSM inertia versus droop speed

The transition to ultra-weak grids (SCR < 2) introduces a fundamental stability trade-off between the two dominant Grid-Forming (GFM) control paradigms (Guerrero et al., 2011): Virtual Synchronous Machine (VSM) and droop-based control (Rodriguez-Cabero et al., 2020; Wald et al., 2024). As correctly highlighted by the reviewer, this trade-off arises from the intrinsic difference in their synchronization mechanisms and dynamic time constants. The principal advantage of VSM control lies in its emulation of synchronous generator dynamics through the swing equation, introducing virtual inertia $J$and damping D. This second-order structure provides energy buffering, phase stiffness, and improved robustness against sustained disturbances in weak grids. However, the same inertial mechanism introduces a deliberate time constant that slows the instantaneous frequency and phase response. In ultra-weak grids characterized by high grid impedance Z_g, even small power perturbations can induce rapid and large power–angle deviations δ. If virtual inertia is excessively large or poorly tuned, the VSM's inertial response may be unable to track these rapid phase excursions, potentially leading to transient loss of synchronism or power–angle instability (Beck and Hesse, 2007). In contrast, droop-controlled GFM inverters operate without virtual inertia ($J = 0$), relying on first-order algebraic power–frequency and reactive power–voltage relationships (Fazal et al., 2022). Their synchronization dynamics are therefore governed primarily by the fast inner voltage and current control loops. This enables near-instantaneous power–angle adjustment in response to abrupt voltage or phase variations, which can provide superior transient alignment in ultra-weak, highly resistive networks. As a result, a well-tuned adaptive droop controller may exhibit faster initial synchronization than a conventional VSM under severe grid weakness (Vasquez et al., 2013). Crucially, this apparent advantage of droop control does not imply a fundamental incompatibility of VSM strategies with ultra-weak grids. Rather, it reflects a design trade-off between response speed and phase-energy buffering, not a structural limitation of inertia-based control (Wald et al., 2024). While droop control offers rapid adjustment, it lacks intrinsic energy storage and frequency filtering, rendering it highly sensitive to noise, measurement errors, and large-signal disturbances (Aliyu et al., 2025). Consequently, its stability margins deteriorate sharply as SCR approaches unity. The optimal solution therefore lies in adaptive inertia-based strategies, will be discussed in Section 3.5 and be extended in Section 3.10. Adaptive VSM and AI-augmented GFM controllers dynamically tune the virtual inertia $J$and damping Din real time based on grid conditions (Lu and Zhuan, 2024). During steady-state operation, higher inertia enhances frequency filtering and robustness. During fast transients or rapid power–angle excursions in ultra-weak grids, the controller can temporarily reduce J(or increase D), effectively emulating the fast, non-inertial response of droop control to preserve synchronism. Once the transient subsides, inertia is restored to maintain stability and power quality (Zhang et al.,

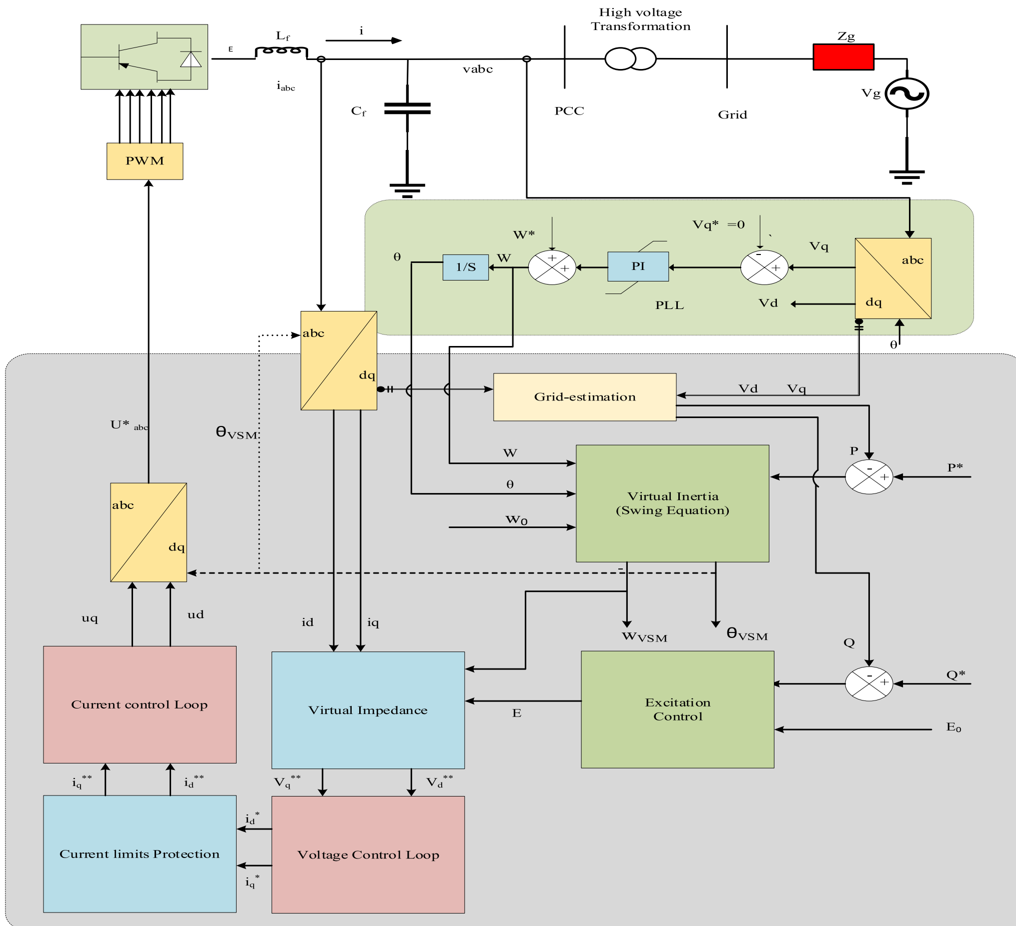

Fig. 3–6. Comprehensive Control Architecture of a Virtual Synchronous Machine (VSM) Grid-Forming Inverter.

2020). This dynamic adaptation reconciles the apparent conflict between inertia and speed, providing a unified control framework that combines the fast transient responsiveness of droop control with the superior large-signal stability and resilience of VSM-based grid-forming strategies. Accordingly, when properly tuned and adaptively coordinated, VSM-based GFM control offers higher overall stability margins than droop control in ultra-weak grid environments (Lu and Zhuan, 2024), (Zhang et al., 2020).

3.4.4. P–Q decoupling in resistive grids: limits of virtual impedance and emerging control approaches

In weak-grid environments with non-negligible R/Xratios, the classical decoupling between active and reactive power becomes significantly degraded (Wang et al., 2025a). In conventional inductive networks, active power is predominantly governed by the power angle, while reactive power is primarily regulated through voltage magnitude. However, as grid resistance increases, strong cross-coupling emerges between active power and voltage magnitude, as well as between reactive power and phase angle, posing a fundamental challenge for grid-forming inverter control (Gao et al., 2023). Virtual impedance methods, reviewed in Section 2.7, are commonly employed to shape inverter output characteristics, improve power sharing, and enhance stability by emulating synchronous machine behavior through synthetic resistive and inductive elements (Rahman et al., 2024). While such techniques can partially mitigate P–Q coupling in moderately weak or inductive grids, their effectiveness diminishes significantly in highly resistive networks for several reasons (Wang et al., 2023):

- **Inherent Physical Coupling:** In resistive grids, the coupling between power and voltage variables is a fundamental property of the network. Virtual impedance alone cannot fully eliminate this interaction, particularly when grid impedance varies dynamically.
- **Stability–Performance Trade-Off:** Increasing virtual impedance to improve decoupling often degrades transient performance, slows voltage recovery, and reduces power transfer capability due to excessive voltage drops.
- **Tuning Sensitivity:** Achieving optimal virtual impedance settings across a wide range of R/Xconditions is nontrivial and typically requires adaptive or grid-aware tuning mechanisms. As a result, virtual impedance should be viewed as mitigating rather than a fully decoupling solution in ultra-weak and resistive grids (Rahman et al., 2024).

To address P–Q coupling more fundamentally, several advanced control paradigms have been proposed that move beyond static virtual impedance shaping (Labella et al., 2020):

- **Power Angle Control (PAC):** PAC explicitly assigns active power regulation to voltage angles and reactive power regulation to voltage magnitude, even in resistive grids. By redefining the control structure, PAC re-establishes the desired P–δ and Q–V relationships by design, although it relies on accurate grid impedance estimation and is sensitive to measurement noise.
- **Matching Control (MC):** Matching control aims to actively align the inverter output impedance with the grid impedance or a desired reference profile. This impedance-aware strategy enables improved power decoupling and stability over a wide range of R/Xratios but requires real-time impedance identification and adaptive control mechanisms.

- **Model Predictive Control (MPC):** MPC incorporates grid impedance characteristics directly into an optimization framework, allowing the controller to anticipate and compensate for P–Q coupling effects. While highly effective in principle, MPC introduces significant computational complexity and depends on accurate system modeling. These approaches offer structurally deeper solutions to the coupled stability problem by redefining control objectives, actively shaping inverter–grid interactions or leveraging predictive optimization. Furthermore, the integration of AI-based supervisory layers will be discussed in Section 3.10, can enhance these paradigms by enabling real-time adaptation to changing grid conditions and uncertainty ("AI-Enhanced Stability Control of Grid-Forming Inverters via Inertia, Damping, and Impedance Regulation and Request PDF.", 2025).

3.4.5. Power sharing and frequency regulation in islanded microgrids: VSM vs. droop

In communication-less islanded microgrids, grid-forming inverters are required to ensure both stable frequency regulation and proportional power sharing using only local measurements. Among the available grid-forming strategies, droop control and virtual synchronous machine control represent two widely adopted approaches with fundamentally different dynamic characteristics and performance trade-offs. Droop control emulates the steady-state primary frequency and voltage regulation behavior of synchronous generators by establishing proportional relationships between active power and frequency, and between reactive power and voltage magnitude (Guerrero et al., 2011). In predominantly inductive networks, these relationships are approximately decoupled, which enables decentralized and communication-free power sharing among parallel inverters through appropriate selection of droop coefficients. This characteristic allows droop-controlled inverters to achieve reliable proportional power sharing with fast response to disturbances (Moustafa et al., 2025). However, droop-based operation inherently leads to a steady-state frequency deviation from nominal value, since frequency regulation is achieved through intentional frequency offsets rather than inertia-based stabilization. Virtual synchronous machine control extends beyond steady-state droop behavior by explicitly incorporating the swing equation of a synchronous generator. By introducing virtual inertia and damping, VSM-based inverters actively contribute to the system's inertial response and reduce the rate of change of frequency following power imbalances. This dynamic behavior significantly improves frequency regulation and enhances disturbance rejection in islanded microgrids. As a result, VSM-controlled systems generally exhibit superior frequency stability compared to droop-controlled systems, particularly during large and sudden variations (Wald et al., 2024). Despite these advantages, the inclusion of virtual inertia introduces second-order dynamics that affect transient power sharing in communication-less multi-inverter systems. While steady-state power sharing is still governed by droop-like characteristics, the dynamic interaction between multiple virtual inertias can produce oscillatory behavior and deviations from ideal proportional power sharing during transients (Beck and Hesse, 2007). In contrast, droop-controlled inverters respond instantaneously to frequency deviations due to their effective first-order dynamics, which results in more predictable transient power sharing but weaker frequency stabilization. The fundamental trade-off between droop control and virtual synchronous machine control therefore lies in their dynamic response properties. Droop control prioritizes simplicity and accurate proportional power sharing with fast transient response, at the expense of steady-state frequency deviation. Virtual synchronous machine control prioritizes improved frequency stability and inertial support, at the cost of increased control complexity and potentially reduced accuracy of transient power sharing in the absence of coordination mechanisms (Mallemaci et al., 2023).

3.5. Comparative stability characteristics of droop-controlled and virtual synchronous machine grid-forming inverters

As discussed in Sections 3.3 and 3.4, droop-based and Virtual Synchronous Machine (VSM) strategies represent dominant approaches for implementing Grid-Forming (GFM) behavior. While both enable autonomous voltage and frequency regulation without phase-locked loops, their underlying stability mechanisms differ fundamentally, leading to distinct performance trade-offs in weak grids, particularly as the short-circuit ratio approaches unity (Rocabert et al., 2012b). Droop-controlled GFM inverters achieve synchronization through algebraic power–frequency and reactive power–voltage relationships, offering simplicity and effective power sharing in moderate grid-strength conditions (Guerrero et al., 2011). However, as grid strength deteriorates, the absence of explicit inertial dynamics limits synchronization stability margins. In ultra-weak grids, small disturbances produce rapid frequency deviations with insufficient inherent damping, rendering droop-controlled systems increasingly sensitive to parameter tuning and network impedance variations. In contrast, VSM-based strategies explicitly embed second-order electromechanical dynamics by emulating the swing equation of synchronous generators. This dynamic structure provides intrinsic energy buffering and phase inertia, enhancing synchronization stability and tolerance to sudden power imbalances in weak grids (Vasquez et al., 2013). As SCR approaches unity, the virtual inertia and damping inherent in VSM control enable significantly larger stability margins compared to droop implementations, reducing sensitivity to grid impedance uncertainty and transient disturbances. Consequently, VSM strategies demonstrate superior resilience under ultra-weak conditions, though at the cost of increased control complexity and potential responsiveness degradation if improperly tuned (Zhang et al., 2010). Despite improved synchronization robustness, VSM approaches introduce susceptibility to sub-synchronous oscillations. The interaction between virtual inertia, damping coefficients, and grid impedance can excite low-frequency oscillatory modes (0.5–15 Hz), especially in resistive or mixed R/X networks (Rocabert et al., 2012b). These modes are typically absent in droop-controlled systems due to their first-order algebraic nature. Therefore, while VSM control enhances stability margins in weak grids, careful damping design is essential to prevent oscillatory behavior (Beck and Hesse, 2007). The comparison reveals a fundamental trade-off between simplicity and robustness. Droop-based GFM control offers straightforward implementation with reduced oscillatory risk but exhibits limited synchronization margins as grid strength declines. VSM-based strategies provide superior stability and inertia emulation in ultra-weak grids at the expense of increased sub-synchronous oscillation susceptibility and higher implementation complexity (Wald et al., 2024)

3.6. System-level barriers to large-scale deployment of grid-forming inverters

Although Grid-Forming (GFM) inverters have demonstrated strong potential for enhancing stability in weak and ultra-weak power systems, their transition from pilot deployments to large-scale adoption remains constrained by deeply interconnected system-level barriers. These challenges emerge from the complex interplay between protection philosophies, heterogeneous inverter dynamics, and the absence of harmonized performance specifications ("Guerrero et al., 2013)

3.6.1. Protection scheme redesign and coordination challenges

One of the most significant limitations arises from the fundamental misalignment between conventional protection schemes and GFM inverter fault characteristics. Traditional protection systems are designed around high fault currents (5–10 p.u.) produced by synchronous generators, enabling reliable discrimination through overcurrent and distance relays (Kroposki et al., 2017). In contrast, GFM inverters exhibit current-limited fault responses constrained to 1.2–1.5 p.u. to protect semiconductor devices while simultaneously providing voltage support that fundamentally alters measured impedance at relay locations. This creates three critical challenges: overcurrent relays become desensitized and may fail to detect faults in radial feeders; distance relays mis operate due to voltage support maintaining higher-than-expected voltages during faults; and directional elements malfunction as phase relationships between voltage and current deviate from traditional patterns (Kroposki et al., 2017). Reliable operation in GFM-dominated systems necessitates a paradigm shift toward protection architectures explicitly accommodating inverter-based resource characteristics, including voltage-based fault detection, differential protection schemes utilizing high-speed communication, and adaptive protection algorithms that adjust settings based on real-time system topology (Lin et al., 2026). However, implementation requires substantial infrastructure investment, with estimated costs of $2–5 million per substation for communication-enabled protection systems, creating significant economic barriers.

3.6.2. Dynamic interactions in heterogeneous inverter populations

Power systems during the transition period will operate with heterogeneous populations comprising synchronous generators, Grid-Following (GFL) inverters, and Grid-Forming (GFM) inverters, each exhibiting distinct dynamics. This heterogeneity introduces three adverse phenomena: sub synchronous oscillations (1–15 Hz) emerging from eigenvalue coupling between GFL phase-locked loop dynamics and GFM virtual inertia, with damping degrading as $\zeta \approx \zeta_0 \exp(-0.15\ N_{inv})$ for $N_{inv} > 5$ parallel inverters; harmonic instability when LCL filter resonances of multiple inverters coincide, demonstrated where three converters at 1.2 kHz resonance produced 8% total harmonic distortion; and unequal power sharing under unbalanced faults due to divergent negative-sequence control strategies (Rocabert et al., 2012b; Pogaku et al., 2007). The voltage-source characteristic of GFM inverters can interact unfavorably with PLL-synchronized GFL units in weak grids, creating feedback where GFM voltage oscillations drive PLL tracking errors, which inject oscillatory currents that further destabilize the common coupling point. This bidirectional coupling triggers instability at short-circuit ratios where both converter types would operate stably if deployed homogeneously, revealing that GFM integration is fundamentally a system-level coordination problem (Lin et al., 2026).

3.6.3. Standardization fragmentation and performance specification gaps

A critical barrier is the absence of comprehensive, harmonized performance specifications across jurisdictions. While conventional generation benefits from standardized definitions in IEEE 1547 and IEC 61400, comparable GFM benchmarks remain fragmented ("IEEE SA - IEEE, 1547–2018.", 2025). Specific gaps include lack of quantitative metrics for frequency stiffness and inertial response; undefined voltage recovery profiles following faults; absence of standardized fault current shaping requirements; and inconsistent reactive power capability specifications, with European ENTSO-E requirements diverging from North American NERC standards (Pogaku et al., 2007). This fragmentation increases manufacturer development costs and undermines system operator confidence, particularly without standardized testing protocols for validating GFM stability in ultra-weak conditions (SCR $<$ 1.5) (Rocabert et al., 2012b).

3.6.4. Interdependency analysis and deployment implications

These barriers exhibit strong interdependencies creating compounding obstacles. Protection redesign is constrained by the lack of standardized fault response specifications, as utilities cannot finalize protection schemes without clear definitions of expected GFM behavior (Kroposki et al., 2017). Conversely, meaningful standardization requires resolution of dynamic interaction issues, since specifications must ensure stability for heterogeneous populations. The economic barrier is acute: utilities hesitate to invest in protection upgrades without regulatory mandates, yet regulators cannot establish mandates without proven solutions to interaction and standardization challenges (Rocabert et al., 2012b). This interdependency necessitates a coordinated framework simultaneously advancing: GFM-aware protection architectures through industry-academic-utility consortia; harmonization of international standards establishing quantitative benchmarks and test protocols; system-level stability analysis tools for mixed GFL-GFM populations; and phased deployment strategies positioning early GFM installations at critical buses to maximize benefits while minimizing interaction risks (Pogaku et al., 2007). Only through such holistic coordination can the technical potential of Grid-Forming inverters translate into reliable, scalable integration within future low-inertia power systems.

3.7. GFM inverter performance in low-SCR grids: challenges and adaptive solutions

The rapid growth of Inverter-Based Resources (IBRs) naturally contributes to weaker power systems, reflected by lower Short-Circuit Ratio (SCR) values. Although Grid-Forming (GFM) inverters are generally more resilient than Grid-Following types under such conditions, their stability and effectiveness still depend heavily on grid strength. This section examines how low-SCR environments affect both droop-controlled and Virtual Synchronous Machine (VSM) based GFMs, highlighting their different behaviors and the adjustments required for reliable operation (Liu et al., 2023a; Dash et al., 2025).

3.7.1. The low-SCR environment: fundamental challenges for GFM inverters

In low-SCR grids (SCR $<$ 3), the high grid impedance increases the sensitivity of power transfer to the power angle (δ) between inverter and grid voltages. As impedance rises, the slope of the power–angle curve decreases, making the curve flatter:

$$\frac{dP}{d\delta} = \frac{3EV_g}{X_g}\cos\delta \tag{3-19}$$

In strong grids (low X_g, high SCR), the curve is steep, so small angle changes are enough to transfer significant power. By contrast, in weak grids (high X_g, low SCR), the curve flattens, meaning larger angle swings are required to deliver the same power. This not only reduces the system's margin of stability but also drives the inverter closer to the critical limit around $\delta \approx 90^\circ$, increasing the risk of synchronism loss or oscillatory behavior. Simply, in strong grids an inverter needs only a small "push" (small δ change) to transfer power, whereas in weak grids it requires a much bigger "push" (large δ change), making the system inherently less stable this is illustrated in Fig 3–7. In weak grids, two additional challenges appear (Liu et al., 2023a). First is enhanced P–Q coupling: normally, active power (P) depends mostly on the power angle, while reactive power (Q) depends mostly on voltage. This separation allows easy control. But in weak grids, because of the high grid impedance, P and Q start to influence each other more strongly. As a result, adjusting active power also affects reactive power and vice versa, which makes control more complicated, even when using virtual impedance techniques designed to decouple them (Han et al., 2024). The second challenge is reduced voltage stiffness: in strong grids, the grid can hold the voltage steady, but in weak grids the inverter's terminal voltage is easily disturbed by load variations or interactions with other nearby converters. This reduced ability to maintain a stable voltage leads to complex dynamics when several inverters operate together, making coordination and stability harder to achieve (Han et al., 2024).

3.7.2. Impact on droop-controlled GFM inverters

For droop-controlled Grid-Forming (GFM) inverters, weak grids introduce both stability problems and performance limitations. From a stability perspective, the phase margin in the synchronization loop de-

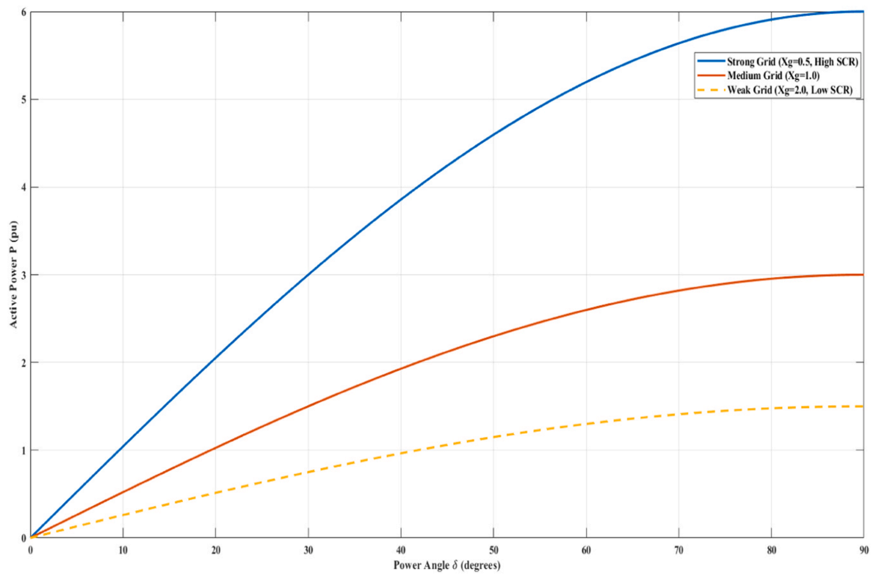

Fig. 3–7. Power-Angle Curves for Different Grid Strengths.

creases as grid impedance grows. In control terms, the open loop transfer function (Liu et al., 2023a; Han et al., 2024):

$$G_{ol}(s) = G_{droop}(s).G_{grid}(s)G_{inner}(s) \tag{3-20}$$

This net open loop transfer function is affected because $G_{grid}(s)$ adds extra phase delay in weak conditions. This reduced margin makes the inverter more prone to instability. In addition, weak grids trigger oscillatory modes at low frequencies (around 0.5–5 Hz), and the damping of these oscillations becomes weaker as SCR decreases, meaning oscillations last longer and are harder to control (Venkataramanan et al., 2023). On the performance side, power sharing accuracy suffers because droop control relies on the assumption that grid lines are mostly inductive. In weak grids, this assumption breaks down, so inverters no longer share active and reactive power proportionally as intended. Finally, the system exhibits a slower and more oscillatory transient response: after disturbances, it takes longer to settle, and the oscillations are stronger. To keep the system stable while still achieving reasonable dynamic performance, engineers must carefully retune the droop coefficients (Zhao et al., 2023).

3.7.2.1. Adaptive solutions for droop control in weak grids. In weak grids with low Short-Circuit Ratio (SCR), droop-controlled Grid-Forming (GFM) inverters often face instability, oscillations, inaccurate power sharing, and slow dynamic response. To enhance stability, researchers have developed adaptive control methods, where the inverter automatically adjusts its parameters depending on the measured grid strength (Mohammed et al., 2024). This approach relies on estimating SCR in real time and tuning droop coefficients and virtual impedance accordingly (Wang et al., 2025b). The first key strategy is adaptive droop coefficients, where the active power–frequency slope (mp) and reactive power–voltage slope (nq) are no longer fixed but are adjusted based on the estimated SCR. In strong grids with high SCR, the system is inherently stable, so smaller droop coefficients are sufficient, maintaining flexibility and responsiveness. By contrast, in weak grids with low SCR, larger coefficients are required to provide additional damping and preserve stability (Mohammed et al., 2024; Wang et al., 2025b). This adaptation is expressed as:

$$m_p(SCR) = m_{p,min} + (m_{p,max} - m_{p,min}) * f(SCR)$$

$$n_p(SCR) = n_{p,min} + (n_{p,max} - n_{p,min}) * g(SCR) \tag{3-21}$$

where f(SCR) and g(SCR) represent functions derived from real-time grid strength estimation. As SCR decreases, the inverter automatically increases m_p and n_q, effectively “stiffening” its response to maintain stability margins. To enable this adjustment, GFM inverters employ grid strength estimation techniques. Impedance-based methods inject small perturbation signals and measure the voltage–current response to determine grid impedance, from which SCR is calculated (Reisner and Weiss, 2024a).

$$\widehat{Z_g}(f) = \frac{\Delta V_{PCC}(f)}{\Delta I_{inv}(f)}$$

$$SCR_{est} = \frac{V_{nom}^2}{P_{rated} * \left|\widehat{Z_g}\right|} \tag{3-22}$$

Alternatively, natural perturbations such as load variations or system transients can be used to estimate impedance without active injection, relying on statistical operators like recursive least squares or moving averages. A third approach uses steady-state power-flow equations to approximate impedance directly from normal operating data (Wang et al., 2025b).

$$\begin{bmatrix} R_g \\ X_g \end{bmatrix} = \begin{bmatrix} \Delta P & -\Delta Q \\ \Delta Q & \Delta P \end{bmatrix}^{-1} \begin{bmatrix} V_{PCC}.\Delta V_{PCC} \\ 0 \end{bmatrix} \tag{3-23}$$

Alongside impedance estimation, stability margin indicators such as Nyquist-based criteria, damping ratio measurements, and synchronization indices can provide additional real-time feedback on system robustness. Despite these advantages, adaptive droop control with real-time SCR estimation also has important limitations (Mohammed et al., 2024). One challenge is estimation delay: the methods require time to process measurements, so sudden grid changes, like faults or switching events, may not be captured quickly enough, leaving the inverter momentarily tuned for the wrong conditions. In addition, measurement noise and harmonics can distort voltage and current signals, reducing the accuracy of impedance estimation (Moustafa et al., 2025). If active signal injection is used, it creates a trade-off: strong injections improve accuracy but disturb power quality, while weak injections are less intrusive but less reliable (Mohammed et al., 2024). There are also practical challenges. Implementing recursive estimation or advanced algorithms adds complexity and computational burden, which may be difficult for low-cost or real-time embedded controllers. In multi-inverter systems, each unit adapting independently can cause coordination issues, leading to uneven power sharing or interaction-induced oscillations. Moreover, estimation accuracy degrades under nonlinear or unbalanced conditions, such as during faults or with converter saturation (Moustafa et al., 2025). Finally, in fast transient like line trips, adaptation may not keep up, risking temporary instability.

3.7.2.2. Passivity and multi-converter considerations for adaptive virtual impedance in GFM. Grid-Forming inverters employ adaptive virtual impedance for output characteristic shaping and performance optimization in weak grids. However, the interaction between adaptive impedance and GFM dynamics (swing equation in VSM, droop characteristics) introduces additional stability considerations beyond those in GFL systems. The constrained optimization formulation for GFM adaptive impedance must ensure positive-real output impedance while coordinating with virtual inertia and damping adaptation. The optimization problem is formulated as (Reisner and Weiss, 2024a):

$$\begin{aligned}\min_{R_v,X_v} \quad & \| Z_{target}(\omega) - Z_{actual}(R_v, X_v, \omega)\|_2 \\ \text{subject to} \quad & \mathrm{Re}\{Z_{out}(j\omega)\} \geq \epsilon \forall \omega \in [0, \omega_{max}] \\ & \angle Z_{out}(j\omega) \in [\phi_{min}, \phi_{max}] \\ & R_v \in [R_{v,min}, R_{v,max}] \\ & X_v \in [X_{v,min}, X_{v,max}]\end{aligned} \tag{3-24}$$

This constraint prevents non-passive dynamics that could destabilize power-angle stability in droop-controlled GFM or interact adversely with virtual inertia in VSM implementations. In multi-GFM scenarios, adaptive virtual impedance coordination becomes critical for reactive power sharing and voltage regulation. Unlike GFL systems where current-source behavior naturally decouples units, voltage-source GFM inverters exhibit strong electromagnetic coupling through shared grid impedance. Uncoordinated adaptation can produce circulating reactive currents and voltage oscillations at the point of common coupling (Bao et al., 2014). Consensus protocols with impedance averaging mitigate these effects while maintaining individual converter adaptability to local conditions (Wang et al., 2014).

3.7.2.3. AI-enhanced adaptive control architectures. Artificial Intelligence (AI), particularly Machine Learning (ML) and Deep Reinforcement Learning (DRL), provide advanced tools to enhance the adaptive control of Grid-Forming (GFM) inverters in weak and dynamically changing grids (Abdekader Morsy A et al., 2025). Traditional adaptive droop relies on real-time Short-Circuit Ratio (SCR) estimation, which can be affected by delays, noise, and coordination challenges. AI methods overcome these drawbacks by learning nonlinear mappings, predicting grid behavior, and optimizing control parameters in real time (Williams et al., 2025; Issa et al., 2023).

1- AI-Based Parameter Adaptation

One approach is to use fuzzy logic control to adapt droop coefficients and virtual impedance. The inputs are grid condition indicators such as the estimated SCR (SCR_{est}), the rates of change of active and reactive power (dP/dt, dQ/dt), and voltage deviation. The outputs are the adapted droop coefficients and impedance parameters (Omotoso et al., 2023):

$$\left\{m_p^{adapt}, n_q^{adapt}, R_v^{adapt}, X_v^{adapt}\right\}$$

Fuzzy rules define the adaptation strategy. For example:

- IF SCR is very low and dP/dt is high, then m_p is very high.
- IF SCR is low and voltage deviation is medium, then n_q is high.
- IF SCR is high and dQ/dt is low, then R_v is low.

Beyond fuzzy logic, neural networks can directly predict optimal control parameters by learning from historical data and system conditions. A deep neural network (DNN) maps measured features to control parameters such as (Vigneysh and Kumarappan, 2016):

$$\begin{bmatrix} m_p^{adapt} \\ n_q^{adapt} \\ R_v^{adapt} \\ X_v^{adapt} \end{bmatrix} = \mathrm{NN}\left(SCR, \frac{dP}{dt}, \frac{dQ}{dt}, V_{dev}, \theta_{dev}, \text{Historical Data}\right) \tag{3-25}$$

This allows the inverter to instantly select the best droop and impedance values, even under nonlinear or unbalanced conditions, without the delay of classical estimation.

2- Deep Reinforcement Learning (DRL) for Optimal Control

While fuzzy and neural methods provide parameter tuning, DRL takes it further by learning an optimal policy through interaction with the grid environment. The state vector is defined as (Chandrakar et al., 2024):

$$s_t = \left[SCR_{est}, P, Q, V_{PCC}, w, \frac{dw}{dt}, \frac{dv}{dt}, i_d, i_q\right]$$

The control action adjusts droop slopes, virtual impedance, inertia, and damping:

$$a_t = \left[\Delta m_p, \Delta n_p, \Delta R_v, \Delta X_v, \Delta J, \Delta D_p\right]$$

The reward function is designed to encourage frequency and voltage stability, harmonic suppression, and adequate stability margins, while penalizing excessive control effort:

$$\begin{aligned} r_t = & w_1(1 - |\Delta f|) + w_2(1 - |\Delta V|) + w_3 e^{-THD} + w_4(\text{stability magin}) \\ & - w_5 \quad (\text{control Effort}) \end{aligned} \tag{3-26}$$

The DRL agent learns a policy $\pi^*(s)$ that maximizes the expected long-term reward:

$$\pi^*(s) = \mathrm{argmax}\, E\left[\sum_{t=0}^{\infty} \gamma^t r_t | s_0 = s\right] \tag{3-27}$$

Through repeated training, the agent discovers how to adapt inverter

Table 3–2
Benefits and Drawbacks of AI in Droop Control.

Category	Benefits	Drawbacks
Adaptability	Adapts inverter response automatically to varying grid strength.	Requires careful tuning to avoid instability in extreme conditions.
Prediction	Learns system patterns and predicts dynamic behavior.	Limited accuracy when facing rare or unseen operating scenarios.
Noise Robustness	Handles noise measurement and system uncertainties effectively.	Still sensitive to severe disturbances and sensor errors.
Coordination	Enables better coordination between multiple inverters.	Risk of conflicting actions when AI agents operate independently.
Stability Guarantee	Provides adaptive stability support in weak grids.	Lacks formal mathematical proof of stability in all operating conditions.
Data Needs	Utilizes system data to improve control strategies.	Requires large and diverse datasets for reliable training.
Complexity	Supports advanced adaptive control strategies.	High computational demand, challenging for real-time embedded controllers.
Explainability	Limited interpretability tools exist for AI decision-making.	Acts as a “black box,” making debugging and validation difficult.
Cybersecurity	Can detect anomalies and abnormal operating conditions.	Vulnerable to cyberattacks and adversarial data manipulation.
Cost	May improve long-term efficiency and reliability.	Increases deployment cost due to sensors, training, and powerful hardware

parameters optimally for both stability and efficiency, even in rapidly changing grid conditions (Issa et al., 2022b). Table 3–2 summarizes the key benefits and drawbacks of integrating Artificial Intelligence (AI) into droop control strategies for grid-forming inverters. AI-enhanced droop control offers significant advantages, including improved adaptability to varying grid conditions, predictive capabilities, robustness against measurement noise, and enhanced coordination among multiple inverters. However, despite these potential benefits, AI implementation also introduces several challenges. These include increased system complexity, high computational requirements, data dependency, limited interpretability, and potential cybersecurity risks. The table provides a concise overview of these pros and cons, highlighting both the opportunities and limitations associated with AI-assisted droop control (Issa et al., 2022c; "AI-Enhanced Stability Control of Grid-Forming Inverters via Inertia, Damping, and Impedance Regulation and Request PDF.", 2025).

3.7.3. Impact on virtual synchronous machine (VSM) GFM inverters

The virtual inertia (J) and damping (D_p) in a VSM must be carefully tuned depending on grid strength. While higher inertia values generally improve performance in strong grids, applying the same settings in weak grids can result in low-frequency oscillations that are not well damped. In other words, an excessive inertia setting can make the system behave like a pendulum that swings too long, so both J and D_p need to be adjusted to maintain stability. Unlike grid-following inverters that use a PLL, a VSM relies on a power synchronization loop (Reisner and Weiss, 2024b). In weak grids with high impedance, this loop can become unstable more easily. The stability requirements therefore become stricter, and the VSM must be carefully tuned to avoid losing synchronization with the grid. When VSMs operate in weak grids, their dynamics can interact with the grid impedance and trigger oscillations in the 1–15 Hz range (sub synchronous oscillations) (Li et al., 2019). This issue becomes more critical when multiple VSMs run in parallel, as their interactions can amplify these oscillations and threaten system stability. In weak grids, Virtual Synchronous Machines (VSMs) can still deliver effective virtual inertia, but they require more energy to maintain frequency stability because the voltage angle fluctuates more widely. At the same time, voltage regulation becomes more difficult, as the VSM's AVR-like control must handle a terminal voltage that is highly sensitive to variations in both active and reactive power (Wang et al., 2023).

3.7.3.1. Adaptive solutions for virtual synchronous machines (VSMs). As the electrical grid strength changes, the stability and dynamic response of Virtual Synchronous Machines (VSMs) can vary significantly. To ensure reliable operation under both strong and weak grid conditions, adaptive control strategies are introduced. These strategies allow the inverter to automatically adjust its key dynamic parameters namely, the virtual inertia J and damping coefficient D_p based on the real-time grid strength, which is usually measured by the Short-Circuit Ratio (SCR) or grid impedance Z_g. Virtual inertia and damping determine how the VSM reacts to frequency deviations and oscillations. In strong grids with high SCR values, the grid is electrically stiff, so the inverter can operate with smaller inertia and damping. However, in weak grids with low SCR, the grid becomes more sensitive to power fluctuations, requiring higher inertia and damping to maintain stability. To automate this adjustment, the virtual inertia and damping can be expressed as functions of SCR, given by (Li et al., 2019):

$$\mathrm{J(SCR)} = J_{base} * \left(1 + + \propto \frac{SCR_{base}}{SCR}\right)$$

$$D_P(\mathrm{SCR}) = D_{P,base} * \left(1 + + \beta \frac{SCR_{base}}{SCR}\right) \tag{3-28}$$

where J_{base} and D_P are the base values, SCR_{base} is the nominal short-circuit ratio, and α and β are positive tuning constants. As the grid becomes weaker and the SCR decreases, the terms $\frac{SCR_{base}}{SCR}$ increase, automatically raising both inertia and damping. This ensures that the VSM maintains stable frequency and voltage control, effectively suppressing oscillations and enhancing damping performance in low-inertia networks. For the adaptive control to function, the VSM must first estimate the grid strength in real time. This is achieved by monitoring small changes in voltage and current at the Point of Common Coupling (PCC) to estimate the grid impedance as is described in Eq.(3–22) (Reisner and Weiss, 2024b; Li et al., 2019). Through this self-tuning mechanism, the VSM becomes flexible and adaptive, capable of maintaining synchronization and stability even as grid conditions change. This approach enables seamless operation across different levels of system strength, ensuring both robust frequency support and effective voltage regulation in renewable-dominated or weak grid environments (Wang et al., 2023).

3.7.3.2. Comparative analysis: droop vs. VSM in low-SCR grids. In low short-circuit ratio (SCR) conditions, the performance of grid-forming (GFM) control strategies varies significantly depending on how they handle stability, inertia, and adaptability. Traditional droop-based GFM control provides satisfactory voltage and frequency regulation but can struggle under weak grid conditions due to limited dynamic response and dependence on parameter tuning. In contrast, the Virtual Synchronous Machine (VSM) approach offers improved stability and inertial support by emulating synchronous generator dynamics, making it more resilient to grid impedance variations. Table 3–3 summarizes a comparative analysis between Droop Control and VSM under low-SCR grid conditions, emphasizing their respective advantages, limitations, and adaptability characteristics (Venkataramanan et al., 2023; Li et al., 2019).

3.7.3.3. AI-enhanced virtual synchronous machine control for low-SCR grids. The integration of Artificial Intelligence (AI) with Virtual Synchronous Machine (VSM) control represents a transformative advancement in stabilizing power systems operating under low Short Circuit Ratio (SCR) conditions. Conventional VSMs mimic the inertial and damping behavior of synchronous generators but struggle to maintain performance in weak or highly dynamic grids due to fixed parameter settings (Issa et al., 2022c). AI-enhanced VSMs overcome these limitations by continuously learning from grid behavior and adjusting their control parameters in real time. Through intelligent inference, prediction, and adaptation, these systems enhance frequency stability, damping, and fault resilience under uncertain and fluctuating grid conditions. The AI-VSM combines a standard VSM framework with intelligent modules for perception, learning, and decision-making. The perception layer collects real-time system measurements such as voltage, current, and phase angle. The learning layer applies deep learning and reinforcement learning algorithms to model dynamic grid behavior, while the decision layer adaptively tunes inertia, damping, and virtual

Table 3–3
Performance Comparison of GFM Strategies in Low-SCR Conditions.

Aspect	Droop Control	Virtual Synchronous Machine
Stability Margin	Moderate requires careful droop tuning	Higher inherent stability due to inertia
Inertial Response	None (unless enhanced)	Excellent, provides RoCoF mitigation
Parameter Sensitivity	Low to moderate	High, requires adaptive tuning
Oscillation Damping	Good with proper virtual impedance	Excellent with proper damping design
Implementation Complexity	Low to moderate	High, requires sophisticated algorithms
Adaptation Requirements	Moderate (droop coefficients + virtual impedance)	High (inertia, damping, current limiting)
Multi-unit Operation	Good with communication, challenging without	Excellent inherent synchronization

impedance parameters. This structure ensures robust operation across a wide range of SCR values without requiring manual returning. The AI-VSM architecture, illustrated in Fig 3–8, incorporates intelligent layers that enhance dynamic performance, stability margin, and robustness under varying grid conditions. AI algorithms integrate various grid indicators to assess overall grid strength using a nonlinear model (Liu et al., 2023b):

$$\text{Grid strength Index} = AI - Model \left\{ \begin{matrix} SCR_{est} \\ Z_g \\ P_{oscillation} \\ V_{sensitivity} \\ \text{Harmonic content} \end{matrix} \right\} \tag{3-29}$$

This model fuses electrical features such as estimated SCR, grid impedance, voltage sensitivity, and harmonic distortion to produce a comprehensive stability indicator (Mohammed et al., 2025).

$$Margin_{pm}(t + \Delta t) = LSTM(X_t, Grid_{\ topology}) \tag{3-30}$$

where Xt includes recent time-series data of voltage, current, and power signals. This predictive layer enables proactive stabilization before instability emerges. AI dynamically modifies the virtual inertia constant according to real-time SCR and disturbance forecasts (Pratap et al., 2021):

$$J_{opt}(t) = \quad J_{base}. \quad [1 + \propto sigmoid(\beta.\frac{SCR_{base} - SCR_{est}}{SCR_{est}})].f_{disturbance}(t) \tag{3-31}$$

This mechanism enhances the system's capacity to resist frequency fluctuations in weak grids. Reinforcement learning (RL) agents optimize the inertia coefficient across frequency variations:

$$J_{RL} = \quad \pi_{RL}. \quad (\frac{dw}{dt}, \Delta w, SCR_{est}, P_{Load}) \tag{3-32}$$

This allows real-time adaptation to transient frequency dynamics based on reward-driven learning. AI identifies specific oscillation modes and applies targeted damping:

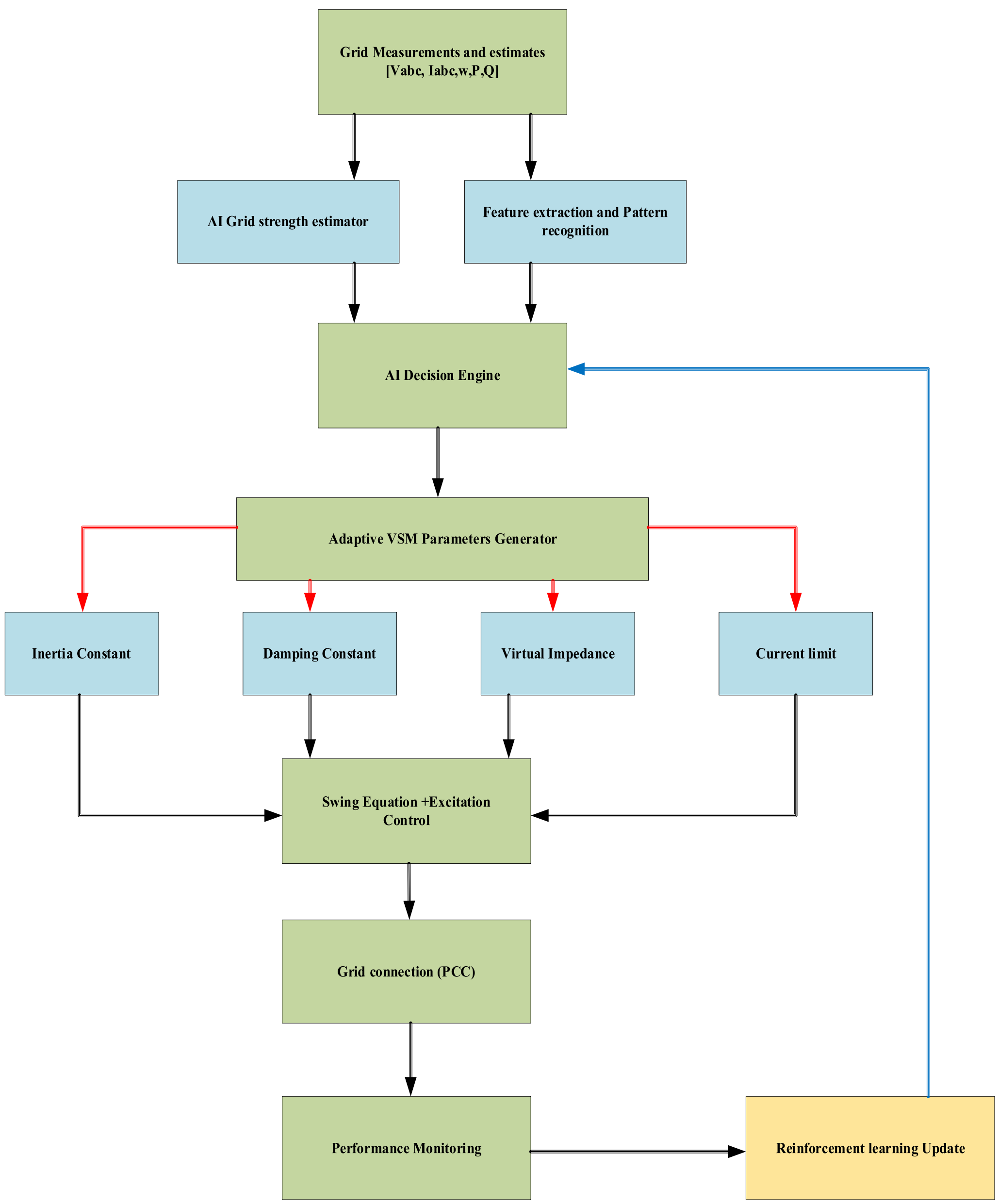

Fig. 3–8. AI-VSM Control Architecture.

$$D_P^{AI} = D_{P,base} + \sum_{i=1}^{n} K_i^{AI}.mode_i(w_{osc,i}, \xi_{target}) \quad (3\text{-}33)$$

Neural networks anticipate oscillations and apply pre-emptive damping:

$$D_P^{predictive} = NN_{damping}(\textbf{\textit{oscillation precursors}}, \textbf{\textit{load patterns}}, \textbf{\textit{neighbor inverter states}}) \quad (3\text{-}34)$$

The AI system dynamically shapes virtual impedance to maximize stability margins:

$$Z_V^{AI} = R_V^{AI} + JX_V^{AI} = AI - Impedance\ Shaping \left\{ \begin{matrix} SCR_{est} \\ P_{angle,\quad sensetivity} \\ V_{Stability,\quad Margin} \\ Intraction\ Index \end{matrix} \right\} \quad (3\text{-}35)$$

Frequency-Dependent Impedance Adaptation:

$$Z_V^{AI} = AI - filter \quad (Z_{V,base}.f_{resonance}, \quad harmonic\ spectrum) \quad (3\text{-}36)$$

Machine learning models predict fault conditions and optimize current limiting (Liu et al., 2023b):

$$I_{limit}^{AI} = \quad I_{rated}. \quad (1 + \gamma.fault\ probability(t).stability\ criticality(t)) \quad (3\text{-}37)$$

During current limiting, AI determines optimal dq-axis current distribution:

$$\begin{bmatrix} i_d^{limit} \\ i_q^{limit} \end{bmatrix} = AI - Current\ allocation \left\{ \begin{matrix} Voltage\ Support \\ Frequency\ Support \\ Device\ Thermal\ State \end{matrix} \right\} \quad (3\text{-}38)$$

In low short-circuit ratio (SCR) systems, conventional Virtual Synchronous Machine (VSM) controllers often face challenges in maintaining optimal stability and dynamic performance under rapidly changing grid conditions. To address these limitations, a Deep Reinforcement Learning (DRL) framework is proposed for online optimization of VSM parameters (Balouji et al., 2023). The DRL agent continuously interacts with the grid environment, observing its dynamic state and adapting key control parameters such as virtual inertia, damping, droop coefficients, and virtual impedance to enhance frequency and voltage stability (Alkuwari et al., 2025). State space encapsulates critical indicators of system dynamics, including estimated SCR, power angle deviation, active and reactive power, PCC voltage and its rate of change, system frequency and its derivative, grid impedance characteristics, and oscillation energy (Rajak and Pudur, 2025).

$$s_t = \left[SCR_{est}, P, Q, V_{PCC}, w, \frac{dw}{dt}, \frac{dV_{PCC}}{dt}, Z_g, \gamma, Oscillation\ Energy \right]$$

The action space defines the set of tunable VSM parameters such as moment of inertia, damping, virtual resistance and reactance, and active–reactive droop coefficients along with a current priority weighting mechanism for overload management (Rajak and Pudur, 2025).

$$a_t = [\Delta m_p, \Delta n_p, \Delta R_v, \Delta X_v, \Delta J, \Delta D_p, Current\ periority\ weight]$$

The reward function is designed to balance transient performance and control effort by rewarding stability margin, frequency and voltage regulation, and fault ride-through capability, while penalizing oscillation energy and excessive control actions (Ghidewon-Abay et al., 2022).

$$\begin{aligned} r_t = & w_1(1 - |\Delta f|) + w_2(1 - |\Delta V|) + w_3(\text{stability magin}) \\ & - w_4 \quad (\text{control Effort}) - w_5 \quad (\text{Oscillation Energy}) \\ & + w_6 \quad (\text{Fault ride through Prformance}) \end{aligned} \quad (3\text{-}39)$$

This learning-based adaptation enables the VSM to achieve optimal resilience and dynamic stability across varying low-SCR scenarios (Balouji et al., 2023; Rajak and Pudur, 2025). To achieve robust and flexible grid-forming control under varying grid conditions, the proposed AI-driven framework operates across multiple timescales, ensuring both fast dynamic response and long-term adaptability. At the fast timescale (in the order of milliseconds), the AI controller focuses on rapid corrective actions such as current limiting adaptation, virtual impedance adjustment, and oscillation damping injection (Lu and Zhuan, 2024). These functions mitigate immediate disturbances and protect electronic power components during transient or faulty events. At the medium timescale (ranging from hundreds of milliseconds to one second), the AI system performs inertia and damping optimization, power sharing coordination among multiple inverters, and stability margin maintenance to ensure synchronized and stable operation under fluctuating loads and generation. Finally, at the slow timescale (spanning seconds to minutes), the controller engages in higher-level decision-making processes, including control strategy adaptation, parameter scheduling in response to grid topology variations, and learning algorithm updates based on accumulated system data. This hierarchical adaptation across multiple timescales enables the AI-enhanced Virtual Synchronous Machine (VSM) to maintain dynamic stability, operational resilience, and long-term learning capability in low-inertia, weak-grid environments (Afifi et al., 2024).

3.8. *Grid-following inverter performance analysis at high SCR (SCR=7)*

3.8.1. *Introduction and experimental framework*

This comprehensive analysis examines the performance characteristics of a grid-following inverter operating under high short-circuit ratio conditions (SCR=7). The evaluation focuses specifically on voltage-related performance metrics, including voltage regulation capability, power quality in terms of harmonic distortion, dynamic response during power transitions, and overall compliance with international standards. The test scenario involves a 5 MW inverter connected to a 690 V, 50 Hz grid, subjected to a structured power ramp test from 2.5 MW to 6.0 MW over a 15-second duration. This analysis provides crucial insights into the inverter's behavior in strong grid environments and identifies both strengths and limitations in its voltage performance characteristics. Table 3–4 summarizes the key experimental parameters used in evaluating the grid-following inverter performance under high short-circuit

Table 3–4
Experimental Test Parameters.

Parameter	Value	Unit
Grid Parameters		
Nominal Voltage	690	V
Grid Frequency	50	Hz
Short-Circuit Ratio	7	-
Inverter Parameters		
Rated Power	5	MW
Test Duration	15	s
Power Test Profile		
Time Intervals	0–5, 5–10, 10–15	s
Power Levels	2.5, 5.0, 6.0	MW

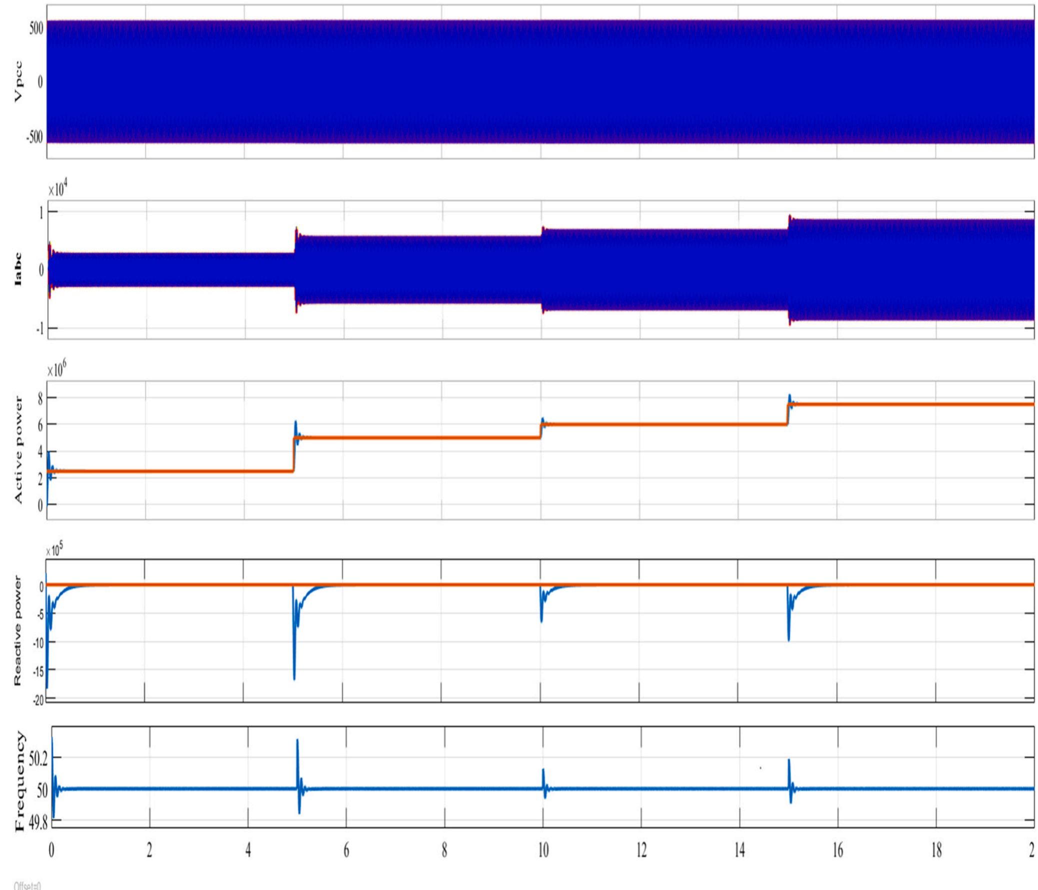

Fig. 3–9. illustrates the integrated performance metrics during the stepped power reference test providing a complete characterization of inverter capabilities under high-SCR conditions.

ratio (SCR = 7) conditions. The simulation results in Fig 3–9 presented in this section provide comprehensive validation of grid-forming inverter performance under high short-circuit ratio (SCR=7) conditions, demonstrating both the capabilities and limitations of modern power electronic interfaces in strong grid environments. As renewable penetration increases globally, understanding inverter behavior in various grid strength conditions becomes crucial for system planning and operation. The following analysis employs rigorous simulation methodologies aligned with IEEE 1547–2018 standards to evaluate critical performance metrics including voltage regulation, power quality, and dynamic response ("IEEE SA - IEEE, 1547–2018.", 2025; "IEEE SA - IEEE, 1547.2–2023.", 2025).

3.8.2. Voltage regulation performance analysis

The voltage regulation analysis reveals a significant operational concern regarding steady-state voltage maintenance. The measured line-to-line voltage consistently operated at approximately 590 V throughout the entire test duration, representing a substantial 14.5% deviation below the nominal 690 V reference. This deviation calculates an absolute voltage drop of 100 V, which persists uniformly across all power levels from 2.5 MW to 6.0 MW. Table 3–5 presents the measured voltage regulation performance of the inverter, comparing actual test results with IEEE 1547 compliance limits under high-SCR operating conditions ("IEEE SA - IEEE, 1547–2018.", 2025).

Table 3–5
Voltage Regulation Performance.

Parameter	Nominal Value	Measured Value	Deviation	Status
Line-to-Line Voltage	690 V	590 V	-100 V (-14.5%)	Non-Compliant
IEEE 1547 Requirement	±10% (621-759V)	-14.5%	Outside Range	Fail
Voltage Stability	Stable	Stable	Consistent across loads	Good

The consistency of this voltage depression across varying power conditions suggests a systematic issue rather than a load-dependent phenomenon. According to IEEE 1547–2018 standards, medium-voltage systems must maintain voltages within ±10% of nominal values, corresponding to an acceptable range of 621–759 V for a 690 V system. The measured 590 V falls significantly outside this permissible range, indicating non-compliance with voltage magnitude requirements.

3.8.3. Voltage quality and harmonic performance

The voltage quality assessment demonstrates exceptionally positive results in terms of harmonic distortion performance. The measured voltage total harmonic distortion (THD) of 0.28% represents outstanding waveform purity, significantly exceeding the IEEE 1547–2018 requirement of 5% maximum THD. Table 3–6 summarizes the voltage quality and harmonic performance results with IEEE 1547

Table 3–6
Voltage Quality and Harmonic Performance.

Parameter	IEEE 1547 Limit	Measured Value	Compliance Margin	Rating
Voltage THD	< 5.0%	0.28%	94% below limit	Excellent
Individual Harmonics	< 3.0%	< 0.1%	> 96% below limit	Excellent

Table 3–7
Dynamic Performance Metrics.

Performance Metric	Measured Value	Industry Standard	Compliance Status
Voltage Recovery Time	0.02 s	< 2.0 s	Excellent
Transient Overshoot	< 1%	< 5%	Excellent
Stability during Steps	No oscillations	Stable operation	Excellent
Frequency Decoupling	Effective	Required	Good

Table 3–8
Standards Compliance Summary.

Standard	Requirement	Measured Value	Compliance Status	Severity
IEEE 1547–2018	Voltage THD < 5%	0.28%	Fully Compliant	Excellent
IEEE 1547–2018	Voltage Range ±10%	-14.5%	Non-Compliant	Critical
IEC 61000 ("IEC TR 61000-3-6:2008 and IEC.", 2025)	Voltage Quality	0.28% THD	Fully Compliant	Excellent
Dynamic Response	< 2.0 s	0.02 s	Exceeds Requirements	Excellent

harmonic distortion limits ("IEEE SA - IEEE, 1547–2018.", 2025; "IEEE SA - IEEE, 1547.2–2023.", 2025).

The dynamic voltage response analysis reveals stable performance during active power transitions between operating points. The voltage magnitude maintains remarkable stability at approximately 590 V throughout the step changes in power reference, showing minimal transient deviations or oscillatory behavior. Table 3–7 presents the dynamic performance metrics of the inverter, highlighting its rapid voltage recovery, minimal overshoot, and stable operation during power transition events.

This stability persists during the power increments from 2.5 MW to 5.0 MW at the 5-second mark, and subsequently to 6.0 MW at the 10-second mark. The absence of significant voltage dips or overshoots during these transitions indicates well-designed current control loops and proper synchronization mechanisms. Table 3–8 provides a consolidated summary of the inverter's compliance with key international standards, illustrating strong harmonic and dynamic performance but a critical deviation in voltage magnitude regulation.

For voltage quality metrics, the system demonstrates excellent compliance, with the 0.28% THD measurement substantially outperforming the 5% limit specified in both IEEE 1547–2018 and IEC 61000 standards ("IEEE SA - IEEE, 1547–2018.", 2025; "IEC TR 61000–3-6:2008 and IEC.", 2025). However, the voltage magnitude compliance reveals a significant shortcoming, with the 590 V operating point representing a 14.5% deviation from nominal. The investigation into the underlying causes of voltage depression reveals several potential contributing factors despite the high short-circuit ratio environment. The consistent 590 V operating point across all power levels suggests that the voltage depression originates primarily from system-level configuration rather than inverter hardware limitations. A key contributing factor identified in the control setup is that the reactive power reference (Qref) of the grid-following inverter was set to zero, resulting in unity power factor operation. Under this condition, the inverter injects only active power without providing reactive support to maintain voltage magnitude. Consequently, even in a strong grid (SCR = 7), the inverter cannot counteract upstream voltage drops or deviations caused by network impedance or transformer settings. This operational configuration, combined with possible substation tap setting or upstream regulation constraints, explains the persistent 100 V voltage deficit observed throughout the test.

Table 3–9
Critical Instability Parameters.

Parameter	Normal Operation	During Collapse	Deviation	Severity
Voltage Magnitude	590 V	200 V	-66%	CATASTROPHIC
Current Magnitude	1.0×10^4 A	1.5×10^4 A	+ 50%	CRITICAL
Frequency	50.2 Hz	51.5 Hz	+ 1.5 Hz	SEVERE
Power Oscillations	Stable	Sustained	100% modulation	UNSTABLE

3.9. *Critical stability analysis at low SCR (SCR=1.5) - voltage collapse scenario*

The system experiences catastrophic instability at t = 10 s following the power reference step to 1.2 pu under weak grid conditions (SCR=1.5, R/X = 10). This represents a severe voltage collapse scenario characterized by extreme operational parameters that exceed all safety margins and operational limits. The critical instability parameters presented in Table 3–9 capture the severe dynamic deviations observed during the voltage collapse scenario, highlighting the system's transient vulnerability under weak-grid or low-reactive-support conditions. These findings align with reported instability mechanisms in grid-following inverters, where the loss of voltage regulation and excessive current injections trigger rapid deterioration of voltage and frequency stability. The voltage collapse to 200 V represents a 66% reduction from the nominal operating voltage, indicating complete loss of voltage stability. The simultaneous current surge to 1.5×10^4 A exceeds the system's rated capacity by 50%, creating hazardous operating conditions. The frequency runaway to 51.5 Hz represents a 3% deviation from nominal, far exceeding the IEEE 1547 limit of ±1%. This indicates complete loss of synchronization of grid and poses significant risks to connected equipment ("IEEE SA - IEEE, 1547–2018.", 2025). The critical instability phenomena captured in Fig 3–10 demonstrate the severe operational limitations of grid-following inverters under weak grid conditions (SCR=1.5), revealing voltage collapse to 200 V, current surge to 1.5×10^4 A, and frequency runaway to 51.5 Hz that validate recent research on synchronization stability challenges in low-SCR networks

3.9.1. *Towards a critical system strength index (CSSI)*

The catastrophic voltage collapse observed at a short-circuit ratio (SCR) of 1.5, as detailed in Section 3.9, underscores a fundamental shortcoming in conventional grid stability assessment: SCR alone is an inadequate, one-dimensional indicator for predicting stability boundaries in inverter-dominated power systems. To overcome this limitation, we propose the conceptual framework of a Critical System Strength Index (CSSI), a multi-dimensional metric that holistically captures the three dominant factors influencing inverter stability. First, the Short-Circuit Ratio (SCR) remains a foundational measure of grid stiffness; however, its effectiveness as a stability predictor is significantly influenced by the phase angle of the grid impedance. Second, the grid impedance angle (ϕ_g), or equivalently the R/X ratio, plays a decisive role in reshaping the power-voltage coupling characteristics. In highly resistive grids (high R/X), active power (P) becomes strongly coupled to voltage magnitude (V), while the traditional Q-V relationship weakens. This altered coupling intensifies phase-locked loop (PLL) sensitivity to active power variations in Grid-Following (GFL) inverters, degrading synchronization stability. Although metrics like the Weighted Short-Circuit Ratio (WSCR) partially account for this effect, they do not fully capture its dynamic implications. Third, the Adjacent Resource Dynamics, quantified as the Inertia and Damping Contribution (IDC), reflects the aggregate stabilizing support from neighboring resources, including virtual inertia and damping from Grid-Forming (GFM) inverters as well as physical inertia from any remaining synchronous generators. The presence of GFM units can substantially elevate the

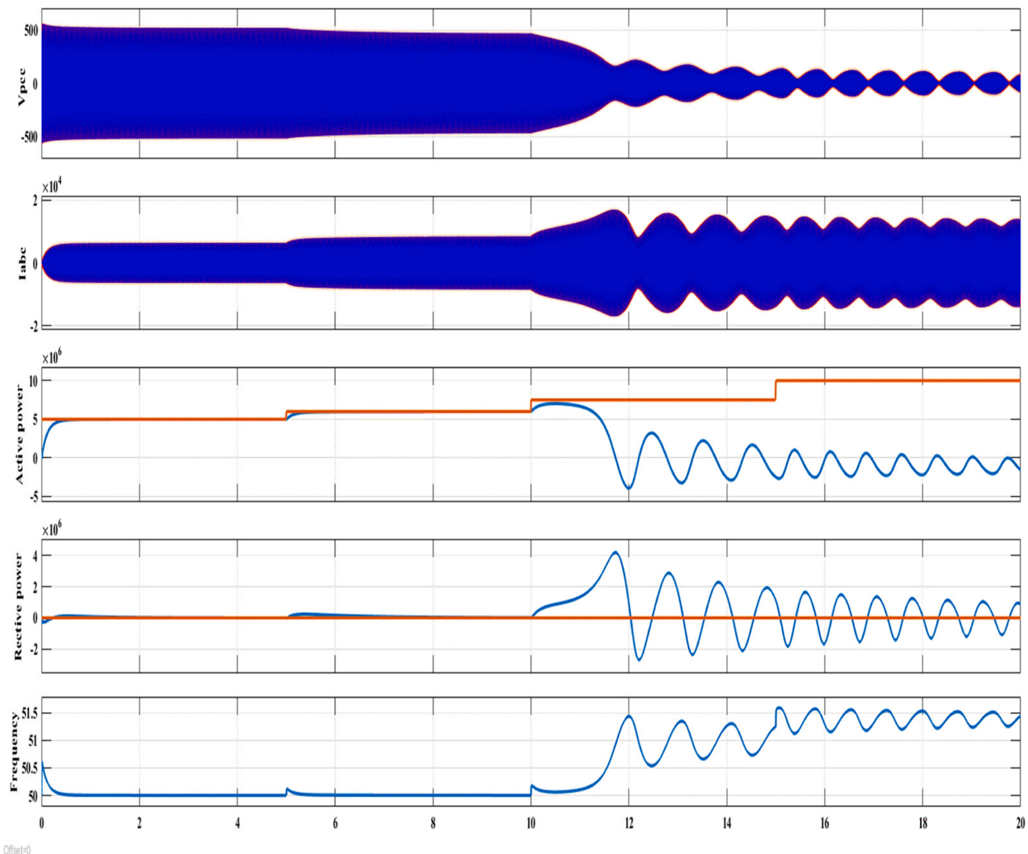

Fig. 3–10. illustrates the integrated performance metrics during the stepped power reference test providing a complete characterization of inverter capabilities under low-SCR conditions.

system's effective stability margin, even under low SCR conditions, by providing a stiff, self-sustaining voltage reference and active damping. The CSSI is thus conceptualized as a nonlinear function of these three interdependent variables:

$$\mathrm{CSSI} = \mathrm{f}(\mathrm{SCR}, \phi_g, \mathrm{IDC}) \tag{3-40}$$

A low CSSI value would offer a more accurate and robust predictor of impending synchronization instability and voltage collapse than SCR alone, enabling improved security assessment in planning and real-time operations. Future work should focus on rigorously deriving the analytical form of *f* through comprehensive small-signal stability studies of hybrid systems comprising both GFL and GFM inverters.

3.9.2. Bifurcation analysis of catastrophic instability and role of current limiting

In ultra-weak grid conditions, catastrophic voltage collapse has been frequently observed in inverter-dominated systems operating near their stability limits. Understanding whether such collapse is governed by oscillatory mechanisms or by large-signal equilibrium loss is essential for the design of robust grid-forming control strategy. This subsection analyzes the catastrophic instability observed at SCR = 1.5 using a bifurcation-based interpretation and examines the role of current-limiting mechanisms in shaping the dominant instability mode (Li et al., 2019).

3.9.2.1. Saddle-node bifurcation as the dominant instability mechanism. The collapse behavior observed at SCR = 1.5 is characterized by a rapid loss of voltage magnitude at the point of common coupling, accompanied by a sharp increase in current demand and the inability of the system to recover its pre-disturbance operating point (Liu et al., 2023a). Such behavior is indicative of a saddle-node bifurcation, where a stable and an unstable equilibrium merge and disappear as a system parameter crosses a critical value. In weak and ultra-weak grids with elevated R/X ratios, the strong coupling between active power injection and voltage magnitude imposes a maximum transferable power limit. As grid strength deteriorates or power demand increases, the operating equilibrium approaches this limit (Niu et al., 2025). Once exceeded, no feasible steady-state solution exists, resulting in an abrupt transition to a low-voltage state. The absence of sustained oscillatory growth prior to collapse, together with the irreversible nature of the voltage drop, strongly supports equilibrium loss, which is rather than oscillatory instability, as the primary failure mechanism. Although saddle-node bifurcation dominates the collapse process, oscillatory behavior may emerge in the vicinity of the stability boundary. Under certain parameter configurations, lightly damp power oscillations can appear as eigenvalues approach the imaginary axis. However, in the observed SCR = 1.5 scenario, these oscillations do not develop into sustained growing modes characteristic of a Hopf bifurcation. Instead, the system transitions directly to voltage collapse once the equilibrium disappears, indicating that oscillatory instability plays a secondary role (Chatterjee and Geng, 2025).

3.9.2.2. Influence of current limiting strategy on instability evolution. Current limiting, while essential for protecting semiconductor devices, fundamentally alters inverter dynamics during large-signal disturbances and directly influences the instability trajectory. When current saturation is reached, the inverter's ability to regulate voltage and power is constrained, effectively modifying its source characteristics (Fan et al., 2022). If the current-limiting strategy prioritizes active current injection, reactive current support is reduced, accelerating voltage degradation in resistive weak grids. Conversely, reactive-current-priority strategies preserve voltage support but may reduce active power delivery, potentially inducing frequency excursions. In both cases, the current ceiling imposed restricts control authority, causing the system to traverse more rapidly toward the stability boundary (Panya et al., 2024). Aggressive current limiting tends to sharpen the saddle-node bifurcation by abruptly removing voltage support, thereby hastening equilibrium loss. More adaptive current-limiting approaches such as dynamic reactive current prioritization that can delay collapse and slightly extend the stable operating region, although they cannot eliminate the fundamental power-transfer limit imposed by grid impedance (Fan et al., 2022). The catastrophic failure observed at SCR $= 1.5$ is therefore best explained as a large-signal saddle-node bifurcation driven by equilibrium loss, with current limiting acting as an accelerating factor rather than the root cause. While oscillatory dynamics may arise near the stability boundary, they remain subordinate to the dominant voltage-collapse mechanism. These findings highlight the importance of bifurcation-aware control design and adaptive current-limiting strategies to maximize stability margins in ultra-weak grid environments.

3.10. Hierarchical AI-augmented GFM architecture for ultra-weak grids

While Section 3.5 introduced adaptive solutions for Virtual Synchronous Machine control in weak grids through real-time parameter tuning of virtual inertia and damping coefficients, those approaches relied on explicit grid strength estimation and predefined adaptation laws. The framework presented in this section extends beyond classical adaptive control by integrating artificial intelligence to autonomously learn optimal adaptation strategies, predict grid disturbances before they manifest, and coordinate multiple layers of control across different timescales. This AI-augmented architecture represents the next evolutionary step, addressing the limitations of model-based adaptive methods when confronted with the severe uncertainties and stochastic dynamics characteristic of ultra-weak grids with SCR < 2 (Rocabert et al., 2012b).

3.10.1. Multi-layer control architecture

The proposed hierarchical architecture comprises three functionally distinct layers operating across different temporal scales, as illustrated in Fig. 3–8. The perception and estimation layer executes at 1–10 ms, performing real-time data acquisition and grid parameter identification through recursive least squares and Kalman filter-based estimators for online impedance tracking (Wang et al., 2020). Prony decomposition methods extract dominant oscillation modes from measured power signals, while Bayesian inference quantifies parameter estimation uncertainty. The intermediate AI supervisory layer operates at 10–100 ms, employing deep reinforcement learning agents trained through proximal policy optimization to determine optimal control parameters (Lin et al., 2026). Long short-term memory networks capture temporal dependencies for predictive feedforward compensation, anticipating disturbances 50–100 ms ahead. A fuzzy logic-based stability assessor processes multiple indicators—eigenvalue locations, damping ratios, and voltage sensitivities—to provide unified robustness evaluation. Multi-agent coordination through IEC 61850 GOOSE (Generic Object-Oriented Substation Events) messaging ensures coherent system-wide responses (Rocabert et al., 2012b). The core GFM execution layer operates at 0.1–1 millisecond intervals, implementing virtual synchronous machine emulation or droop control with adaptive virtual impedance that maintains strict passivity constraints (Zhang et al., 2010). Current limiting with priority-based dq-axis allocation protects semiconductor devices during faults.

3.10.1.1. Role of the AI layer in grid-forming inverters: supervisory versus direct control. key architectural consideration in AI-augmented grid-forming (GFM) inverters is the timescale at which the artificial intelligence layer should operate. Specifically, the AI layer may function either as a slow-timescale supervisory parameter optimizer or as a direct generator of fast control signals to address sub-cycle transients ("AI-Enhanced Stability Control of Grid-Forming Inverters via Inertia, Damping, and Impedance Regulation and Request PDF.", 2025). In this work, a hierarchical control architecture is adopted in which the AI layer operates in a supervisory role, while fast control actions are executed by conventional physics-based GFM controllers (Liu et al., 2023b). In the proposed architecture, the AI layer operates at intermediate timescales (on the order of 10–100 ms) and adaptively tunes the parameters of the underlying GFM controller, such as virtual inertia, damping, droop coefficients, and virtual impedance, in response to changing grid conditions. The inner control loops, responsible for voltage and current regulation at sub-millisecond timescales, remain fully deterministic and are implemented using established GFM control laws. This separation ensures that high-speed control actions are handled by controllers with proven stability and real-time performance, while the AI layer provides adaptive optimization without directly interfering with fast dynamics (Liu et al., 2023b). This supervisory approach offers several advantages. First, it preserves robustness and stability by maintaining physics-based control structures that can be analytically analyzed and certified. Second, it avoids the computational and latency challenges associated with executing complex AI algorithms at switching-frequency timescales (Issa et al., 2023). Third, it enhances interpretability and facilitates compliance with existing grid codes and certification procedures, as the core control behavior remains transparent and verifiable. By contrast, architecture in which the AI layer directly generates fast control signals, such as voltage references or PWM commands, pose significant risks. These include limited real-time feasibility, the absence of formal stability guarantees due to the black-box nature of neural networks, and vulnerability to untrained or out-of-distribution operating conditions. Consequently, direct AI control is not adopted in this study. Overall, positioning the AI layer as a supervisory parameter optimizer provides a practical and reliable framework that balances adaptability and performance with stability, safety, and deplorability in inverter-dominated power systems.

3.10.2. AI feature set and real-time estimation

To enable situational awareness and adaptive control, the AI supervisory layer utilizes a multivariate state vector $\mathbf{s}(t) \in \mathbb{R}^{27}$ comprising 27 real-time measurements and estimates, organized into five functional categories. Each category captures distinct aspects of system dynamics essential for stability assessment in weak and ultra-weak grid environments.

3.10.2.1. Category 1: grid impedance characterization (6 features). Grid strength and topology are characterized by six impedance-related quantities: magnitude $|Z_g|$, angle $\angle Z_g$, resistance R_g, reactance X_g, estimated short-circuit ratio $\mathrm{SCR}_{\mathrm{est}}$, and rate of change dZ_g/dt. These are obtained via a Recursive Least-Squares (RLS) estimator with exponential forgetting factor ($\lambda = 0.98$) applied to the voltage–current relationship at the point of common coupling. Updates occur every 10 ms using a 50-sample sliding window, with outlier rejection ensuring robustness. Estimation errors remain below 8 % for signal-to-noise ratios exceeding 20 dB.

3.10.2.2. Category 2: oscillation modal content (8 features). Poorly damped oscillations in the sub-synchronous range (0.5–15 Hz) are captured by the frequencies f_i and damping ratios ζ_i of the four dominant modes. Prony analysis decomposes the active-power signal over a 2-s window (sampled at 1 kHz) into a sum of damped sinusoids. The top four modes, ranked by amplitude, are retained and updated every 500 ms.

3.10.2.3. Category 3: voltage dynamics and sensitivity (5 features). Voltage stability is assessed through the PCC voltage magnitude V_{PCC}, its rate of change dV/dt, sensitivities to active and reactive power ($\partial V/\partial P$,

$\partial V/\partial Q$), and total harmonic distortion THD_V. Sensitivities are estimated every 2 s via controlled power perturbations ($\Delta P = \pm 0.01$ p.u.) and central-difference formulas. THD is computed via a one-cycle FFT.

3.10.2.4. Category 4: local inverter operating state (4 features). Direct measurements from the inverter active and reactive power output (P_{out}, Q_{out}), power angle δ, and frequency deviation Δf are sampled at 1 kHz and down-sampled to 100 Hz for AI processing.

3.10.2.5. Category 5: neighbor inverter coordination states (4 features). Coordination with neighboring inverters uses the number of active neighbors N_{active}, their average active and reactive power ($P_{neighbors,\ avg}$, $Q_{neighbors,\ avg}$), and the power-sharing error $\varepsilon_{sharing}$. IEC 61850 GOOSE messaging provides deterministic, low-latency communication, with authenticated status messages broadcast every 100 ms. All features are normalized to $[0|1]$ via min-max scaling based on expected operational ranges. Temporal embedding incorporates three historical timesteps (at 100 ms intervals), yielding a 108-dimensional input for recurrent neural networks (e.g., LSTM) to capture temporal dependencies. The total computational load for feature estimation is 5.2 ms per cycle, well within the 10 ms budget of the perception layer. Table 3-10 details the breakdown per category, confirming real-time feasibility on embedded processors such as the Texas Instruments TMS320C6748 DSP (456 MHz).

3.10.3. Intelligence-enhanced parameter adaptation

The AI supervisory layer interacts with the core GFM algorithm through three mechanisms. The parameter adaptation interface enables the deep reinforcement learning agent to adjust six critical parameters: virtual inertia J, damping D, droop slopes mp and nq, and virtual impedance R_V and X_V, following by:

$$\theta\ (k+1) = \theta(k) + (\propto.\pi_{DRL}(s(t))) \tag{3-41}$$

The stability-constrained reward function incorporates Lyapunov barrier terms that penalize parameter updates yielding positive energy function derivatives, restricting the policy search to provably stable configurations (Lin et al., 2026). Long short-term memory networks provide predictive feedback, generating disturbance forecasts that enable preemptive parameter adjustments (Rocabert et al., 2012b). Three mechanisms address vulnerabilities of conventional adaptive control in ultra-weak grids. Measurement uncertainty-aware adaptation employs Bayesian neural networks to compute posterior probability distributions over impedance estimates, weighting control actions inversely with uncertainty magnitude (Lin et al., 2026). Passivity-enforced virtual impedance maintains the positive-real constraint Re $\{Zout(j\omega)\} \geq 0$ through constrained optimization, ensuring the inverter never exhibits destabilizing negative resistance (Zhang et al., 2010). Multi-timescale hybrid learning coordinates fast model predictive control (1–10 ms), medium-timescale DRL optimization (10–100 ms), and slow offline policy updates (100–1000 ms) (Wu and Wang, 2020).

3.10.4. Stability certification and implementation

Multi-layered stability assurance verifies that maximum eigenvalue real parts of the closed-loop state matrix remain strictly negative at each iteration, while energy-based metrics ensure bounded power imbalances (Zhang et al., 2010). Minimum gain and phase margins of 6 dB and 30 ° are maintained through online Nyquist analysis. Implementation requires GPU/TPU hardware achieving neural network inference latencies below 5 ms, with 2–4 GB memory for experience replay buffers (Lin et al., 2026). A fallback strategy reverts to conservative fixed-parameter GFM mode upon AI layer failure, ensuring graceful degradation. Validation through simulation at SCR = 1.5 demonstrates frequency deviation reduction from ±0.8 Hz to ±0.2 Hz, voltage recovery improvement from 500 to 100 ms, and oscillation damping enhancement from 0.05 to 0.3, while maintaining THD below 3% despite 2% measurement noise (Lin et al., 2026). Hardware-in-the-loop testing on OPAL-RT platforms and planned field demonstration in a 10 kV network with SCR = 1.2 will provide comprehensive validation. Table 3–11summarizes the functional allocation across layers. The architecture achieves superior performance through adaptivity to topology changes, predictive instability anticipation 50–100 ms in advance, robustness to ±20% parameter errors, and coordinated multi-inverter power sharing optimization (Wu and Wang, 2020; Zhang et al., 2010).

3.10.5. Verification and validation frameworks for AI-based grid controllers

The deployment of artificial intelligence–based controllers in power systems necessitates a fundamental rethinking of verification and validation (V&V) methodologies. Conventional V&V practices that are largely grounded in extensive time-domain simulations and empirical testing which are inadequate for AI-driven control due to the nonlinear, data-dependent, and partially opaque nature of learning-based models (Xiang and Johnson, 2018). While statistical performance indicators provide useful insights, they cannot guarantee stability or safety under rare, extreme, or previously unseen operating conditions, nor can they account for intentional data manipulation or cyber-physical attacks. To ensure safe operation in critical infrastructure applications, V&V frameworks must evolve toward approaches that provide formal or probabilistic guarantees of stability and safety. One promising direction involves formal verification techniques, which aim to mathematically prove that an AI-controlled system satisfies predefined constraints. Reachability analysis can be used to compute admissible state sets and ensure that unsafe regions are never reached, although its computational complexity limits scalability (Cleaveland et al., 2022). Complementary methods such as satisfiability modulo theories (SMT)–based verification and abstract interpretation enable the analysis of neural-network-driven controllers by bounding their behavior without exhaustive state exploration. For systems of realistic scale where formal proofs become intractable, probabilistic validation approaches offer a practical alternative. Statistical model checking employs Monte Carlo–based simulations to estimate the probability of violating safety or stability constraints, often augmented by rare-event sampling techniques. Similarly, probabilistic safety assessment can be extended to incorporate AI components, enabling the identification of dominant failure modes and quantification of risk associated with control misbehavior (Xiang and Johnson, 2018). A critical aspect of AI controller validation is robustness against adversarial data patterns and cyber-physical threats (Xiang and Johnson, 2018). Learning-based controllers may be vulnerable to carefully crafted input perturbations or malicious sensors and communication attacks that induce unsafe actions (Alvand and Shadmand, 2023). Robustness certification techniques aim to quantify the minimum perturbation required to destabilize the controller and verify that this threshold exceeds acceptable safety margins. In parallel, adversarial training strategies and online anomaly detection mechanisms can improve resilience by exposing the controller to hostile scenarios during development and by monitoring inputs during operation. Secure-by-design architectures that incorporating cryptographic protection, authenticated communication, and redundancy which further reduce vulnerability to targeted attacks. Beyond analytical methods, hardware-in-the-loop (HIL) and

Table 3–10
Computational Requirements for Feature Estimation.

Feature Category	Algorithm	Computation Time
Grid Impedance (6 features)	RLS	0.8 ms
Oscillation Modes (8 features)	Prony Analysis	3.2 ms
Voltage Sensitivity (5 features)	Numerical Differentiation	0.5 ms
THD Computation (1 feature)	FFT (1 cycle)	0.4 ms
Communication (4 features)	GOOSE Decode	0.3 ms
Total (27 features)	Combined	5.2 ms

Table 3–11
AI-Augmented GFM Architecture Components and Functions.

Layer	Component	Function	Timescale	Robustness Feature
Perception	Grid Impedance Estimator	Estimates Z_g, X_g/R_g	1–5 ms	RLS with forgetting factor for time-varying grids
	Oscillation Detector	Identifies 0.5–15 Hz modes	10 ms	Prony method with noise immunity
	Uncertainty Quantifier	Computes measurement confidence	5 ms	Bayesian inference with prior distributions
AI Supervisory	DRL Agent	Optimizes control parameters	10–50 ms	Stability-constrained reward function
	LSTM Predictor	Forecasts grid disturbances	50–100 ms	Attention mechanism for key features
	Stability Assessor	Evaluates stability margins	20 ms	Fuzzy logic with adaptive thresholds
Core GFM	VSM/Droop Core	Voltage/frequency formation	0.1–1 ms	Passivity-enforced implementation
	Adaptive Virtual Impedance	Shapes output characteristics	1 ms	Positive-real constraint enforcement
	Current Limiter	Protects semiconductor devices	0.1 ms	Priority-based dq-axis allocation

power-hardware-in-the-loop (PHIL) testing remain indispensable for validating AI controllers under realistic operating conditions. When combined with adversarial testing scenarios, HIL and PHIL platforms provide a high-fidelity environment for assessing controller behavior under extreme disturbances, parameter uncertainty, and cyber-physical attack vectors prior to field deployment (Issa et al., 2023). Overall, the most effective V&V strategies for AI-augmented grid controllers are inherently hybrid, integrating formal verification for critical safety properties, probabilistic analysis for complex and uncertain dynamics, and experimental validation for real-world realism. Coupled with continuous monitoring and explainable AI techniques, such frameworks are essential for establishing trust and ensuring the reliable operation of AI-enabled control systems in future low-inertia power grids (Xiang and Johnson, 2018).

4. Conclusion and future work

This comprehensive review has systematically analyzed the transformative journey of power systems from a synchronous machine-dominated paradigm to one increasingly reliant on inverter-based resources. We have elucidated the fundamental stability challenges posed by conventional Grid-Following (GFL) inverters in weak grids, particularly the synchronization instability driven by the Phase-Locked Loop (PLL) and the negative incremental resistance effect. Our detailed small-signal impedance model precisely quantifies this phenomenon and dictates the critical SCR thresholds for both single and multi-inverter systems, providing a robust analytical framework for understanding GFL limitations. The paper then transitioned to the paradigm-shifting role of Grid-Forming (GFM) inverters, which are indispensable for stabilizing future renewable-rich power networks. We explored various GFM control strategies, including Droop Control and Virtual Synchronous Machines (VSMs), and critically examined their performance and inherent trade-offs. Specifically, we addressed the nuanced challenge of operating in ultra-weak grids (SCR < 2), highlighting the potential conflict between the inherent time constant of virtual inertia in VSMs and the need for extremely fast power-angle adjustment. Our analysis suggests that while VSMs offer superior frequency regulation due to inertial support, communication-less droop controllers can provide more robust proportional power sharing, with adaptive VSMs emerging as a hybrid solution. Furthermore, we delved into the complexities of P-Q decoupling in resistive grids, demonstrating the limitations of conventional virtual impedance techniques and proposing novel control paradigms such as Power Angle Control, Matching Control, and Model Predictive Control as more fundamental solutions. Crucially, this review extended to the analysis of large-signal instabilities, particularly the catastrophic failures observed at low SCRs. Our bifurcation analysis clarified that such collapses are primarily driven by saddle-node bifurcations (loss of equilibrium), with current limiting strategies playing a significant role in influencing the dominant mode and accelerating the loss of voltage support. The transformative potential of Artificial Intelligence (AI) in enhancing GFM capabilities was thoroughly investigated, emphasizing a hierarchical architecture where AI functions as a slow-timescale supervisory parameter optimizer. We meticulously outlined the advantages of this approach—robustness, computational feasibility, and interpretability—while also detailing the significant risks associated with direct, fast AI control, such as black-box behavior and lack of verifiability. Finally, recognizing the paramount importance of safety and reliability in critical infrastructure, we charted a forward-looking research trajectory for developing robust Verification and Validation (V&V) frameworks for AI-based grid controllers. These frameworks must move beyond statistical performance to provide formal or probabilistic guarantees of stability, especially when confronting adversarial data patterns and cyber-physical attacks. This includes the integration of formal verification methods, probabilistic safety analysis, robustness certification, and secure-by-design AI architectures. The insights presented in this paper provide a clear pathway for overcoming the most pressing stability barriers, fostering the secure, reliability, and sustainable integration of renewable energy into the global power system.

CRediT authorship contribution statement

Abdelwahab Ammar: Writing – original draft, Validation, Software, Methodology, Funding acquisition, Data curation, Conceptualization. **István Vokony:** Writing – review & editing, Supervision, Investigation, Funding acquisition.

Declaration of Competing Interest

The authors declare that they have no known competing financial interests or personal relationships that could have appeared to influence the work reported in this paper.

Acknowledgments

Ammar Samir Abdelwahab acknowledges the support of the Bolyai János Research Scholarship of the Hungarian Academy of Sciences (BO/50/24). This publication was supported by the HYNET - this project has received funding from the European Union's Horizon Europe research and innovation program under grant agreement No. 101172757. I would like to express my sincere gratitude to my beloved family, my father, my mother, and my siblings for their unwavering support, encouragement, and prayers throughout my academic journey. Their love and sacrifices have been a constant source of strength and inspiration.

Data availability

Data will be made available on request.

References

"(PDF) A review on Microgrid operation and control." Accessed: Oct. 14, 2025. [Online]. Available: ⟨https://www.researchgate.net/publication/334726089_A_review_on_Microgrid_operation_and_control⟩.

"AI-Enhanced Stability Control of Grid-Forming Inverters via Inertia, Damping, and Impedance Regulation | Request PDF." Accessed: Oct. 10, 2025. [Online]. Available: ⟨https://www.researchgate.net/publication/395791188_AI-Enhanced_Stability_Control_of_Grid-Forming_Inverters_via_Inertia_Damping_and_Impedance_Regulation⟩.

"Guerrero, J.M., et al., 'Control of Power Converters in Distributed Generation Microgrids,' IEEE Transactions on Industrial Electronics, vol. 60, no. 4, pp. 1263–1270, 2013. - Google Search." Accessed: Nov. 18, 2024. [Online]. Available: ⟨https://www.google.com/search?q=Guerrero%2C+J.+M.%2C+et+al.%2C+%22Control+of+Power+Converters+in+Distributed+Generation+Microgrids%2C%22+IEEE+Transactions+on+Industrial+Electronics%2C+vol.+60%2C+no.+4%2C+pp.+1263%E2%80%931270%2C+2013.&oq=Guerrero%2C+J.+M.%2C+et+al.%2C+%22Control+of+Power+Converters+in+Distributed+Generation+Microgrids%2C%22+IEEE+Transactions+on+Industrial+Electronics%2C+vol.+60%2C+no.+4%2C+pp.+1263%E2%80%931270%2C+2013.&gs_lcrp=EgZjaHJvbWUyBggAEEUYOTIGCAEQLhhA0gEHNjUxajBqMagCALACAA&sourceid=chrome&ie=UTF-8⟩.

"IEC TR 61000-3-6:2008 | IEC." Accessed: May 23, 2025. [Online]. Available: ⟨https://webstore.iec.ch/en/publication/4155⟩.

"IEEE SA - IEEE 1547.2-2023." Accessed: May 14, 2025. [Online]. Available: ⟨https://standards.ieee.org/ieee/1547.2/7166/⟩.

"IEEE SA - IEEE 1547-2018." Accessed: Jun. 17, 2025. [Online]. Available: ⟨https://standards.ieee.org/ieee/1547/5915/⟩.

Abdekader Morsy A, A.S., Setianingsih, C., Molnár, B., Kiss, J., Bereczki, B., Hartmann, B., 2025. AI-enhanced MCDA-based evaluation of grid reliability in the nordic-baltic region (Aug). 2025 10th Int. Youth Conf. Energy (IYCE) 1–5. https://doi.org/10.1109/IYCE66046.2025.11155050.

Afifi, M.A., Marei, M.I., Mohamad, A.M.I., 2024. Reinforcement-learning-based virtual inertia controller for frequency support in islanded microgrids (Mar). Technol. 2024 Vol. 12 Page 39 12 (3), 39. https://doi.org/10.3390/TECHNOLOGIES12030039.

Aliyu, A.J., Kannan, R., Wei, H.T., 2025. Impact of grid strength on grid-forming inverter performance: a comparative study of droop and virtual synchronous generator controls (May). Eng. Res. Express 7 (2), 025340. https://doi.org/10.1088/2631-8695/ADD2D4.

Alkuwari, A.N., Albaseer, A., Al-Kuwari, S., Qaraqe, M., 2025. Robust ConvLSTM Model with Deep Reinforcement Learning for Stealth Attack Detection in Smart Grids. IEEE Open J. Ind. Electron. Soc. https://doi.org/10.1109/OJIES.2025.3594618.

Alvand, H., Shadmand, M.B., 2023. AI-based self-driving grid-following inverters with compromised supervisory layer controller. IECON Proc. (Ind. Electron. Conf.). https://doi.org/10.1109/IECON51785.2023.10312338.

Bai, K., Sindhu, V., Haque, A., 2023. Fault Ride Through approach for Grid-Connected Photovoltaic System (Sep). ePrime Adv. Electr. Eng. Electron. Energy 5. https://doi.org/10.1016/j.prime.2023.100232.

Balouji, E., Backstrom, K., McKelvey, T., 2023. Deep reinforcement learning based grid-forming inverter. 2023 IEEE Ind. Appl. Soc. Annu. Meet. IAS 2023. https://doi.org/10.1109/IAS54024.2023.10406664.

Bamigbade, A., 2023. H∞Robust Control of a Grid-Connected Inverter. 2023 IEEE Tex. Power Energy Conf. TPEC 2023. https://doi.org/10.1109/TPEC56611.2023.10078550.

Bao, C., Ruan, X., Wang, X., Li, W., Pan, D., Weng, K., 2014. Step-by-step controller design for LCL-Type Grid-Connected inverter with capacitor-current-feedback active-damping. IEEE Trans. Power Electron 29 (3), 1239–1253. https://doi.org/10.1109/TPEL.2013.2262378.

Barac, B., Krpan, M., Capuder, T., Kuzle, I., 2021. Modeling and Initialization of a Virtual Synchronous Machine for Power System Fundamental Frequency Simulations. IEEE Access 9, 160116–160134. https://doi.org/10.1109/ACCESS.2021.3130375.

Barsali, S., et al., 2025. Grid forming inverters for electric vehicle charging stations to enhance distribution grid resilience. IEEE Access 13, 109687–109700. https://doi.org/10.1109/ACCESS.2025.3582070.

Beck, H.P., Hesse, R., 2007. Virtual synchronous machine. 2007 9th Int. Conf. Electr. Power Qual. Util. EPQU. https://doi.org/10.1109/EPQU.2007.4424220.

Benner, P., Heiland, J., Werner, S.W.R., 2022. "Robust output-feedback stabilization for incompressible flows using low-dimensional H∞ -controllers," (May). Comput. Optim. Appl. 82 (1), 225–249. https://doi.org/10.1007/S10589-022-00359-X.

Castilla, M., De Vicuña, L.G., Miret, J., 2018. Control of power converters in AC microgrids (Nov). Micro Des. Implement. 139–170. https://doi.org/10.1007/978-3-319-98687-6_5.

Chandrakar, R., Dubey, R.K., Panigrahi, B.K., 2024. Deep Learning-Based Islanding Detection Method for Droop-Controlled Grid-Forming Inverters (Dec). IEEE J. Emerg. Sel. Top. Ind. Electron. 6 (2), 687–698. https://doi.org/10.1109/JESTIE.2024.3512937.

Chatterjee, S., Geng, S., 2025. Effects of line dynamics on the stability margin to Hopf bifurcation in grid-forming inverters (Dec). Sustain. Energy Grids Netw. 44, 101947. https://doi.org/10.1016/J.SEGAN.2025.101947.

Chatterjee, S., Kumar, P., Chatterjee, S., 2018. A techno-commercial review on grid connected photovoltaic system (Jan). Renew. Sustain. Energy Rev. 81, 2371–2397. https://doi.org/10.1016/j.rser.2017.06.045.

B.M. Chen, "Robust and H∞ Control," 2000, doi: 10.1007/978-1-4471-3653-8.

M. Cleaveland, L. Lindemann, R. Ivanov, and G.J. Pappas, "Risk Verification of Stochastic Systems with Neural Network Controllers," Aug. 2022, Accessed: Feb. 01, 2026. [Online]. Available: https://arxiv.org/pdf/2209.09881.

Das, T.S., Annakkage, U.D., Muthumuni, D., 2024. Input-Output Feedback Linearized Control of Grid-Forming Converters in Virtual Synchronous Machine Mode. Proc. 2024 23rd Natl. Power Syst. Conf. Achiev. Decarbonized Digit. Energy Electr. Transp. Syst. NPSC 2024. https://doi.org/10.1109/NPSC61626.2024.10987027.

Dash, G., Jain, P., Pandey, V., Senroy, N., 2025. Stability Enhancement in Power Systems with High Renewable Penetration: The Role of Grid-Forming Inverters. 2025 IEEE 1st Int. Conf. Smart Sustain. Dev. Electr. Eng. SSDEE 2025. https://doi.org/10.1109/SSDEE64538.2025.10968505.

Fan, B., Liu, T., Zhao, F., Wu, H., Wang, X., 2022. A Review of Current-Limiting Control of Grid-Forming Inverters under Symmetrical Disturbances. IEEE Open J. Power Electron. 3, 955–969. https://doi.org/10.1109/OJPEL.2022.3227507.

Fazal, S., Haque, M.E., Arif, M.T., Gargoom, A., 2022. Droop Control Techniques for Grid Forming Inverter. vol. 2022-November AsiaPac. Power Energy Eng. Conf. APPEEC. https://doi.org/10.1109/APPEEC53445.2022.10072251.

X.; Gao, D.; Zhou, A.; Anvari-Moghaddam, and F. Blaabjerg, "Analysis of X/R Ratio Effect on Stability of Grid-Following and Grid-Forming Converters," vol. 14, p. 2025, 2023, doi: 10.1109/CPE-POWERENG58103.2023.10227503.

Geekiyanage, V., Seppänen, J., 2024. Power System Stability Improvements Through Grid Forming Inverters for Systems with High Penetration of Grid Following Inverters. IEEE PES Innov. Smart Grid Technol. Eur. ISGT Eur. 2024. https://doi.org/10.1109/ISGTEUROPE62998.2024.10863434.

S. Ghidewon-Abay, A. Mehrizi-Sani, C. Mazheruddin, H. Syed, and M. Jin, "Control of Grid-Connected Converters using Deep Learning," 2022.

Guerrero, J.M., Vasquez, J.C., Matas, J., De, L.G., 2011. Vicuña, and M. Castilla, "Hierarchical control of droop-controlled AC and DC microgrids - A general approach toward standardization (Jan). IEEE Trans. Ind. Electron. 58 (1), 158–172. https://doi.org/10.1109/TIE.2010.2066534.

Han, F., Zhang, X., Li, M., Li, F., Zhao, W., 2024. Stability Control for Grid-Connected Inverters Based on Hybrid-Mode of Grid-Following and Grid-Forming (Sep). IEEE Trans. Ind. Electron. 71 (9), 10750–10760. https://doi.org/10.1109/TIE.2023.3335325.

He, X., Desai, M.A., Huang, L., Dorfler, F., 2025. Cross-Forming Control and Fault Current Limiting for Grid-Forming Inverters. IEEE Trans. Power Electron 40 (3), 3980–4007. https://doi.org/10.1109/TPEL.2024.3500885.

Huang, L., Blaabjerg, F., 2025. An Improved RFR Method for Enhancing Large-Signal Stability of Grid-Following Inverter Under Weak and Faulty Grid Conditions. IEEE Trans. Ind. Electron. 1–6. https://doi.org/10.1109/TIE.2025.3591655.

H. Issa *et al.*, "Artificial Intelligence-Based Controller for Grid-Forming Inverter-Based Generators," p. 3852923, 2022a, Accessed: Oct. 04, 2025. [Online]. Available: ⟨https://hal.science/hal-03852923v1⟩.

H. Issa *et al.*, "AI-based controller for grid-forming inverter-based generators under extreme dynamics," pp. 12–15, 2023, doi: 10.1049/icp.2023.0701ï.

Issa, H., Debusschere, V., Garbuio, L., Lalanda, P., Hadjsaid, N., 2022b. Artificial Intelligence-Based Controller for Grid-Forming Inverter-Based Generators. vol. 2022-October IEEE PES Innov. Smart Grid Technol. Conf. Eur.. https://doi.org/10.1109/ISGT-EUROPE54678.2022.9960593.

Issa, H., Debusschere, V., Garbuio, L., Lalanda, P., Hadjsaid, N., 2022c. Artificial Intelligence-Based Controller for Grid-Forming Inverter-Based Generators. vol. 2022-October IEEE PES Innov. Smart Grid Technol. Conf. Eur.. https://doi.org/10.1109/ISGT-EUROPE54678.2022.9960593.

Kannan, A., et al., 2024. Performance of Grid Forming Compared to Grid Following STATCOM in Weak Power Systems. IEEE PES Innov. Smart Grid Technol. Eur. ISGT Eur. 2024. https://doi.org/10.1109/ISGTEUROPE62998.2024.10863099.

Keddar, M., Doumbia, M.L., Belmokhtar, K., Krachai, M.Della, 2021. Experimental Validation of an Accurate Reactive Power-Sharing Approach Based on Adaptive Virtual Impedance and Consensus Control. 2021 12th Int. Renew. Energy Congr. IREC 2021. https://doi.org/10.1109/IREC52758.2021.9624770.

Kroposki, B., et al., 2017. Achieving a 100% Renewable Grid: Operating Electric Power Systems with Extremely High Levels of Variable Renewable Energy (Mar). IEEE Power Energy Mag. 15 (2), 61–73. https://doi.org/10.1109/MPE.2016.2637122.

Labella, A., Filipovic, F., Petronijevic, M., Bonfiglio, A., Procopio, R., 2020. An MPC Approach for Grid-Forming Inverters: Theory and Experiment (May). Energ. 2020 Vol. 13 Page 2270 13 (9), 2270. https://doi.org/10.3390/EN13092270.

Li, F., Lin, X., Yang, L., Wang, J., Zhang, D., 2024. An Adaptive Reverse Droop Control for Coordinated Power Sharing Strategy of GFM and GFL Inverters. CPSS ISESC 2024 2024 CPSS IEEE Int. Symp Energy Storage Convers. 683–685. https://doi.org/10.1109/ISESC63657.2024.10785315.

Li, Y., Meng, K., Dong, Z.Y., 2019. Frequency enhancement of grid-forming inverters under low-SCR weak grid. IET Conf. Publ. 2019 (CP764). https://doi.org/10.1049/CP.2019.0287.

Lin, X., Li, Z., Yang, Z., Wang, J., Cao, J., Yang, S., 2025. A Reverse Droop Control for More Adjustable Grid-following Inverters Under Weak Grid. 2025 4th Int. Conf. N. Energy Syst. Power Eng. NESP 2025 261–266. https://doi.org/10.1109/NESP65198.2025.11041275.

Y. Lin *et al.*, "Research Roadmap on Grid-Forming Inverters With editing and support from Hariharan Krishnaswami", Accessed: Jan. 28, 2026. [Online]. Available: www.nrel.gov/publications.

Liu, J., Wang, W., Fan, Y., Zhao, X., 2024. Stability Improvement for Grid-Following Inverter by Virtual Damping Enhancement With Current Compensation. Proc. 2024 4th Power Syst. Green. Energy Conf. PSGEC 2024 1217–1221. https://doi.org/10.1109/PSGEC62376.2024.10721068.

Liu, W., Kerekes, T., Dragicevic, T., Teodorescu, R., 2023b. Review of Grid Stability Assessment Based on AI and a New Concept of Converter-Dominated Power System State of Stability Assessment (Jan). IEEE J. Emerg. Sel. Top. Ind. Electron. 4 (3), 928–938. https://doi.org/10.1109/JESTIE.2023.3236885.

Liu, W., Wang, R., Kerekes, T., Dragicevic, T., Teodorescu, R., 2023a. Modulation-Compensated Power Synchronization Control for Modular Multilevel Converters with Enhanced Performance under Varying SCR (Oct). IEEE J. Emerg. Sel. Top. Power Electron 11 (5), 4714–4725. https://doi.org/10.1109/JESTPE.2023.3293431.

Lu, C., Zhuan, X., 2024. Adaptive Control for Virtual Synchronous Generator Parameters Based on Soft Actor Critic (Apr). Sens. (Basel) 24 (7). https://doi.org/10.3390/S24072035.

Ma, Z., 2025. From Grid-Following to Grid-Forming: A Review of Converter Technology Paradigm Shift and Its Applications in Renewable-Rich Power Systems (Aug). Adv. Eng. Res. Possib.. Chall. 2 (2), 37. https://doi.org/10.63313/AERPC.9047.

Mallemaci, V., Mandrile, F., Carpaneto, E., Bojoi, R., 2023. Simplified virtual synchronous compensator with grid-forming capability (Sep). IEEE Trans. Ind. Appl. 59 (5), 6203–6219. https://doi.org/10.1109/TIA.2023.3285523.

Meraj, S.T., Yu, S.S., Hasan, K., Trinh, H.M., Shi, P., 2025. An advanced frequency adaptive pll for grid connected inverters under abnormal grid conditions. IEEE Trans. Ind. Appl. 61 (2), 1863–1875. https://doi.org/10.1109/TIA.2024.3524481.

Mohammed, N., Udawatte, H., Zhou, W., Hill, D.J., Bahrani, B., 2024. Grid-Forming Inverters: A Comparative Study of Different Control Strategies in Frequency and Time Domains. IEEE Open J. Ind. Electron. Soc. 5, 185–214. https://doi.org/10.1109/OJIES.2024.3371985.

Mohammed, N., Zhou, W., Ramasubramanian, D., Bahrani, B., Dutta, S., Bello, M., 2025. Data-driven estimation of impedance of inverter-based resources for efficient stability evaluation (Jul). Electr. Power Syst. Res. 244, 111559. https://doi.org/10.1016/J.EPSR.2025.111559.

Moustafa, S.H., Taha, R.A., Ibrahim, A.M., Soliman, A.S., Amin, M.M., Mohammad, O.A., 2025. "Dynamic Droop-Controlled Grid-Forming Inverter Strategy for Stable Power Sharing in PV-Integrated AC Islanded Microgrids," (Jul). 2025 IEEE Int. Conf. Environ. Electr. Eng. 2025 IEEE Ind. Commer. Power Syst. Eur. (EEEIC / I&ampCPS Eur.) 1–5. https://doi.org/10.1109/EEEIC/ICPSEUROPE64998.2025.11169087.

T.-T. Nguyen, T. Vu, S. Paudyal, F. Blaabjerg, and T.L. Vu, "Grid-Forming Inverter-based Wind Turbine Generators: Comprehensive Review, Comparative Analysis, and Recommendations," Jul. 2022, Accessed: Oct. 04, 2025. [Online]. Available: ⟨http://arxiv.org/abs/2203.02105⟩.

Niu, X., et al., 2025. A Tight Grid-Forming Control Framework for Grid-connected Inverters under Large Grid Frequency Drops with Wide Range of SCR and X/R. IEEE Trans. Power Electron. https://doi.org/10.1109/TPEL.2025.3643503.

Omotoso, H.O., et al., 2023. Machine Learning Supervisory Control of Grid-Forming Inverters in Islanded Mode (May). Sustain. 2023 Vol. 15 Page 8018 15 (10), 8018. https://doi.org/10.3390/SU15108018.

Panya, P., Suwankawin, S., Sangwongwanich, S., 2024. A Current-Limiting Scheme with Adjustable Virtual Impedance for Three-Phase Four-Wire Grid Forming Inverters. 2024 27th Int. Conf. Electr. Mach. Syst. ICEMS 2024 1990–1996. https://doi.org/10.23919/ICEMS60997.2024.10920971.

Park, J., Jeong, S., Yoon, M., 2024. Grid Forming Inverter Power Control Stability Analysis. IEEE Access 12, 112626–112636. https://doi.org/10.1109/ACCESS.2024.3443611.

Pepermans, G., Driesen, J., Haeseldonckx, D., Belmans, R., D'haeseleer, W., 2005. Distributed generation: Definition, benefits and issues (Apr). Energy Policy 33 (6), 787–798. https://doi.org/10.1016/j.enpol.2003.10.004.

Pogaku, N., Prodanović, M., Green, T.C., 2007. Modeling, analysis and testing of autonomous operation of an inverter-based microgrid (Mar). IEEE Trans. Power Electron 22 (2), 613–625. https://doi.org/10.1109/TPEL.2006.890003.

Pratap, A., Sharma, S.K., Khandelwal, A., 2021. A Review of Modern Virtual Inertia Control Strategies for Microgrid Implementation. 2021 IEEE 2nd Int. Conf. Electr. Power Energy Syst. ICEPES 2021. https://doi.org/10.1109/ICEPES52894.2021.9699804.

Quan, X., et al., 2020. Photovoltaic Synchronous Generator: Architecture and Control Strategy for a Grid-Forming PV Energy System (Jun). IEEE J. Emerg. Sel. Top. Power Electron 8 (2), 936–948. https://doi.org/10.1109/JESTPE.2019.2953178.

Rahman, K., Hashimoto, J., Orihara, D., 2024. Virtual Impedance Control for Enhanced Current Limitation in Grid-Forming Inverters. Proc. 3rd IEEE Int. Conf. Power Electron. Intell. Control Energy Syst. ICPEICES 2024 1078–1083. https://doi.org/10.1109/ICPEICES62430.2024.10719306.

Rajak, M.K., Pudur, R., 2025. Deep reinforcement learning framework for adaptive power control in grid-forming inverters: A multi-objective optimization approach (Apr). J. Renew. Sustain. Energy 17 (2). https://doi.org/10.1063/5.0249385.

Reisner, F., Weiss, G., 2024b. Grid impedance measurement for inverters with current controllers and virtual impedances. 2024 22nd Int. Conf. Intell. Syst. Appl. Power Syst. ISAP 2024. https://doi.org/10.1109/ISAP63260.2024.10744252.

Reisner, F., Weiss, G., 2024a. Grid impedance measurement for inverters with current controllers and virtual impedances. 2024 22nd Int. Conf. Intell. Syst. Appl. Power Syst. ISAP 2024. https://doi.org/10.1109/ISAP63260.2024.10744252.

Reißner, F., De Carne, G., 2024. Virtual Synchronous Machine integration on a Commercial Flywheel for Frequency Grid Support. IEEE Trans. Power Electron 39 (10), 12086–12090. https://doi.org/10.1109/TPEL.2024.3369980.

Rocabert, J., Luna, A., Blaabjerg, F., Rodríguez, P., 2012a. "Control of Power Converters in AC Microgrids,". IEEE Trans. Power Electron 27 (11), 4734–4749. https://doi.org/10.1109/TPEL.2012.2199334.

Rocabert, J., Luna, A., Blaabjerg, F., Rodríguez, P., 2012b. "Control of power converters in AC microgrids,". IEEE Trans. Power Electron 27 (11), 4734–4749. https://doi.org/10.1109/TPEL.2012.2199334.

Rodriguez-Cabero, A., Roldan-Perez, J., Prodanovic, M., 2020. Virtual Impedance Design Considerations for Virtual Synchronous Machines in Weak Grids (Jun). IEEE J. Emerg. Sel. Top. Power Electron 8 (2), 1477–1489. https://doi.org/10.1109/JESTPE.2019.2912071.

Roldan-Perez, J., Rodriguez-Cabero, A., Prodanovic, M., 2019. Design and Analysis of Virtual Synchronous Machines in Inductive and Resistive Weak Grids (Dec). IEEE Trans. Energy Convers. 34 (4), 1818–1828. https://doi.org/10.1109/TEC.2019.2930643.

Saleh, A., Rastegarnia, A., Farzamnia, A., Kin, K.T.T., 2022. Power and Current Limiting Strategy Based on Droop Controller with Floating Characteristic for Grid-Connected Distributed Generations. IEEE Access 10, 13966–13973. https://doi.org/10.1109/ACCESS.2022.3146147.

Song, G., Cao, B., Chang, L., 2022. Review of Grid-forming Inverters in Support of Power System Operation (Mar). Chin. J. Electr. Eng. 8 (1), 1–15. https://doi.org/10.23919/CJEE.2022.000001.

Thommessen, A., Hackl, C.M., 2024. Virtual Synchronous Machine Control for Doubly Fed Induction Machine-Based Wind Energy Conversion Systems. IEEE Open J. Ind. Electron. Soc. 5, 264–301. https://doi.org/10.1109/OJIES.2024.3366082.

Vasquez, J.C., Guerrero, J.M., Savaghebi, M., Eloy-Garcia, J., Teodorescu, R., 2013. "Modeling, analysis, and design of stationary-reference-frame droop-controlled parallel three-phase voltage source inverters,". IEEE Trans. Ind. Electron. 60 (4), 1271–1280. https://doi.org/10.1109/TIE.2012.2194951.

Venkataramanan, A., Wang, W., Ramasubramanian, D., Huque, A., Key, T., Mehrizi-Sani, A., 2023. GRID-FORMING DISTRIBUTED ENERGY RESOURCES: VALUE IN HIGH RENEWABLE PENETRATION AND WEAK GRID SCENARIOS. IET Conf. Proc. 2023 (20), 321–330. https://doi.org/10.1049/ICP.2023.2755.

Vigneysh, T., Kumarappan, N., 2016. Artificial Neural Network Based Droop-Control Technique for Accurate Power Sharing in an Islanded Microgrid (Sep). Int. J. Comput. Intell. Syst. 9 (5), 827–838. https://doi.org/10.1080/18756891.2016.1237183.

Wald, F., Tao, Q., De Carne, G., 2024. Virtual Synchronous Machine Control for Asynchronous Grid Connections (Feb). IEEE Trans. Power Deliv. 39 (1), 397–406. https://doi.org/10.1109/TPWRD.2023.3235149.

Wang, J., Liu, Z., Feng, K., Liu, J., 2025b. An adaptive droop and feedforward control based transient power sharing and decoupling method for grid-forming inverters in islanded microgrids. IEEE Trans. Ind. Electron. 72 (5), 4800–4810. https://doi.org/10.1109/TIE.2024.3463024.

J. Wang, S. Ganguly, and B. Kroposki, "Experimental Evaluation of Impact of Short-Circuit Ratio (SCR) and X/R Ratio on Stability of Grid-Forming and Grid-Following Inverters," pp. 1–5, Nov. 2025a, doi: 10.1109/PESGM52009.2025.11225025.

Wang, T., Zhou, Y., Yan, S., Wang, B., Zhang, H., 2023. Output Impedance Modeling and Parameter Disturbance Stability Analysis of Photovoltaic Virtual Synchronous Generator. 2022 1st Int. Conf. CyberEnergy Syst. Intell. Energy ICCSIE 2022. https://doi.org/10.1109/ICCSIE55183.2023.10175259.

Wang, X., Blaabjerg, F., Wu, W., 2014. Modeling and analysis of harmonic stability in an AC power-electronics- based power system. IEEE Trans. Power Electron 29 (12), 6421–6432. https://doi.org/10.1109/TPEL.2014.2306432.

Wang, X., Taul, M.G., Wu, H., Liao, Y., Blaabjerg, F., Harnefors, L., 2020. Grid-Synchronization Stability of Converter-Based Resources - An Overview. IEEE Open J. Ind. Appl. 1, 115–134. https://doi.org/10.1109/OJIA.2020.3020392.

Wang, Y., Wang, J., Zeng, W., Liu, H., Chai, Y., 2018. H∞ robust control of an LCL-Type grid-connected inverter with large-scale grid impedance perturbation (Jan). Energ. (Basel) 11 (1). https://doi.org/10.3390/EN11010057.

Wei, W., Yao, L., Liang, S., Deng, J., Ruan, D., Zhang, X., 2025. VSG Control with Adaptive Virtual Impedance Compensation for Enhanced Small-Signal Stability Under Varying Grid SCRs. 2025 IEEE Int. Conf. Power Syst. Smart Grid Technol. PSSGT 2025 100–105. https://doi.org/10.1109/PSSGT64932.2025.11033926.

Williams, D.O., Li, Z.S., Megahed, T.F., Luo, X., 2025. Enhancing Power Quality in Low-Inertia Grids Using NILM-Enabled Grid-Forming Inverters. 2025 IEEE Int. Conf. Progn. Health Manag. ICPHM 2025. https://doi.org/10.1109/ICPHM65385.2025.11061818.

Wu, H., Wang, X., 2019. Design-Oriented Transient Stability Analysis of PLL-Synchronized Voltage-Source Converters (Sep). IEEE Trans. Power Electron 35 (4), 3573–3589. https://doi.org/10.1109/TPEL.2019.2937942.

Wu, H., Wang, X., 2020. Design-Oriented Transient Stability Analysis of PLL-Synchronized Voltage-Source Converters (Apr). IEEE Trans. Power Electron 35 (4), 3573–3589. https://doi.org/10.1109/TPEL.2019.2937942.

W. Xiang and T.T. Johnson, "Reachability Analysis and Safety Verification for Neural Network Control Systems," May 2018, Accessed: Feb. 01, 2026. [Online]. Available: http://arxiv.org/abs/1805.09944.

Zeb, K., et al., 2022. Faults and Fault Ride Through strategies for grid-connected photovoltaic system: A comprehensive review (Apr). Renew. Sustain. Energy Rev. 158. https://doi.org/10.1016/j.rser.2022.112125.

Zhang, L., Harnefors, L., Nee, H.P., 2010. Power-synchronization control of grid-connected voltage-source converters (May). IEEE Trans. Power Syst. 25 (2), 809–820. https://doi.org/10.1109/TPWRS.2009.2032231.

Zhang, L., Harnefors, L., Nee, H.P., 2011. Interconnection of two very weak AC systems by VSC-HVDC links using power-synchronization control (Feb). IEEE Trans. Power Syst. 26 (1), 344–355. https://doi.org/10.1109/TPWRS.2010.2047875.

Zhang, L., Zheng, H., Hu, Q., Su, B., Lyu, L., 2020. An Adaptive Droop Control Strategy for Islanded Microgrid Based on Improved Particle Swarm Optimization. IEEE Access 8, 3579–3593. https://doi.org/10.1109/ACCESS.2019.2960871.

Zhao, F., Wang, X., Zhou, Z., Sun, Y., Harnefors, L., Zhu, T., 2023. Robust grid-forming control with active susceptance (Mar). IEEE Trans. Power Electron 38 (3), 2872–2877. https://doi.org/10.1109/TPEL.2022.3223511.